Theoretical studies of metal-metal cooperativity in pyrazolate-bridged complexes

Dissertation
for the award of the degree
"Doctor rerum naturalium" (Dr.rer.nat.)
of the Georg-August-Universität Göttingen

within the doctoral program Chemistry
of the Georg-August University School of Science (GAUSS)

submitted by
Anton Römer
from Bremen

Göttingen, April 2023

Thesis Committee

Prof. Dr. Ricardo A. Mata
Institute for Physical Chemistry, Georg-August-University Göttingen

Prof. Dr. Peter E. Blöchl
Institute of Theoretical Physics, Clausthal University of Technology

Prof. Dr. Jörg Behler,
Center for Theoretical Chemistry, Ruhr University Bochum

Members of the Examination Board

Reviewer: Prof. Dr. Ricardo A. Mata
Institute for Physical Chemistry, Georg-August-University Göttingen

Second Reviewer: Prof. Dr. Peter Blöchl
Institute of Theoretical Physics, Clausthal University of Technology

Further members of the Examination Board

Prof. Dr. Franc Meyer
Institute for Anorganic Chemistry, Georg-August-University Göttingen

Prof. Dr. Thomas Zeuch
Institute for Physical Chemistry, Georg-August-University Göttingen

Jun.-Prof. Dr. Daniel Obenchain
Institute for Physical Chemistry, Georg-August-University Göttingen

Dr. Oliver Bünermann
Institute for Physical Chemistry, Georg-August-University Göttingen

Date of the oral examination: 20.06.2023

Statement of Authorship

With my signature I declare to have written this thesis by myself, without assistance from other parties and without the use of other documents, expect for those explicitly stated in the text.

Göttingen, April 2023

Danksagung

Mein vorrangiger Dank gebührt Prof. Dr. Ricardo A. Mata. Dies gilt zum einen für die Bereitstellung des Themas meiner Doktorarbeit und die hervorragende wissenschatfliche Betreuung. Zum anderen, und keineswegs minderen Teil, gilt es aber auch seinen ausdrücklichen Interesse und Bemühungen daran, ein Arbeitsklima zu erhalten, das gleichsam produktiv wie freundlich ist. Geschichten über mangelhafte Betreuung and schlechte Arbeitsklimata während der Promotion sind bedauerlicherweise gang und gäbe, aber meine Zeit in der Arbeitsgruppe Mata ist ein Paradebeispiel dafür, dass es nicht immer so kommen muss. Des Weiteren danke ich Prof. Dr. Peter E. Blöchl und Prof. Dr. Jörg Behler für meine Betreuung und die wissenschaftliche Kooperation.
Das Arbeitsklima könnte ohne die Gruppenmitglieder kaum bestehen. Somit möchte ich allen Mitgliedern der Arbeitsgruppen Mata und Behler, aktuellen wie vorherigen, ebenfalls dafür danken. Dies gilt noch einmal mehr für jene, die an meinen Projekten mitgewirkt und unterstützt haben, spezifisch Lukas Hasecke, Rafael Machleid und Roland Schulz.
Für ein "normales" Leben außerhalb der Uni habe ich (ohne besondere Reihenfolge) außerdem folgenden Personen zu danken: Lennart, Kirstin, Christian, Peter, Dominik, Charlotte, Philipp, Frieda, Sky, und Gordon. Ohne unsere fantastischen Erlebnisse wäre ich kaum derselbe Mensch, der ich heute bin.
Zu guter Letzt danke ich meiner Familie, insbesondere meinen Eltern Martina und Ulrich Römer. Ich mag zeitweise an mir selbst gezweifelt haben, aber auf eure unerschütterliche Unterstützung war stets Verlass.

Abstract

Transition metal complexes can play a variety of important roles in regard to catalysis, materials synthesis, photochemistry, and biological systems through use of their unique electronic structure, and the resulting chemical versatility. These complexes can be tuned towards a multitude of different applications through careful design of their ligand structure. Electronic structure methods can provide great insight into these aspects, being able to predict compound properties even before any synthetic efforts have taken place, or in elucidating reaction mechanisms and unexplained compound behaviour afterwards. The results from one such project are detailed in the first chapter of this work, describing the oxidative splitting of water molecules by a bimetallic Ni^{II} complex, with special attention toward the metal-metal cooperativity.

Furthermore, transition metal complexes often exhibit spin transitions in response to external stimuli such as changes in temperature and pressure, a phenomenon known as spin crossover (SCO). This phenomenon goes hand in hand with changes in physical properties, and the attainable bi- or multistabilities grant these types of complexes wide potential application as molecular switches in display, memory and sensing devices. It is no surprise that they have gathered significant interest for decades, and many attempts are made to design SCO complexes with specific characteristics. Especially of interest currently are complexes containing two or even more transition metal centers. However, it is crucial to balance ligand field stabilization and spin pairing energies to reach magnetic multistability conditions. Again, electronic structure methods should be able to further the understanding of these aspects. However, the widely used general gradient approximation density functional calculations provide only qualitatively correct results, being known to overestimate the stability of low-spin (LS) states. Higher level methods on the other hand are often not available for systems of any significant size.

The aim of this work then is to firstly demonstrate the application of a range of techniques involving density functional theory (DFT), which are currently in everyday use for the validation and explanation of experimental observations. From there on, this work extrapolates from these commonly used methods to develop a methodology to improve DFT techniques both in accuracy and in the range of applicable systems. Specifically, it is attempted to describe the spin states of a [2x2] Fe^{II} grid complex in a self-consistent, *ab initio* approach. Wave function methods are applied to the investigation of smaller model systems, with the result being used to parameterize a local hybrid functional.

Contents

Chapter 1

Introduction

Transition metal complexes

Transition metal complexes play a highly important role in regard to catalysis, materials synthesis, photochemistry, and biological systems [1–3]. Their unique electronic structure results in versatile reactivities, which can be tuned towards a multitude of different applications. In general terms, these systems consist of one or more transition metal center, surrounded (and possibly connected) by a ligand structure. The chemical behaviour is mostly determined by the interaction between the s and p molecular orbitals of the ligands and the d orbitals of the metal(s).

Catalytic reagents containing first row transition metals, such as iron, cobalt or nickel, have been extensively investigated due to their relative abundance, low cost, and ease of handling when compared to lower row transition metals [4]. These complexes can potentially catalyse a wide range of processes, including oxidation, reduction, hydrogenation, carbon-carbon bond formation, and the splitting of water molecules, to name just a few examples [5, 6]. These applications have the potential to contribute greatly to advancements in both industry and academia.

Spin-crossover

Another important aspect of materials containing transition metals is the potential for spin-crossover (SCO) events. Since their initial discovery in 1931 [7], materials exhibiting this behaviour have garnered immense interest. The reason lies in their possible application as molecular switches for use in display, memory, and sensing devices, possibly even as qubits in quantum computation [8–13]. These materials are commonly based on d^4 to d^7 transition metals [14–20], with complexes based on Fe^{II} possibly the most notable example [21, 22].

In general terms, a SCO describes the transition between a low-spin (LS) and high-spin (HS) state, brought on by external stimuli such as temperature, pressure or light irradiation [23–25], and it requires a suitable ligand field at hand [26]. In octahedral Fe^{II} complexes, occupation of the t_{2g} orbitals is favored for large ligand-field splitting energies, resulting in the $^1A_{1g}$ S=0 LS state. For weaker ligand fields, with a spin-pairing energy larger than the ligand-field splitting energy, both t_{2g} and e_g orbitals are occupied, resulting in the $^5T_{2g}$ S=2 HS state. Transitions between the spin states are generally accompanied by changes to the geometry of the metal environment, explained by the shift of electron density between bonding e_g and anti-bonding t_{2g} orbitals. In octahedral Fe^{II} complexes, the Fe-ligand bond is elongated by around 0.2 Å on average, absent other factors such as a distorted ligand environment [26]. Some notable examples of such SCO complexes are shown in figure 1.1.

Up till now, these materials have been composed mainly of single center complexes with abrupt and well-defined transitions. However, supramolecular complexes combining multiple metal centers have come into focus in recent times [28–30]. They exhibit unique SCO properties not found in their single-center counterparts, allowing for hysteretic and multistep transitions, as well as cooperative effects, since changes to one metal center can be communicated to another through changes to the ligand backbone structure. One such complex of interest is the [2x2] Fe^{II} grid complex, synthesized by Meyer and coworkers in 2010 [30], and shown in figure 1.2.

Describing the spin states of SCO complexes from a theoretical perspective has been attempted in a multitude of studies. Because of the inherent difficulties in computing the spin states accurately, internal references are often adopted [31,32]. Calculations

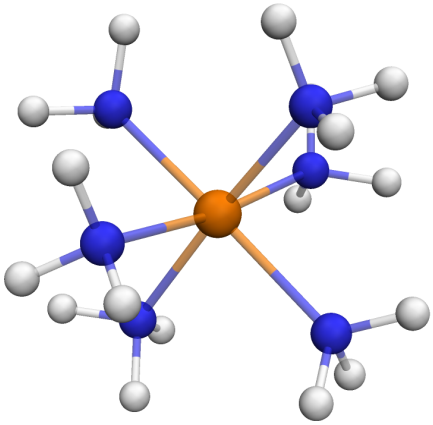

(a) $[Fe^{II}(NH_3)_6]^{2+}$

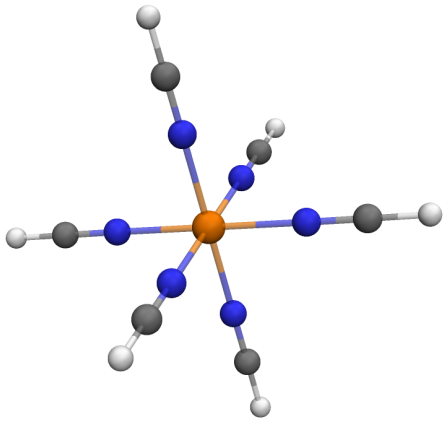

(b) $[Fe^{II}(NCH)_6]^{2+}$

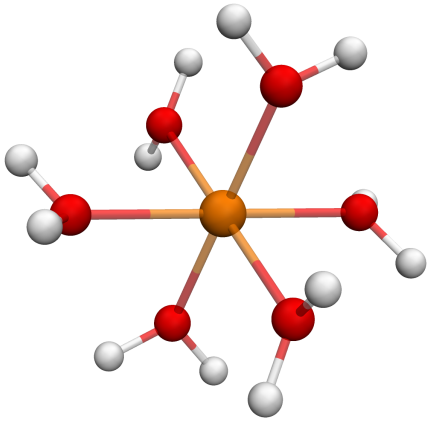

(c) $[Fe^{II}(H_2O)_6]^{2+}$

Figure 1.1: Examples of common small Fe^{II} complexes. Complexes (a) and (b) exhibit the SCO phenomenon. All structures are in the LS state. Fe atoms are orange, N blue, C grey, O red, H white. Visualized with PyMOL [27].

are carried out on both the target and a reference complex, and the resulting values can be discussed in terms of relative trends instead of absolute values. This approach gains viability the more closely related targets and references are to each other.

It is yet a matter of debate which theoretical approaches are most reliable for the simulation of the energetics of Fe(II) SCO complexes. The aforementioned comparison to benchmark data is hampered, since experimental measurements will always include some sort of environment effect [33] and fully converged electronic struc-

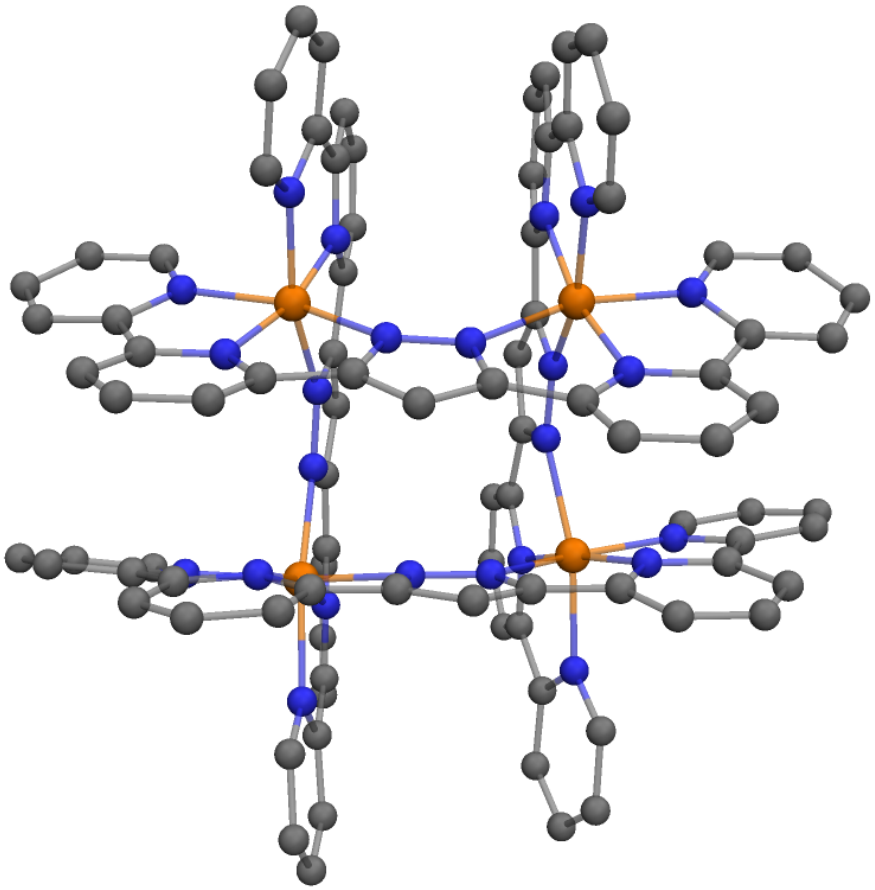

Figure 1.2: Molecular structure of the [2x2] Fe^{II} grid complex. Fe atoms are orange, C grey, N blue. H atoms are omitted for visual clarity. Visualized with PyMOL [27].

ture descriptions are unattainable for systems of any relevant size. Multireference approaches have been reported, including the use of RASSCF/RASPT2, CASSCF/CASPT2, NEVPT2 and SORCI [34–39]. Other studies rely on single-reference methods, such as coupled-cluster methods, though whether this is sufficient has ultimately not been completely determined. Divergence between CASPT2 values [35] and singlet-quintet gaps computed at the CCSD(T) level [40] can be interpreted as a failure in the single-reference description of coupled-cluster. As the weight of different configurations depends on the ligand in question, the validity of a coupled-cluster approach has to be assessed system by system. It is unfortunately unclear

which methods can be relied upon to produce the best results for those cases where multireference becomes a greater issue.

Triple excitations have a sizeable contribution when comparing different spin states, which can be observed by comparing CCSD and CCSD(T) values in several previous studies [41, 42]. Second-order perturbation theory, even in a multi-reference framework, might not reliably capture all of the dynamical correlation differences upon transition. A balance between the two types of correlation is crucial [43]. This issue also arises in regard to the selection of the electron space to be expanded in correlated calculations. Pierloot and coworkers highlighted the importance of electronic correlation effects from the (3s3p) electrons in 2017 [36]. The study also demonstrates the strong basis set dependence in spin gap energetics.

Chapter 2

Theoretical Background

2.1 Density Functional Theory

2.1.1 Introduction

Density functional theory (DFT) is a widely used computational method to investigate the electronic structure of chemical many-body systems. The theory holds that ground-state properties are uniquely determined by the electron density of a system, offering a cost-effective approach when compared to wave function-based methods. In 1998 Walter Kohn was awarded the Nobel Prize in chemistry "for his development of the density-functional theory" [44], a clear statement to the importance of this method.

The basic workings of DFT can be derived in the following manner, starting with the time-independent Schrödinger equation [45–47]

$$\hat{\mathrm{H}} \left|\Psi\right\rangle = E \left|\Psi\right\rangle \tag{2.1}$$

where $\hat{\mathrm{H}}$ is the Hamilton operator, Ψ the wave function and E the energy of the system. The Born-Oppenheimer approximation (BOA) [48,49] allows for separation of the Hamiltonian into nuclear and electronic terms, because of the large difference between their respective masses. For a system containing N nuclei and n electrons the Hamiltonian can be written as

$$\hat{\mathrm{H}} = \underbrace{-\frac{1}{2}\sum_{\mathrm{I}=1}^{N}\frac{1}{M_{\mathrm{I}}}\nabla_{\mathrm{I}}^2}_{\hat{\mathrm{T}}_{\mathrm{N}}} \underbrace{-\frac{1}{2}\sum_{i=1}^{n}\nabla_i^2}_{\hat{\mathrm{T}}_{\mathrm{e}}} \underbrace{-\sum_{i=1}^{n}\sum_{\mathrm{I}=1}^{N}\frac{Z_{\mathrm{I}}}{|\mathrm{R_I}-\mathrm{r}_i|}}_{\hat{\mathrm{V}}_{\mathrm{eN}}} \underbrace{+\sum_{i=1}^{n}\sum_{j>i}^{n}\frac{1}{|\mathrm{r}_i-\mathrm{r}_j|}}_{\hat{\mathrm{V}}_{\mathrm{ee}}} \underbrace{+\sum_{\mathrm{I}=1}^{N}\sum_{\mathrm{J}>\mathrm{I}}^{N}\frac{Z_{\mathrm{I}}Z_{\mathrm{J}}}{|\mathrm{R_I}-\mathrm{R_J}|}}_{\hat{\mathrm{V}}_{\mathrm{NN}}} \tag{2.2}$$

where M are nuclear masses, Z nuclear charges, R nuclear position vectors, r electron position vectors. $\hat{\mathrm{T}}_{\mathrm{N}}$ and $\hat{\mathrm{T}}_{\mathrm{e}}$ denote the kinetic energy operators for the nuclei and electrons, while $\hat{\mathrm{V}}_{\mathrm{eN}}$, $\hat{\mathrm{V}}_{\mathrm{ee}}$ and $\hat{\mathrm{V}}_{\mathrm{NN}}$ denote nucleus-electron, electron-electron, and nucleus-nucleus potential energy operators, respectively. In this "clamped nuclei" approximation the nuclei are considered to be stationary, resulting in a constant potential energy ($\hat{\mathrm{V}}_{\mathrm{NN}}$=const.) The electronic Hamiltonian can now be written as

$$\hat{\mathrm{H}}_{\mathrm{el}}(\mathrm{r}) = \hat{\mathrm{T}}_{\mathrm{e}}(\mathrm{r}) + \hat{\mathrm{V}}_{\mathrm{ee}}(\mathrm{r}) + \hat{\mathrm{V}}_{\mathrm{Ne}}(\mathrm{r}) + \hat{\mathrm{V}}_{\mathrm{NN}}\,. \tag{2.3}$$

By repeatedly solving the electronic Schrödinger equation for sets of different nuclear positions a potential energy surface (PES) $E_n(\mathrm{R})$ can be constructed, which describes the energy of the system as a function of the molecular structure.

The Hartree-Fock (HF) method [50, 51] is the simplest approach for obtaining a solution to the electronic Schrödinger equation. The wave functions are approximated by a single Slater determinant, constructed from the molecular orbitals. A set of N-coupled equations for the N spin orbitals can be derived, which yield the HF wave function and the energy of the system. For simple molecules, this energy amounts to about 99% of the total energy, with the remaining 1% referred to as the correlation energy. Recovering this 1%, or parts thereof, requires higher levels of theory. Some examples are discussed in the next sections.

Hohenberg-Kohn theorems

Pierre Hohenberg and Walter Kohn postulated two theorems regarding systems of electrons moving under the influence of an external potential, which are integral to density functional theory (DFT) [52]. The first, as alluded to in the beginning of this chapter, states that the electronic ground-state of a system is uniquely determined by the electron density. The second theorem states that the variational principle [53]

can be applied to the calculation of the ground state electron density. The variational principle establishes that the ground state energy E_{trial} calculated with a trial wave function Φ has to be greater than the true ground state energy E_0. Thus, E_0 can be found by minimizing the expectation value of the Hamiltonian through variation of the parameters of Φ:

$$E_{trial} = \langle \Phi | \hat{\mathrm{H}} | \Phi \rangle \geq E_0 \,. \tag{2.4}$$

Since the wave function is completely defined by the electron density, the principle applies to the calculation of the electron density as well. This reduces the computational effort significantly. Using ρ_0 for the ground state electron density, the ground state energy can now be calculated with

$$E_0[\rho_0] = \hat{\mathrm{T}}[\rho_0] + E_{\mathrm{Ne}}[\rho_0] + E_{\mathrm{ee}}[\rho_0] + \hat{\mathrm{V}}_{\mathrm{NN}} \,. \tag{2.5}$$

Kohn-Sham approach

Introduced by Walter Kohn and Lu Jeu Sham [54], the Kohn-Sham method simplifies the many-body problem of interacting electrons in a static external potential to a problem of non-interacting electrons moving in an effective potential. The nucleus-electron interaction $E_{\mathrm{Ne}}[\rho_0]$ and the classical part of the electron-electron interaction $\mathrm{J}_{\mathrm{ee}}[\rho_0]$ can be calculated exactly. The kinetic energy $T_S[\rho]$ is calculated from a non-interacting reference system with the same electron density, where the wave function can be represented as a Slater determinant [55] of orbitals. An effective potential is used to consider the indirect interaction of these Kohn-Sham orbitals. The unknown terms are combined into the exchange-correlation functional $E_{\mathrm{XC}}[\rho_0]$, accounting for both the quantum mechanical exchange of identical particles, and the effects of electron correlations due to the Coulomb repulsion between the electrons. In the Kohn-Sham approach the ground state energy can be calculated with

$$E_0[\rho_0] = \hat{\mathrm{T}}_s[\rho_0] + E_{\mathrm{Ne}}[\rho_0] + \mathrm{J}_{\mathrm{ee}}[\rho_0] + E_{\mathrm{XC}}[\rho_0] + \hat{\mathrm{V}}_{\mathrm{NN}} \,. \tag{2.6}$$

2.1.2 Exchange-correlation functionals

The exact terms for the exchange-correlation functional are unknown, except for select model systems like the free electron gas. Molecular properties can only be calculated in this manner by making approximations, leading to various levels of accuracy in the results. The different types of functionals can be classified according to their sophistication [56–58].

LDA

The simplest type of these approaches is the local density approximation (LDA), where $E_{\mathrm{XC}}[\rho_0]$ is approximated for each point in real space by the exchange-correlation energy of a homogeneous electron gas. This is an acceptable assumption for the field of solid state physics, but for chemical systems it leads to an overestimation of bond energies. The first LDA was already proposed by Kohn and Sham. Another example is the VWN functional [59].

GGA

The generalized gradient approximation (GGA) offers an improvement by taking into account both the local electron density and its gradient $\nabla\rho$. This offers a better description of the local variance of the electron density inherent to molecular systems. Functionals based on this approximation demand for comparatively little computational effort and offer good results, especially concerning structural parameters, but are less reliable for other properties. Examples for commonly used GGA type functionals are PBE [60] and BP86 [61, 62].

Meta-GGA

Meta-GGA type functionals are an extension of the GGA type, containing higher-order derivatives of the electron density. Nowadays this definition has shifted slightly to typically include a dependence on the kinetic energy density. Examples include TPSS [63] and M06-L [64].

Hybrid-GGA

Hybrid-GGA type functionals [65] replace a percentage of the GGA exchange energy with the exact HF exchange energy [50, 51], according to the general formula

$$E_{\mathrm{xc}} = E_{\mathrm{xc}}^{\mathrm{GGA}} + a\left(E_{\mathrm{x}}^{\mathrm{HF}} - E_{\mathrm{x}}^{\mathrm{GGA}}\right), \tag{2.7}$$

whereby a is the parameter governing the amount which is exchanged. This is considered an improvement because it alleviates the self-interaction error that GGA type functionals suffer from [66]. The GGA exchange energies are computed differently depending on the functional. For example, the PBE functional is used in the case of PBE0 [67, 68], the Slater-Dirac/B88 exchange energies in the case of B3LYP [69]). The amount of replaced exchange a is found to have a major impact on a variety of properties, indicating that it might be possible to adapt hybrid functionals to best represent a specific system. This is further explored in chapter 4. This type of functional is the currently dominant choice when more complex electronic configurations are of importance, for example in complexes containing transition metals [70, 71].

Range-separated hybrid-GGA

For range-separated hybrid GGA type functionals, the two-electron operator for the exchange is split into a short-range and a long-range term, according to the general formula [72, 73]

$$r_{12}^{-1} = \frac{1 - [\alpha + \beta\mathrm{erf}(\mu r_{12})]}{r_{12}} + \frac{\alpha + \beta\mathrm{erf}(\mu r_{12})}{r_{12}}, \tag{2.8}$$

whereby α, β and μ are adjustable parameters. The first term governs the short-range regime, the second term the long-range. At zero interelectronic distance the admixture of the HF exchange would be determined by α, while at larger distances it would be determined by $\alpha + \beta$. In short, the amount of HF exchange varies depending on the distance, which is especially useful in the case of metallic solid state systems, where pure hybrid-GGA functionals tend to overestimate exchange in the long-range regime [74]. Examples are CAM-B3LYP [73] and wB97 [75].

Local hybrid functionals

Local hybrid functionals are a recent class of functionals, using admixtures of exact exchange dependent on the real-space geometries [76–78]. Specifically the local hybrid functional PBE0r [79,80] is used extensively in this work, and will be discussed in the following.

The approach of the PBE0r functional is based on the idea of formulating the Fock term in a basis of local orbitals $|\chi_\alpha\rangle$ and implementing range separation by truncating the sum over four-center integrals, rather than dividing the Coulomb interaction into short- and long-range contributions. The local orbitals $|\chi_\alpha\rangle$ are divided into sets $\alpha \in \mathcal{C}_R$, which are centered at a specific atom identified by the index R. The orbital index α holds atomic site, angular momenta and spin indices as well as additional quantum numbers.

The exchange energy in the local approximation can be calculated with

$$E_x^{\mathrm{PBE0r}} = -\frac{1}{2}\sum_R \sum_{\alpha,\beta,\gamma,\delta\in\mathcal{C}_R} \langle\alpha\beta|\gamma\delta\rangle \rho^{(1)}_{\gamma\beta}\rho^{(1)}_{\delta,\alpha}\,, \tag{2.9}$$

whereby $\langle\alpha\beta|\gamma\delta\rangle$ are the 4-center, 2-electron integrals. The one-particle reduced density matrix can be calculated from the occupations f_n and Kohn-Sham wave functions $|\psi_n\rangle$

$$\rho^{(1)}(\alpha,\beta) \;=\; \sum_n \langle\pi_\alpha|\psi_n\rangle f_n \langle\psi_n|\pi_\beta\rangle\,, \tag{2.10}$$

as well as the local orbital projector functions $\langle\pi_\alpha|$. These projector functions obey the bi-orthogonality condition $\langle\pi_\alpha|\chi_\beta\rangle = \delta_{\alpha,\beta}$, meaning that the approximate sign becomes an identity if local orbitals span at least the same Hilbert space as the Kohn-Sham wave functions. Eq. 2.9 can be understood as an approximation of the exact exchange, since the four-center terms are limited to quadruples centered on the same atom. This breaks up the Coulomb interaction into atomic contributions. By dividing the hybrid terms into atomic contribution it allows to change the admixture of the HF exchange atom by atom. There are different approaches to finding the optimal parameterization [81–84], which will be discussed further from chapter 4 onward.

To avoid double counting of the exchange term, it is required to subtract the respective PBE exchange. This is achieved by dividing the Coulomb interaction into the contribution of individual atoms using cutoff functions $g_R(\vec{r})$. Specifically, the electron density is partitioned into local contributions

$$n_R(\vec{r}) = \sum_{\alpha,\beta\in\mathcal{C}_R} \sum_{\sigma} \langle \vec{r},\sigma|\chi_\alpha\rangle \rho^{(1)}_{\alpha,\beta} \langle\chi_\beta|\vec{r},\sigma\rangle \tag{2.11}$$

and the cutoff functions defined as $g_R(\vec{r}) = n_R(\vec{r}) / \sum_{R'} n_{R'}(\vec{r})$.

The double counting correction is simplified by evaluating both cutoff functions at the same position $\vec{r}$. This results in the simple expression

$$E^{\text{PBE0r}}_{\text{DC,approx}} = -\sum_R \int d^3r \, \frac{n_R(\vec{r})}{n(\vec{r})} n_R(\vec{r}) \epsilon_{xc}(\vec{r}) \, . \tag{2.12}$$

Within the Car-Parinello Projector Augmented Wave (CP-PAW) code [85, 86], the density $n(\vec{r})$ is expressed in terms of partial wave expansion, while $n_R(\vec{r})$ is represented by local orbitals.

Range separation is achieved by disregarding offsite four-center integrals from the exchange and the corresponding double counting term. This provides a reasonable description of the atomic physics, specifically the atomic self-interaction correction. This makes PBE0r an appropriate functional for the description of transition metal compounds with partially filled d-shells.

2.2 Coupled-cluster theory

Coupled-cluster theory [87, 88] offers an *ab initio* size-consistent and non-variational wave function approach for the computation of electron-electron correlation energy. It is asymptotically converging on the exact results, though this accuracy carries a hefty computational cost when compared to DFT.

The wave function is constructed with an exponential *ansatz* in the following form

$$|\Psi_{\text{CC}}\rangle = \mathrm{e}^{\hat{\mathrm{T}}} |\Phi_0\rangle \ , \tag{2.13}$$

whereby $|\Phi_0\rangle$ is the reference wave function, typically a single Slater determinant constructed from HF molecular orbitals. $\hat{\mathrm{T}}$ is the cluster operator, which yields a linear combination of excited determinants when acting upon $|\Phi_0\rangle$. It is constructed in the following form

$$\hat{\mathrm{T}} = \hat{\mathrm{T}}_1 + \hat{\mathrm{T}}_2 + \hat{\mathrm{T}}_3 + \ldots , \tag{2.14}$$

whereby $\hat{\mathrm{T}}_1$ is the operator for all single excitations, $\hat{\mathrm{T}}_2$ the operator for all double excitations, and so forth. $\hat{\mathrm{T}}_n$ acting upon $|\Phi_0\rangle$ generates excited Slater determinants in the same order

$$\hat{\mathrm{T}}_1 |\Phi_0\rangle = \sum_{i}^{occ} \sum_{a}^{vir} t_i^a \Phi_i^a , \tag{2.15}$$

$$\hat{\mathrm{T}}_2 |\Phi_0\rangle = \sum_{i<j}^{occ} \sum_{a<b}^{vir} t_{ij}^{ab} \Phi_{ij}^{ab} , \tag{2.16}$$

whereby t denotes the expansion coefficients, also called amplitudes. The exponential $\mathrm{e}^{\hat{\mathrm{T}}}$ of equation 2.13 can also be written in the form of a Taylor expansion

$$\mathrm{e}^{\hat{\mathrm{T}}} = 1 + \hat{\mathrm{T}} + \frac{\hat{\mathrm{T}}^2}{2} + \frac{\hat{\mathrm{T}}^3}{6} + \ldots = \sum_{k=0} \frac{\hat{\mathrm{T}}^k}{k!} , \tag{2.17}$$

demonstrating the distinct advantage that upon truncation of the cluster operator, the wave function still contains contributions from higher order substitutions. Using $\hat{\mathrm{T}} = \hat{\mathrm{T}}_2$ as an example, the Taylor expansion contains the term $\frac{1}{2}\hat{\mathrm{T}}_2^2$, yielding a fourfold excitation $\left|\Phi_{ijkl}^{abcd}\right\rangle$ when acting upon $|\Phi_0\rangle$. Using no truncation would mean that the order of the cluster operator is equal to the total number of electrons in the system, and the calculation would converge upon the full configuration interaction (FCI) limit. In practice, some truncation is necessary, since considering the whole number of excitations is computationally not feasible, except for systems with a very small number of electrons, using a small basis set. The most common approach only includes single ("S") and double ("D") excitations ($\hat{\mathrm{T}} = \hat{\mathrm{T}}_1 + \hat{\mathrm{T}}_2$), consequently denoted as CCSD [89, 90]. Adding triple ("T") excitations ($\hat{\mathrm{T}}_3$) yields CCSDT

[91,92], though a perturbative treatment of the triples CCSD(T) [93] is a more cost effective approach, while yielding excellent results for a wide range of systems. For these reasons CCSD(T) has become known as the "gold standard" of computational chemistry [94].

2.3 Nudged elastic band method

The nudged elastic band (NEB) method [95–97] can be used to find a minimum energy path (MEP) on a PES, connecting a given reactant and product state. This can be utilized to determine the transition states of reactions and thereby gain an estimate of the activation energies.

The method generates an initial path by creating a string of discrete intermediate structures, referred to as "images". This can be achieved by simple linear interpolation of the Cartesian coordinates, though more advanced methods exist [98, 99]. The number of these images can be adapted according to the complexity of the MEP. During the NEB calculation the images are iteratively optimized toward the MEP using the atomic force component perpendicular to the current path, while the reactant and product states remain fixed. Virtual spring forces between neighbouring images are included to ensure roughly equal spacing along the path, typically in the range of of 0.01-1.0 Eh/Bohr^2. These can also be energy-weighted, in order to increase the density of images in the vicinity of the barrier [100]. A maximum along the MEP, corresponding to a first order saddle point on the PES, signifies the transition state of the reaction. It is exceedingly unlikely to generate an image exactly at the maximum. Rather, the highest energy image can be converted to a "climbing image", which is pushed uphill in energy along the tangent to the path while relaxing downhill in orthogonal directions. The spring forces are disregarded for this image. In this manner the energy is minimized in respect to all degrees of freedom other than the one degree of freedom corresponding to the direction of the tangent, so that the image converges to the maximum of the MEP, i.e. the transition state. To ascertain the convergence a frequency calculation can be employed. Since the transition state is located at a first order saddle point of the PES, the structure should exhibit exactly one imaginary frequency, also corresponding to the atomic motion relevant to the reaction.

2.4 Molecular dynamics simulations

Treating the movement of the nuclei classically, Newton's equations of motion can be used to simulate the molecular dynamics (MD) of a system [101, 102], with

$$\ddot{x}_N(t) = \frac{F_N(x(t))}{m_N}\,, \tag{2.18}$$

whereby $\ddot{x}$ denotes the acceleration and m the mass of nucleus N, while F is the force acting upon it at time t. As the force is determined by the negative derivative of the PES with respect to the position $x_N(t)$, this is a coupled system of N differential equations. Solving this system analytically is not feasible for all but the simplest of systems. Instead numerical integration methods are applied, based on approximating the movement by taking time steps of finite length. Three common examples for these methods are the Verlet [103], velocity Verlet [104] and the leapfrog algorithm [105].

For the propagation of positions x(t) and velocities v(t), the velocity Verlet algorithm reads

$$x_i(t+\Delta t) = x_i(t) + v_i(t)\Delta t + \frac{F_i(t)}{2m_i}\Delta t^2\,, \tag{2.19}$$

$$v_i(t+\Delta t) = v_i(t) + \frac{F_i(t) + F_i(t+\Delta t)}{2m_i}\Delta t\,, \tag{2.20}$$

with Δt as the length of the timestep. Choosing a suitable Δt is crucial, since the computational cost decreases linearly with the size of the step. On the other hand, atomic motions such as the stretching vibration of hydrogen bonds (on a femtosecond timescale) can be lost when choosing too large a step. The initial atomic structure is given by the system, while initial velocity distributions can be obtained from a Maxwell-Boltzmann distribution, for example.

Following these equations the system would simulate the microcanonical NVE ensemble, with constant particle number N, volume V, and total energy E. The temperature T would deviate from its initial value, since some amount of the initial kinetic

energy will be exchanged with potential energy contributions, for example bond stretching. This runs counter to experimental conditions, which are often maintained at a constant temperature. To simulate the corresponding NVT ensemble, it is necessary to add a temperature control, referred to as a thermostat [106]. Common examples are the Andersen [107], Berendsen [108], and Nose-Hoover [109–111] thermostat.

2.5 Bayesian optimization

Moving away from atomistic simulation methods, the Bayesian optimization (BO) method is a general data analysis tool applied in this work. The BO machine learning tool is frequently used for optimizing objective functions with long evaluation times. The objective function f is considered a *derivative-free* function, signifying that the function can only yield $f(x)$, not any of the derivatives. It is further assumed that f is a continuous function and that it lacks any special structures, like concavities or linearities. In general terms, the Gaussian process regression (GPR) technique is used after the evaluation of f to quantify the uncertainty of the sampled space. This information is then used by an acquisition function to decide on the next point to be sampled. This process can be repeated as often as needed, leading to the optimization of the objective function. The following describes the two main components of the BO technique, the GPR and the acquisition function, in further detail [112, 113].

Gaussian process regression

Firstly the objective function f is evaluated at a finite collection of points $x_1, x_2, ..., x_k \in \mathbb{R}^d$, with d as the number of dimensions to the domain [114]. The resulting values can be collected into a vector $[f(x_1), f(x_2), ...f(x_k)]$. It is assumed that this vector is drawn at random by a probability distribution prior to the GPR. By evaluating a *mean function* μ_0 at each x_i, a mean vector is constructed. For each pair of points x_i, x_j a *covariance function* or *kernel* Σ_0 is evaluated, yielding a covariance matrix. From this, a normal probability distribution can be computed with

$$f(x_{1:k}) \sim \text{Normal}(\mu_0(x_{1:k}), \Sigma_0(x_{1:k}, x_{1:k}))\,, \tag{2.21}$$

Using Bayes' Theorem [115], a *posterior probability distribution* can be obtained, offering a numerical value for the uncertainty of each point. If the prior distribution is acquired using n distributions, the value of f at a new point x can be inferred by calculating the conditional distribution:

$$f(x)|f(x_{1:k}) \sim \text{Normal}(\mu_n(x), \sigma_n^2(x))\,. \tag{2.22}$$

In this, $\mu_n(x)$ is the *posterior mean*, an average between prior mean $\mu_0(x)$ and an estimate based on $f(x_{1:n})$, weighted based on the kernel. It is obtained with

$$\mu_n(x) = \Sigma_0(x, x_{1:n})\Sigma_0(x_{1:n}, x_{1:n})^{-1}(f(x_{1:n}) - \mu_0(x_{1:n})) + \mu_0(x)\,. \tag{2.23}$$

$\sigma_n^2(x)$ is called the *posterior variance* and offers a measure of the uncertainty for the calculated prediction. It is obtained with

$$\sigma_n^2(x) = \Sigma_0(x, x) - \Sigma_0(x, x_{1:n})\Sigma(x_{1:n}, x_{1:n})^{-1}\Sigma(x_{1:n}, x)\,. \tag{2.24}$$

Kernels are required to be positive semi-definite functions. They typically correlate points more strongly the closer they are in the input space. Two common examples are described in the following.

The *Gaussian* kernel (also called *power exponential*) is expressed as

$$\Sigma_0(x, x') = \alpha_0 \exp(-||x - x'||^2)\,, \tag{2.25}$$

whereby $||x-x'||^2 = \sum_{i=1}^{d} \alpha_i(x_i - x_i')^2$ and $\alpha_{0:d}$ are parameters of the kernel. Varying α influences how quickly $f(x)$ changes with x. The *Matérn* kernel is expressed as

$$\Sigma_0(x, x') = \alpha_0 \frac{2^{1-\nu}}{\Gamma(\nu)} (\sqrt{2\nu}||x - x'||)^\nu K_\nu(\sqrt{2\nu}||x - x'||)\,, \tag{2.26}$$

whereby K_ν is the modified Bessel function. The mean function is commonly chosen to be constant, with $\mu_0(x) = \mu$.

Acquisition function

The acquisition function is employed to determine the next point to be sampled, using the posterior probability distribution from the GPR. Most commonly used is the *expected improvement* function [116], which will be described in the following. It proposes that the best next point to be sampled is the one where the expected improvement to the optimization is highest. The function is defined as

$$\mathrm{EI}_n(x) := E_n[[f(x) - f_n^*]^+] \,, \tag{2.27}$$

whereby f_n^* is the point with the best value observed so far. The improvement to this value then is either given by $f(x) - f_n^*$ or set to 0, should it be negative. By maximizing the expected improvement function on the posterior probability distribution, the next point to be sampled is determined [117]. This is solved analytically by employing the normal density function, resulting in

$$\mathrm{EI}_n(x) = \begin{cases} (\mu_n(x) - f_n^*)\Phi(Z) - \sigma_n(x)\phi(Z) & \text{if } \sigma_n(x) > 0 \\ 0 & \text{if } \sigma_n(x) = 0 \,, \end{cases} \tag{2.28}$$

with $Z = \frac{\mu_n(x) - f_n^*}{\sigma_n(x)}$, whereby ϕ and Φ describe the cumulative density and the probability density functions of the normal probability distributions [118].

f is evaluated at the point of highest improvement and the result included in the next iteration of the posterior probability distribution. This in turn can be used again by the acquisition function. This optimization loop finishes upon reaching either a convergence criterion or a maximum number of iterations set beforehand.

Chapter 3

Oxidative H_2O addition to a bimetallic Ni^{II} complex

The findings presented in this chapter and appendix A are currently being prepared for journal publication. In part they have been published in the PhD thesis of Roland Alexander Schulz as well [119]. The content of this chapter and the publication will carry similarities to both works, even though no further explicit citation is given.
I want to explicitly thank Dr. Roland Alexander Schulz and Prof. Dr. Franc Meyer, who were responsible for the experimental part of this publication, as discussed in the introduction of this chapter.

3.1 Introduction

As mentioned in the introduction 1, complexes that can catalyze the splitting of water are of great interest. Many of the complexes currently used in large-scale applications are based on late transition metal complexes [120], making them in general more costly and difficult to handle. Few first-row transition metal complexes capable of activating water are known, though in recent years progress has been made in various ways. Homolytic activation of water has been reported with nickel complexes, where the H-atom equivalent is stored in noninnocent ligand scaffolds [121,122]. Other approaches employ spectator ligands, and the water splitting results in M-OH and M-H bonds forming, with either mono- or bimetallic complexes [123].

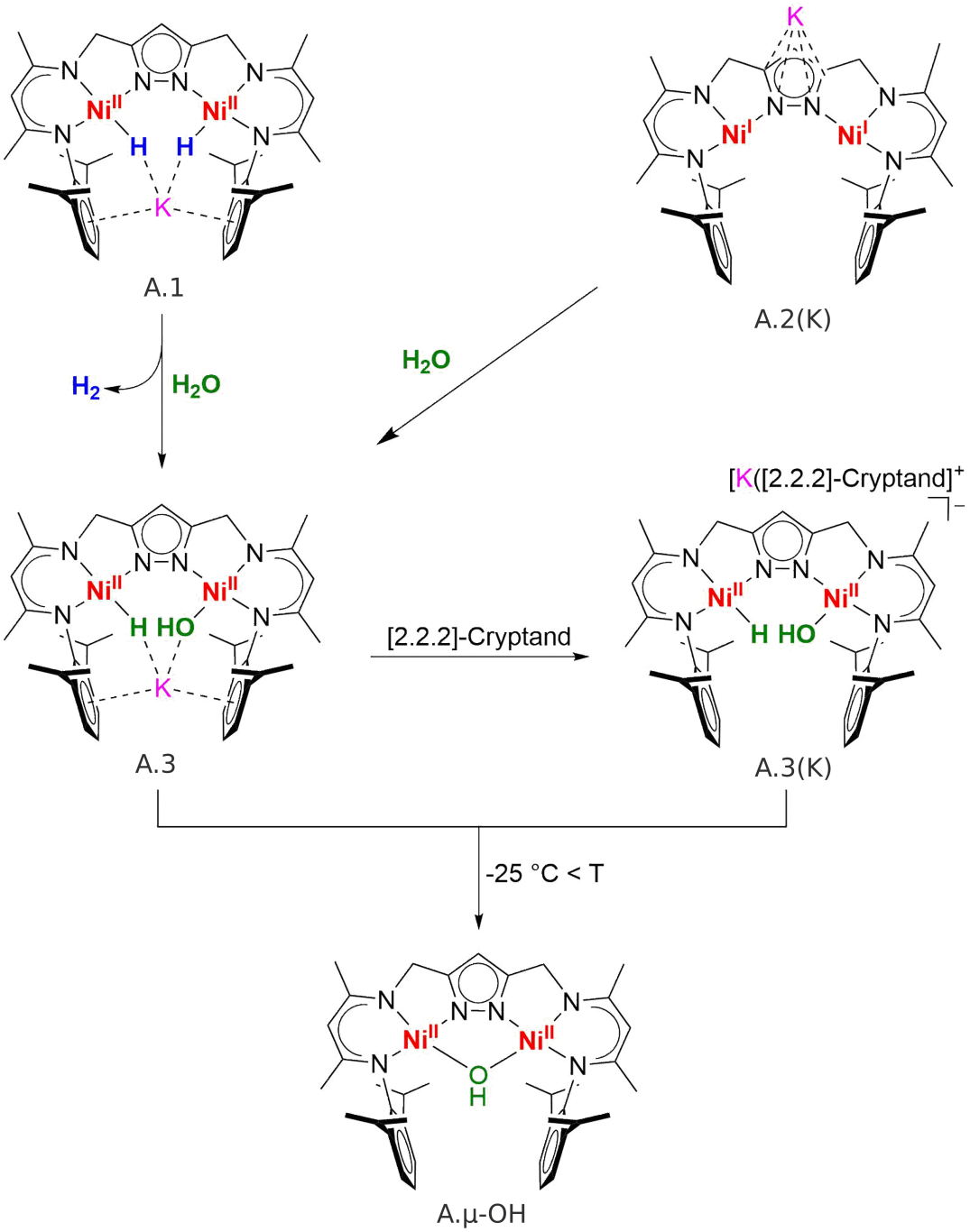

Figure 3.1: Reaction scheme of the oxidative water addition to a bimetallic Ni^{II} complex, including related reactions.

Bimetallic $Ni^{I/II}$ complexes capable of activating a variety of molecules have recently been reported and characterized extensively by Meyer and coworkers [124,125]. As is shown in figure 3.1, the complex is composed of a pyrazolate-bridged compartmental ligand with β-diketiminato (nacnac) chelate arms, providing highly preorganized two pincer-type binding pockets, containing the Ni centers.

Roland Schulz was able to demonstrate the oxidative addition of water to the dinickel complex **A.1**, resulting in the separation into hydride and hydroxyl groups connected to the Ni centers, **A.3**. The release of H_2 forming **A.1** has also been previously demonstrated [125]. This results in **A.2(K)**, which can perform the addition as well. For **A.3** the potassium cation can be sequestered by the addition of a crone ether, resulting in complex **A.3(K)**. Both **A.3** and **A.3(K)** decompose to **A.μ-OH** when heated above -25 C°.

The role of DFT in this project was to elucidate the exact manner of the oxidative H_2O addition, as well as the characterization of the products from this reaction, **A.3** and **A.3(K)**.

3.2 DFT characterization

The ORCA 4.2.1 program package [126, 127] was used for all calculations in this section. Default settings were applied, unless otherwise noted.

3.2.1 Structure optimizations

Crystallographic structure data of complex **A.2(K)** was obtained from [125]. This data was translated into the XYZ format, which could then be used for the calculations in this section.

The geometry optimizations were performed using the BP86 functional [61,62] with the def2-SVP basis set [128], including def2/J auxiliary basis set [129] and Grimme's D3 dispersion correction with Becke-Johnson damping [130, 131].
The BP86 functional is known to yield reasonable structures when used for the geometry optimization of transition metal complexes [132]. The double-zeta basis set def2-SVP is sufficient as well. The use of higher order basis sets has a negligible effect on the structure, though energies and properties should be computed at a higher level of theory [133, 134].

After successfully optimizing the structure of complex **A.2(K)**, structures for **A.1, A.2, A.3, A.3(K)** and **A.μ-OH** were derived by initially adding the respective atoms in the approximate positions and optimizing again at the same level of theory as described above. The broken state symmetry formalism was used for the optimization of the structures of complexes **A.2(K)** and **A.2**, to account for the lone electron present at both Ni centers. The optimized structures of complexes **A.1, A.2(K), A.2, A.3, A.3(K)** and **A.μ-OH** are shown in Figure 3.2. The structural data of complex **A.2(K)** and the input file for the geometry optimization is shown in appendix A.

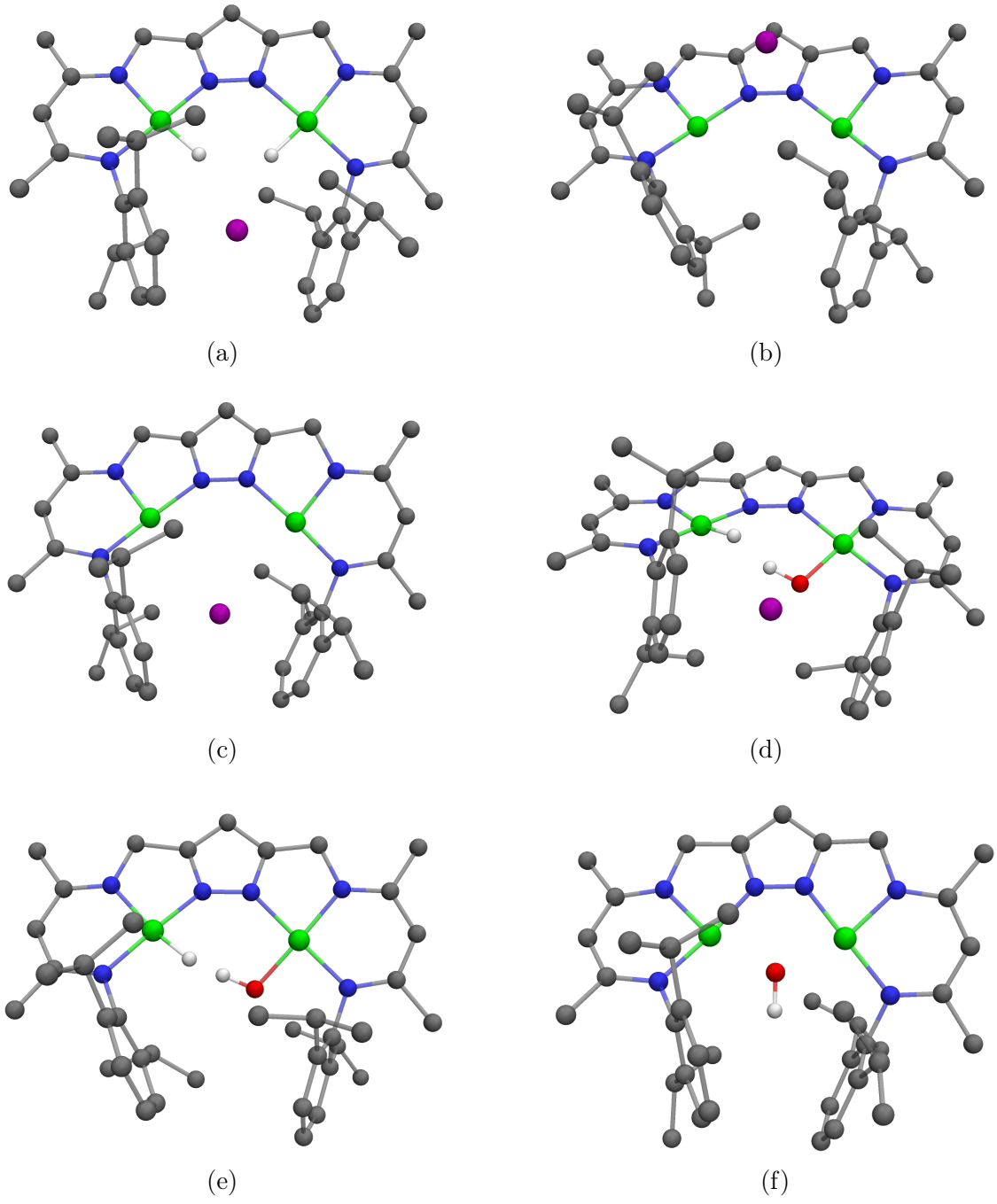

Figure 3.2: DFT optimized molecular structure of (a) **A.1**, (b) **A.2(K)**, (c) **A.2**, (d) **A.3**, (e) **A.3(K)** and (f) **A.μ-OH**. Ni atoms are green, C grey, H white, K purple, N blue, O red. Most H atoms are omitted for clarity. Visualized with PyMOL [27].

3.2.2 Reaction pathway

The release of H_2 from complex **A.1** has already been well described [125], leading to complex **A.2(K)** or **A.2**, respectively. The most important reaction to understand then is the addition of H_2O to these complexes. The full description of a reaction pathway requires the reactants, products and the transition state, according to transition state theory [135]. The NEB method can be a useful approach in the search for transition states, provided that there are reasonably good guesses for the structures of reactants and products. The method is discussed in further detail in 2.3.

Complex **A.3** is already a reasonable structure for the product of the NEB. To search for a reasonable structure for the reactant, H_2O molecules were placed in multiple positions around complex **A.2** and the structure optimized at the same level of theory as described in 3.2.1. Some of the local minima found in this manner are clearly unsuitable as the reactant structure for the NEB, since the H_2O has been moved to other areas of the complex (see figure 3.3a), or away from the complex altogether. However, for one of the local minima, **A.4**, the H_2O has been positioned just slightly above the cleft between the two Ni centers (see figure 3.3b). Manually moving the H_2O further into the cleft before optimizing actually results in complex **A.3**, with the H_2O split into H and HO, connected to the two Ni centers. For these reasons complex **A.4** has been adopted as a reasonable structure for the reactant of the NEB.

The NEB method was employed using BP86-D3/def2-SVP and 8 virtual images, which converged upon a MEP and a climbing image, providing a good estimate for the transition state. This was further improved by using the transition state optimization feature implemented in ORCA, while calculating the exact Hessian. The resulting structure for the transition state **A.TS1** is shown in figure 3.4.

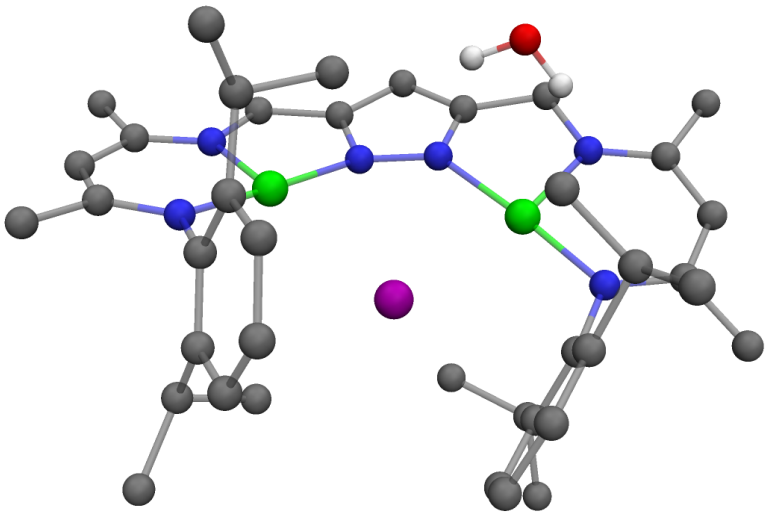

(a)

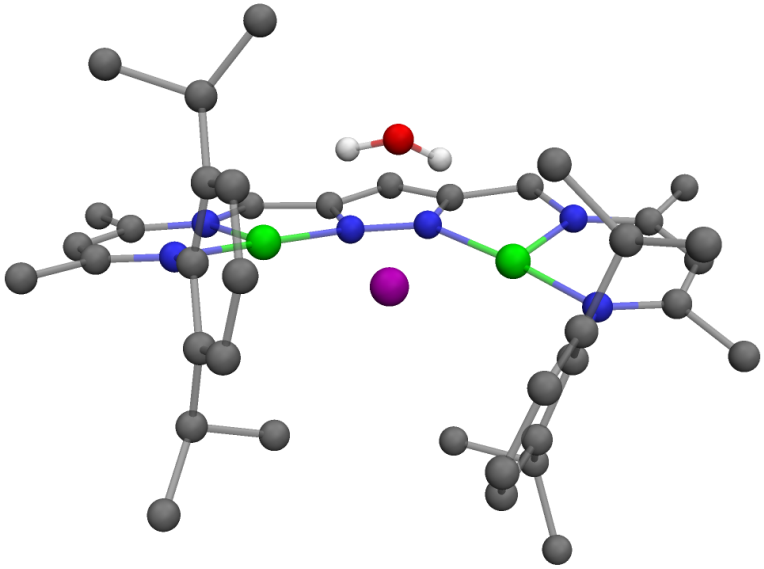

(b)

Figure 3.3: Local minimum structures after DFT optimization of H_2O placed in the vicinity of complex **A.2(K)**. For (a) the H_2O has been moved far away from the active site, while in (b) the H_2O has remained quite close, making it a reasonable structure for the NEB reactant, i.e. **A.4**. Ni atoms are green, C grey, H white, K purple, N blue, O red. Most H atoms are omitted for clarity. Visualized with PyMOL [27].

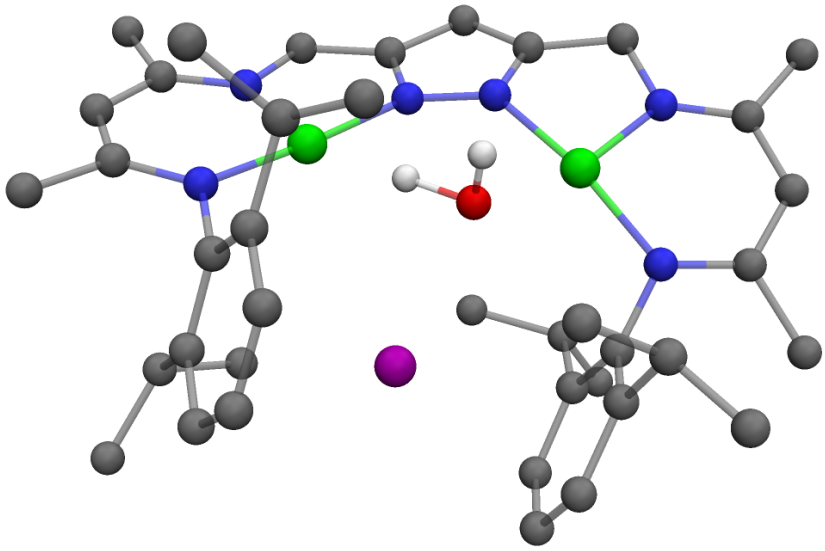

Figure 3.4: Molecular structure of the transition state **A.TS1** for the concerted pathway for the oxidative H_2O addition. Ni atoms are green, C grey, H white, K purple, N blue, O red. Most H atoms are omitted for clarity. Visualized with PyMOL [27].

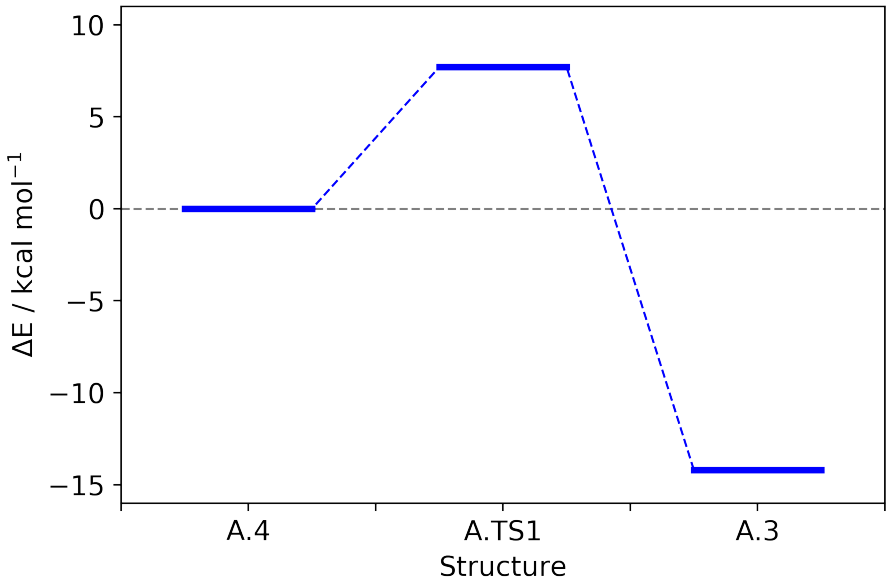

Figure 3.5: Relative electronic energies for the reaction pathway of the concerted oxidative H_2O addition to **A.4**. All energy values are relative to that of reactant **A.4**.

Examining the eigenmodes of **A.TS1** yields exactly one imaginary frequency, which is a crucial characteristic for the recognition of a transition state. Furthermore, the atomic motion connected to this frequency, a stretching of the H-OH bond, is exactly what would be expected for this transition state. For these reasons this has been accepted as a possible reaction path. Figure 3.5 shows the relative energies for this concerted pathway for the oxidative H_2O addition. The structural data for **A.3**, **A.4** and **A.TS1**, as well as the input files related to the search for the transition state can be found in appendix A.

A.5 was another local minima found in the previous step, as shown in figure 3.6. The presence of this minima alluded to the potential existence of another pathway with two distinct steps. The first step of this second pathway would be the approach of the H_2O into the cleft of **A.4**, resulting in **A.5** as an intermediate. In the second step the H_2O would be split, resulting in **A.3** as a final product. Figure 3.7 shows a diagram of this hypothetical pathway. However, **A.5** is already 9.8 kcal/mol higher in energy than **A.4**., making it similar in energy to **A.TS1** of the concerted pathway, as can be seen in the next section 3.2.3. The respective transition states of this stepwise pathway would likewise be even higher in energy than **A.TS1**. It has to be concluded that this process would not be competitive in respect to the concerted pathway, even if theoretically possible. For this reason it was not investigated further.

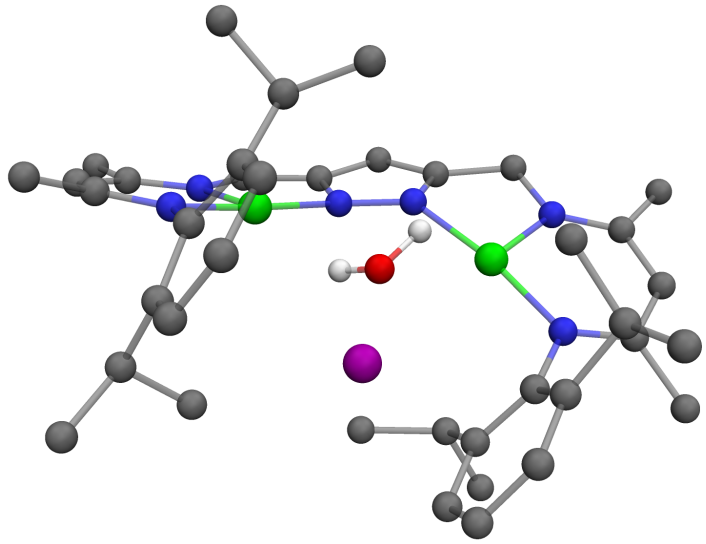

Figure 3.6: Molecular structure of a hypothetical intermediate step **A.5** for the stepwise pathway for the oxidative H_2O addition. Ni atoms are green, C grey, H white, K purple, N blue, O red. Most H atoms are omitted for clarity. Visualized with PyMOL [27].

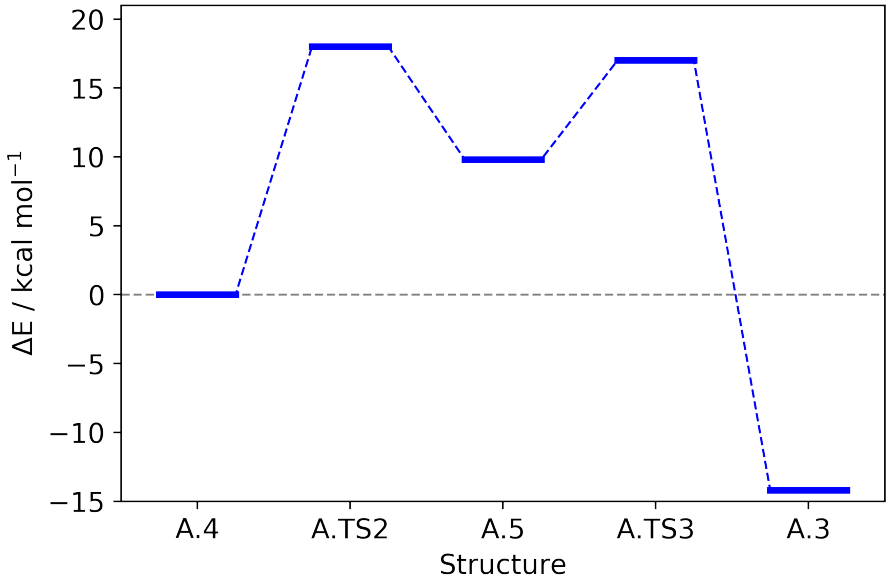

Figure 3.7: Relative electronic energies for a hypothetical *stepwise* addition of H_2O to **A.4**. Energies of **A.4**, **A.3** and **A.5** calculated with BP86-D3/def2-SVP. **A.TS2** and **A.TS3** not calculated.

3.2.3 Exact energies

To improve the accuracy of the proposed reaction path, the electronic energies of **A.4**, **A.3** and **A.TS1** were recalculated using the def2-TZVP basis set [128] and the conductor-like polarizable continuum model (CPCM) solvation model with default settings for THF [136].

Furthermore, frequency calculations (using BP86-D3/def2-SVP) were carried out, yielding an approximation for the zero-point vibrational energy (ZPVE) of each complex. Adding the ZPVE to the electronic energies results in an approximate Gibbs free energy (G^0). The resulting relative energies for **A.4**, **A.3** and **A.TS1** are shown in figure 3.8, with a barrier height of kcal/mol.

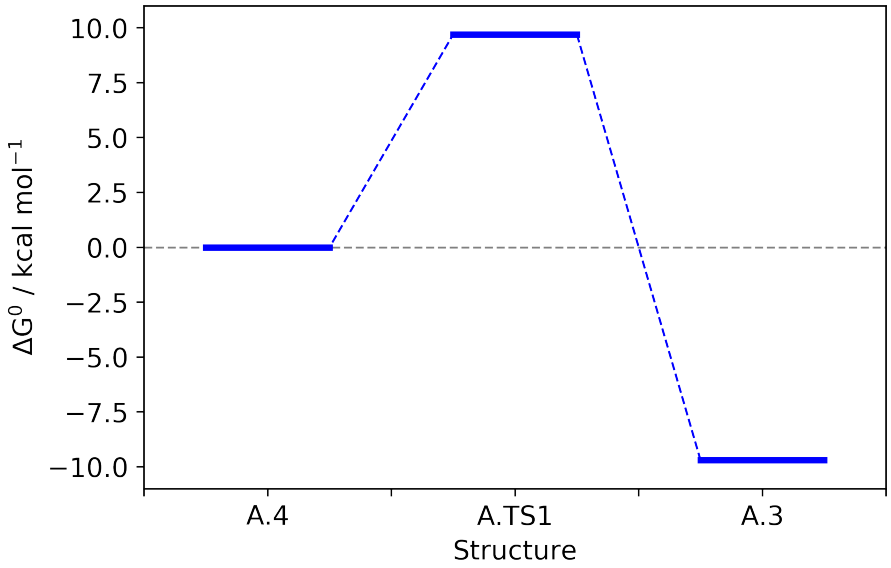

Figure 3.8: Relative energies for the reaction pathway of the oxidative H_2O addition to **A.4**, with approximations for G^0. All energy values are relative to that of the reactant **A.4**.

The Eyring equation 3.1 can be used to calculate the rate of a chemical reaction k, with k_B being the Boltzmann constant, T the Temperature, h the Planck constant, ΔG^* the barrier height and R the ideal gas constant [137–139].

$$k = \frac{k_B T}{h} e^{-\frac{\Delta G^*}{RT}} \tag{3.1}$$

The half-life of a reaction can then be calculated with $t_{1/2} = \frac{ln2}{k}$. For a barrier of 9.7 kcal/mol at a temperature of 213 K (the experimental conditions) the half-life would be 2.8 ms. This is in good agreement to the experimental observation of the reaction occurring almost instantaneously [119].

3.2.4 Further characterization of A.3

Especially of interest was the interaction between the hydroxyl proton and the hydride connected to the Ni center in **A.3**, so an effort was made to further characterize this complex.

Molecular Dynamics

To investigate the evolution of the proton-hydride interaction over time, multiple MD simulations were performed, each running for 5000 timesteps with intervals of 1.0 fs. The Berendsen virtual thermostat was set to 250 K, in accordance with the experimental conditions. For this large amount of calculations the PBEh-3c functional [140] was used instead of BP86-D3/def2-SVP. PBEh-3c is significantly less computationally intensive while still producing reasonably accurate structures of transition metal complexes [141]. These MD simulations were performed for **A.3**, **A.3(K)**, and for an **A.3 with an additional explicit THF molecule**, representing the solvent, the structure of which is shown in figure 3.9. Figure 3.10 shows the evolution of the proton-hydride distance from the simulations. An example for the input file for the MD simulation can be found in appendix A.

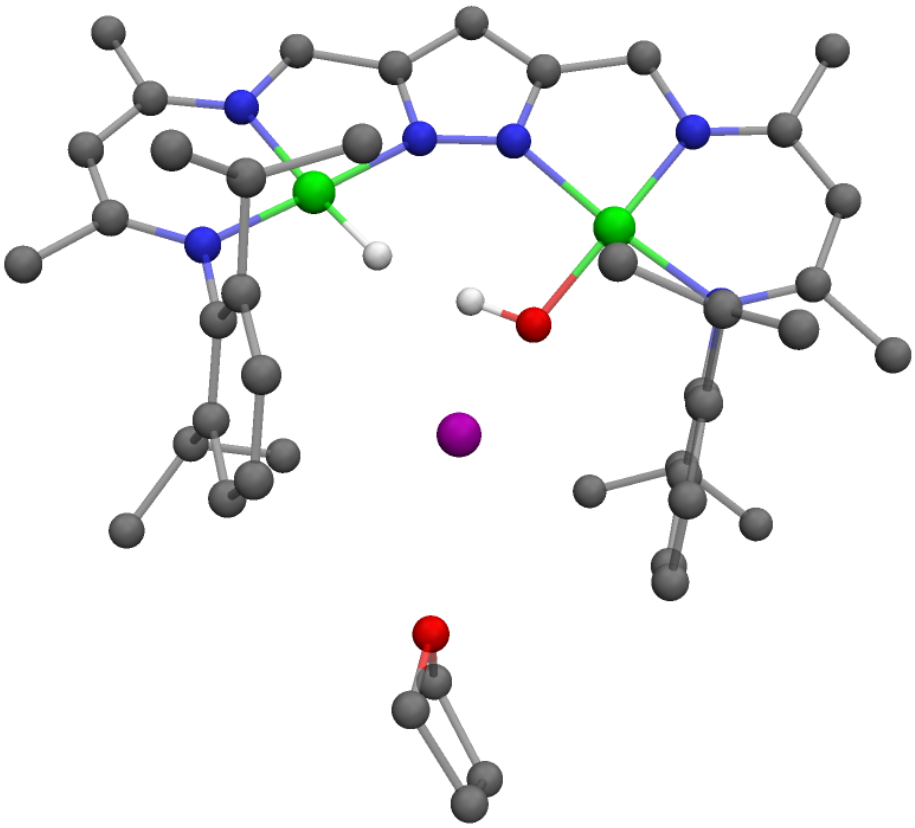

Figure 3.9: Molecular structure of **A.3** with an additional explicit THF molecule, representing the solvent. Ni atoms are green, C grey, H white, K purple, N blue, O red. Most H atoms are omitted for clarity. Visualized with PyMOL [27].

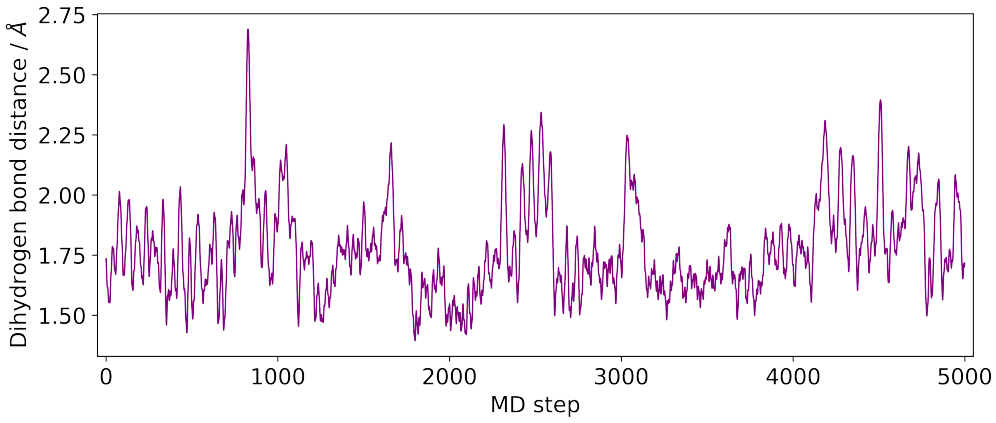

(a)

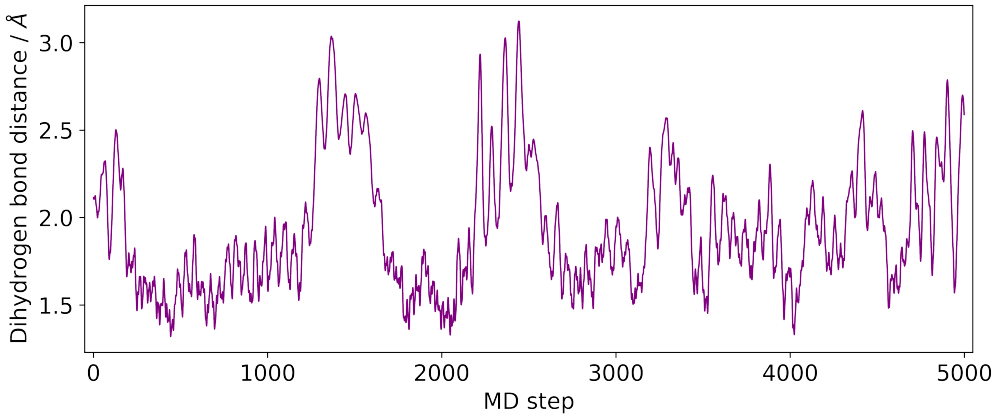

(b)

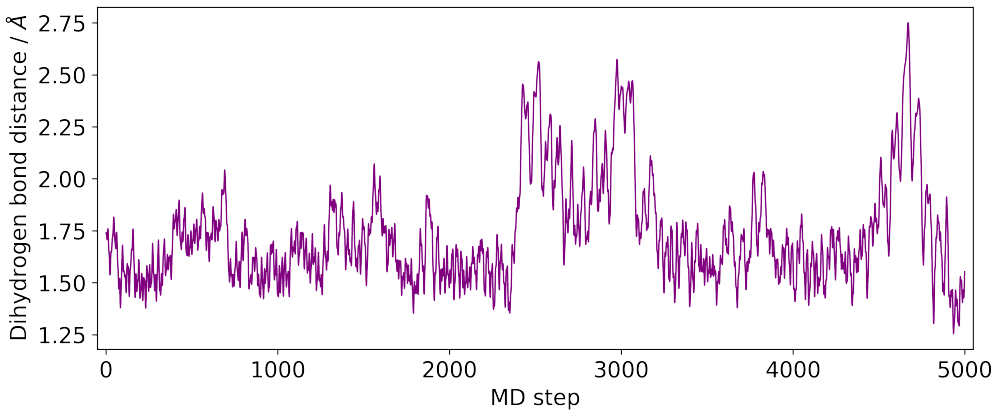

(c)

Figure 3.10: Simulated evolution of the dihydrogen bond distance in (a) **A.3**, (b) **A.3(K)** and (c) **A.3** with explicit THF. Each timestep represents the evolution of the system by 1.0 fs.

Torsional barrier

To determine the strength of the intramolecular proton-hydride interaction a rotation of the hydroxyl group was simulated. Multiple "relaxed scans" were performed (using BP86-D3/def2-SVP), meaning that certain aspects of the structure are set to specific values, while the rest of the structure is allowed to relax during optimization. In this case it pertains to the H-O-Ni-N dihedral angle, which is being changed by 30 degrees for every step, mimicking a rotation. This scan was first performed for complex **A.3**. Then the potassium cation was removed from the structure and the energies recalculated, approximating the torsion for complex **A.3(K)** as well. The resulting energy profile is shown in figure 3.11.

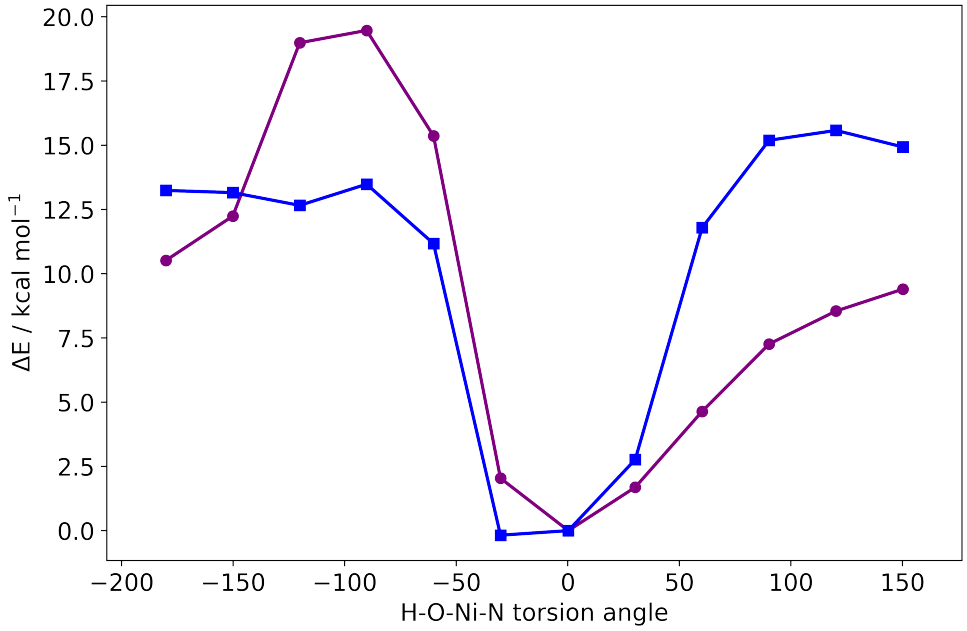

Figure 3.11: Torsional energy profile of **A.3** (in purple) and **A.3(K)** (in red). All energies are relative to the structure at 0° of torsion, with the hydrogen atoms facing each other.

For **A.3** it is evident that 0°, with the two hydrogen atoms facing each other, is indeed the most stable orientation. For **A.3(K)** the most stable configuration would probably be between 0° and -30°, in a region not directly covered by the scan. The differences in energy between this minimum and the height of the torsional barrier are 20 and 14 kcal/mol, respectively.

However, it has to be noted that this rotation is also inhibited by the repulsion between the hydroxyl group and the aryl rings. In an effort to differentiate between proton-hydride interaction and steric hinderances another torsional scan was performed with a truncated structure, where the aryl rings of **A.3** have been exchanged with a single H atom. It has to be noted that for this structure the K^+ has to be fixed in position, lest it is moved away during the relaxation. The rest of the structure was still allowed to relax as described previously. The resulting energy profile is shown in figure 3.12, with a maximum torsional barrier of 14 kcal/mol.

Taking both effects into account allows for an estimation of the strength of the intramolecular proton-hydride interaction of around 10 kcal/mol, which is well in line with previously reported values for dihydrogen bonds [142].

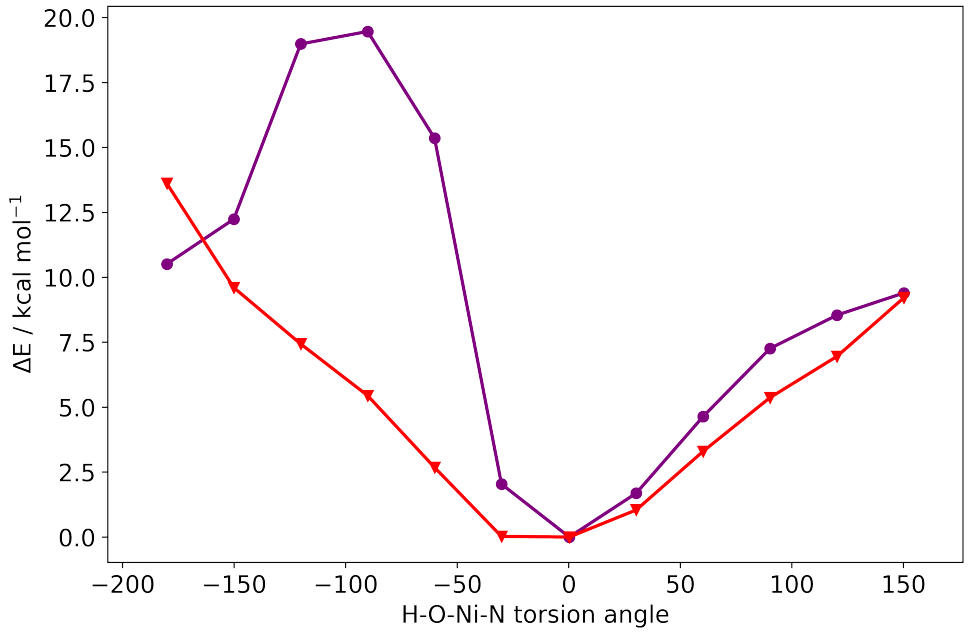

Figure 3.12: Torsional energy profile of both **A.3** (in purple) and the truncated **A.3** (in red), with aryl rings replaced by H atoms. All energies are relative to the structure at 0° of torsion, with the hydrogen atoms facing each other.

IR spectrum

The frequency calculations in 3.2.3 allowed for the simulation of an infrared absorption spectrum, depicted in figure 3.13. Figure 3.14 shows a comparison of the experimental and the simulated spectrum, with the latter shifted by -72 cm^{-1}, so that the nickel-hydroxyl stretching vibrations at 3409 cm^{-1} overlap. Scaling or shifting of simulated IR spectra is commonly done to aid in the comparison to experimental spectra, since this approach of deriving the spectra does make rather large approximations, such as the disregard of anharmonicity [143]. Nonetheless, after overlaying the nickel-hydroxyl stretching vibrations the rest of the relevant absorption peaks are in very good agreement. The nickel-hydride stretching vibration can be assigned to the absorption band at 1890 cm^{-1} in the experimental spectrum, and 1962 cm^{-1} in the simulated spectrum.

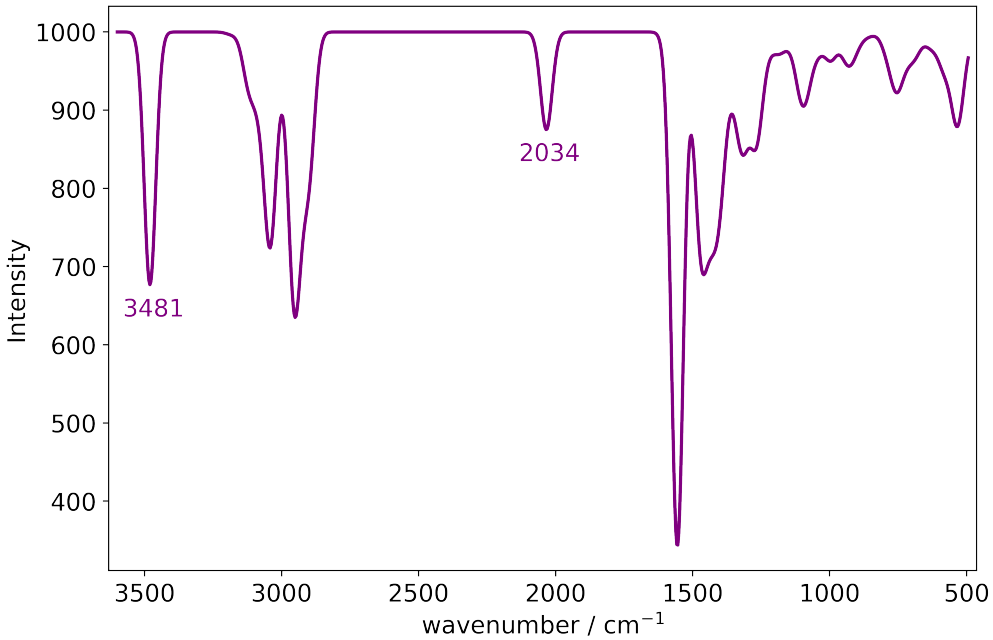

Figure 3.13: Simulated IR absorption spectrum of complex **A.3**, using the numerical frequency routine of ORCA at BP86-D3/def2-SVP level of theory. Marked are the nickel-hydroxyl stretching vibrations at 3481 cm^{-1} and the nickel-hydride stretching vibration at 2034 cm^{-1}.

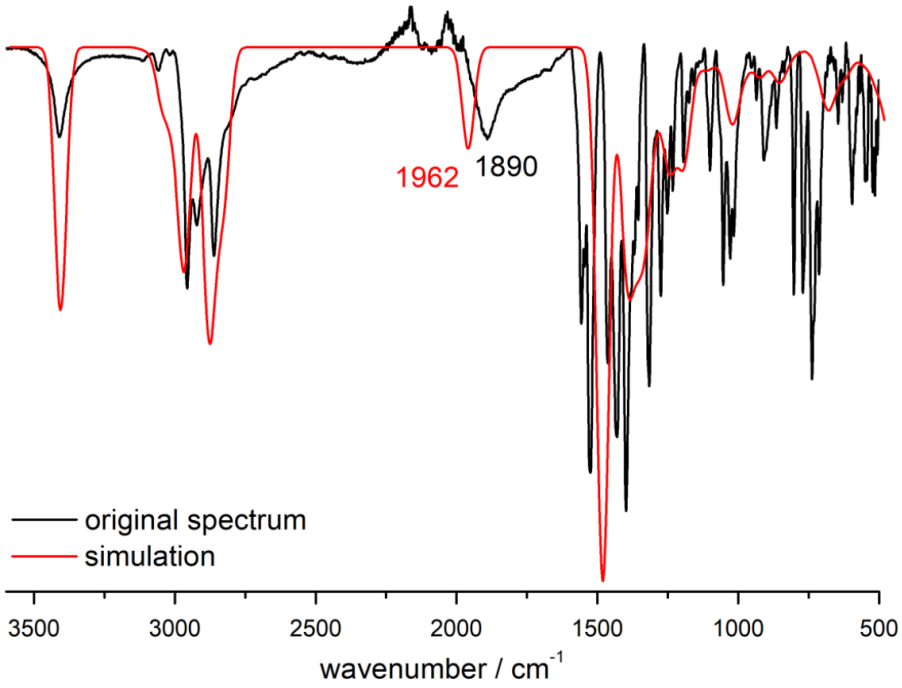

Figure 3.14: Comparison of simulated and experimental IR spectra. The simulated spectrum is shifted by -72 cm^{-1}, so that the nickel-hydroxyl stretching vibrations overlap at 3409 cm^{-1}.

3.3 Discussion

In summary, it was possible to employ various DFT methods to great effect. Optimizing the relevant complexes of the oxidative H_2O addition offered a more detailed picture of the structural information than experimental methods such as NMR or X-ray diffraction are able to provide by themselves. It might be possible to devise experiments to determine energetic values such as the barrier height of the transition state or the strength of the dihydrogen bond, but such experiments would likely prove complicated and costly, while DFT methods allow for comparatively easy access. Comparisons to benchmark values, such as between measured and simulated dihydrogen bond lengths or IR spectra, allow for the confidence that other simulated results can be relied upon as well, within the margin of error inherent to all computational methods.

A probable reaction pathway for the oxidative H_2O addition was demonstrated, elucidating the metal-metal cooperativity of the two Ni^{II} atoms and the role of the intramolecular cleft. The splitting of water, which is otherwise quite costly in energy (119 kcal/mol) [144], would not occur in this manner without this specific configuration.

The product of the addition was characterized as well. The structure of the intramolecular cleft promotes close proximity of the hydride and hydroxyl group after splitting. The extend of the dihydrogen bonding interaction, previously only inferred by NMR and NOE spectroscopy [119], was determined through the investigation of the torsional barrier. The MD simulations further detailed this interaction, demonstrating that the hydride and hydroxyl group are oriented toward each other most of the time, with only small and short deviations in the dihydrogen bond length. The role of the potassium cation was elucidated as well, keeping the cleft closed through its attractive interaction with the negatively charged aryl rings. Removing the cation leads to on average longer bond lengths of the dihydrogen bond, as shown in figure 3.10b.

However, as already mentioned in section 2.1, it has to be acknowledged that DFT is far from being the perfect solution to all problems when it comes to computational chemistry. DFT is not a "black box" method, and the computational parameters, such as the functional and basis set, have to be chosen thoughtfully. There is an ever growing field of functionals and functional types, purporting ever more accuracy, but also complicating these decisions. For example, it has been shown that Hybrid-GGA type functionals, while generally reliable in terms of computed structures, can be problematic when it comes to other properties, such as spin transition energies [34]. In such cases the computed values become directly dependent upon the amount of exact HF exchange used, making this a crucial factor to consider in cases of transition metal compounds exhibiting spin-crossover behaviour.

The severity of these problems, as well as approaches to their resolution, will be the topic of the next chapter(s).

Chapter 4

Parameterization of DFT functionals for Fe^{II} SCO

The findings presented in this chapter and appendix B have previously been published in MDPI's journal Molecules *[145]. The content of this chapter and the publication will therefore be similar, even though no explicit citation is given. Authors retain full copyright over all articles published in MDPI journals.*
I want to explicitly thank Lukas Hasecke, who was responsible for development and application of the UCCSD(T)-F12B method and the Bayesian optimization procedure, and Prof. Dr. Peter E. Blöchl, who contributed with his knowledge about the CP-PAW method.*

4.1 Introduction

As described in the Introduction 1 there are many and varied efforts to improve the computational description of the spin crossover (SCO) phenomenon in Fe^{II} complexes. The findings of Phan *et al.* [146] were especially interesting, suggesting a strong correlation between the spin state of homoleptic diimine complexes of Fe^{II} and the N-N distances in these diimine ligands. This raised the question whether hybrid density functionals can be adequately parameterized to capture the effects of ligand field stabilisation under various geometric constraints.

This approach differs from previous benchmark studies, which focused on altering the chemical properties of the compound. It makes use of the most basic model system for a Fe^{II} complex with N-coordinating ligands, specifically the $[Fe^{II}(NH_3)_6]^{2+}$ species. A series of standard benchmark tests is established that can be applied to other centers and coordination structures as well, focusing on the ligand structure. The primary point of interest is the adiabatic HS-LS energy difference $\Delta E_{HL} = E_{HS}(\mathbf{R}_{HS}) - E_{LS}(\mathbf{R}_{LS})$, where $E_{XS}(\mathbf{R}_{XS})$ refers to the energy of the HS/LS states in their respective geometries. Only electronic energies are discussed, without consideration for environmental effects such as solution or solid-state interactions, although these can be introduced through standard embedding procedures.

4.2 Preparation of the $[Fe^{II}(NH_3)_6]^{2+}$ model system

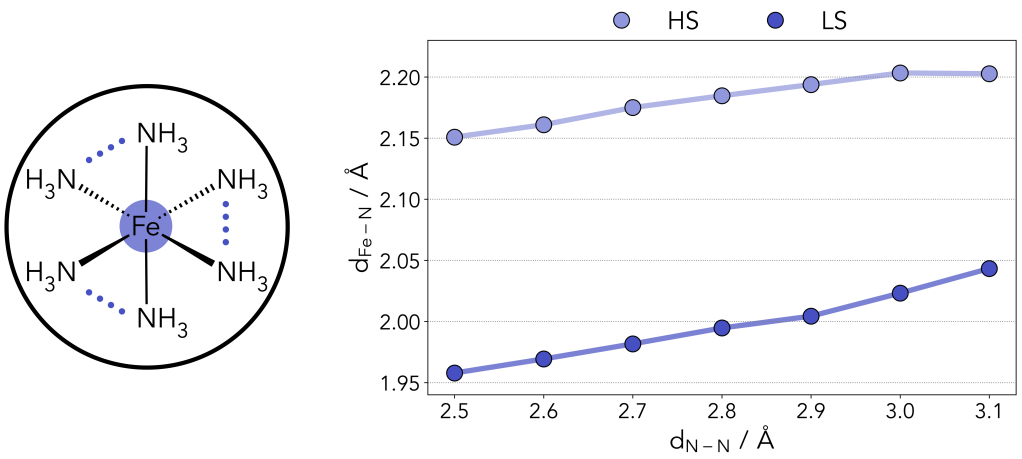

Figure 4.1: Left panel: Conceptual diagram of the $[Fe^{II}(NH_3)_6]^{2+}$ model complexes. The N-N distances were restricted pairwise to set values, marked by the dotted lines. All other geometry parameters are optimized for both HS and LS states.
Right panel: Influence of the N-N pair distance restraint upon the Fe-N distance.

Taking the work of Phan *et al.* [146] as a starting point, a range of model systems was constructed to mimic different ligand geometries. Since many SCO complexes contain bidentate ligands, pairwise restrictions were imposed on the N-N distances of the $[Fe^{II}(NH_3)_6]^{2+}$ model, as depicted in figure 4.1. No symmetry constraints were applied. The range of N-N distances was set from 2.5 to 3.1 Å in steps of 0.1 Å,

covering the optimal SCO range of 2.8-2.9 Å predicted by Phan *et al.* and extending beyond. The complex geometries were optimized for all degrees of freedom other than the pairwise N-N distance, using the PBE0r [147] level of theory. This local hybrid functional is discussed extensively in section 2.1.2.

All calculations with PBE0r were carried out using the CP-PAW code package [85, 86]. Initial geometry optimizations were carried out using 12.5% exact exchange for all atom types. An example of a corresponding input file is provided in appendix B. Also provided are the structures of the model system in HS and LS state with 2.5, 2.8 and 3.1 Å pairwise N-N distance in XYZ format.

As observed from the optimized geometries in figure 4.1, constraining the N-N distance to shorter values also leads to a reduction of the Fe-N coordination distance. The LS geometries exhibit a slightly more pronounced effect. This relationship is determined by the overlap between the nitrogen lone pairs and the Fe e_g orbitals. When the distance between the coordinating nitrogen atoms is reduced, the orbital overlap can be partially preserved by also shortening the Fe-N distance, and vice versa. This change has a less destabilizing effect on the S=0 state, as it can more readily accept density in the e_g levels.

4.3 Coupled-cluster benchmark calculations

Coupled-cluster calculations were carried out to obtain benchmark values for the high-spin (HS)-low-spin (LS) gap ΔE_{HL}. A detailed breakdown of the values discussed in this section can be found in the appendix B.

Explicit correlation methods [148] were utilized to reach almost complete basis set limit accuracy while reducing computational costs as much as possible. The benchmark reference results were obtained using the unrestricted coupled-cluster (UCC) F12B method [149], which includes single, double, and perturbative triple excitations with the fixed amplitude 3C(FIX) *ansatz* [150], implemented in MOLPRO [151]. Additional complementary auxiliary basis set (CABS) singles correction and scaling of the perturbative triples were applied [152]. The method-specific cc-pVTZ-F12 basis sets were used for the ammonia ligands [153], while the aug-cc-pwCVTZ basis was chosen for iron [154] to allow for adequate recovery of the 3s3p correlation. Following

the prior work on explicit correlation methods on transition metal complexes from Bross *et al.* [155], their aug-cc-pwCVTZ/MP2FIT was utilized as the density fitting basis and as the CABS for the resolution of identity. For the density fitting of the Fock matrices, def2-QZVPP [156] was used. The Hartree-Fock calculations for the recovery of the relativistic contributions to the F12B energy were performed using a cc-pwCVQZ-DK/cc-pwCVQZ [154] basis for iron and cc-pVQZ-DK/cc-pVQZ [157] for the remainder. The results for ΔE_{HL} are presented in figure 4.2.

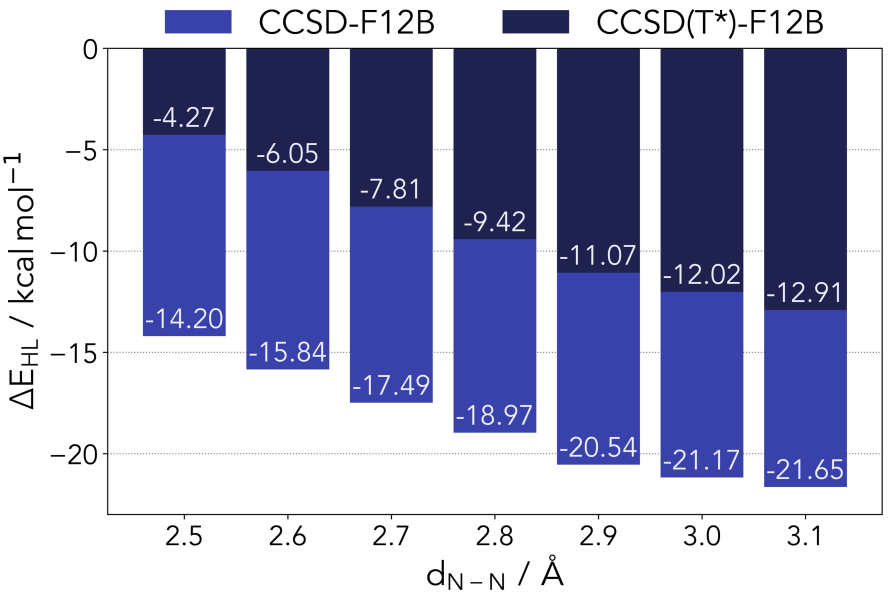

Figure 4.2: Computed HS-LS gap for the $[Fe^{II}(NH_3)_6]^{2+}$ complex with varying N-N distances at the coupled-cluster level (including the DK correction and the scaled triples).

It can be observed that the restraints placed on the ligands contribute to a significant reduction of the ΔE_{HL}, from -12.9 kcal/mol down to -4.3 kcal/mol. However, within the applied range, this reduction is not sufficient to invert the stability of the high-spin state over the low-spin state. For the fully relaxed model system the N-N distances are approximately 3.1 and 2.8 Å for the HS and LS states, respectively.

The triples correction significantly favors the LS state, reducing the gap by approximately 10 kcal/mol. A detailed breakdown of different energy components for the calculation of ΔE_{HL} as a function of the N-N distance is presented in figure 4.3.

Some terms show a geometry dependence, particularly the CCSD correlation energy and the triples correction. It appears that the scaling of the triples (T*) has little impact.

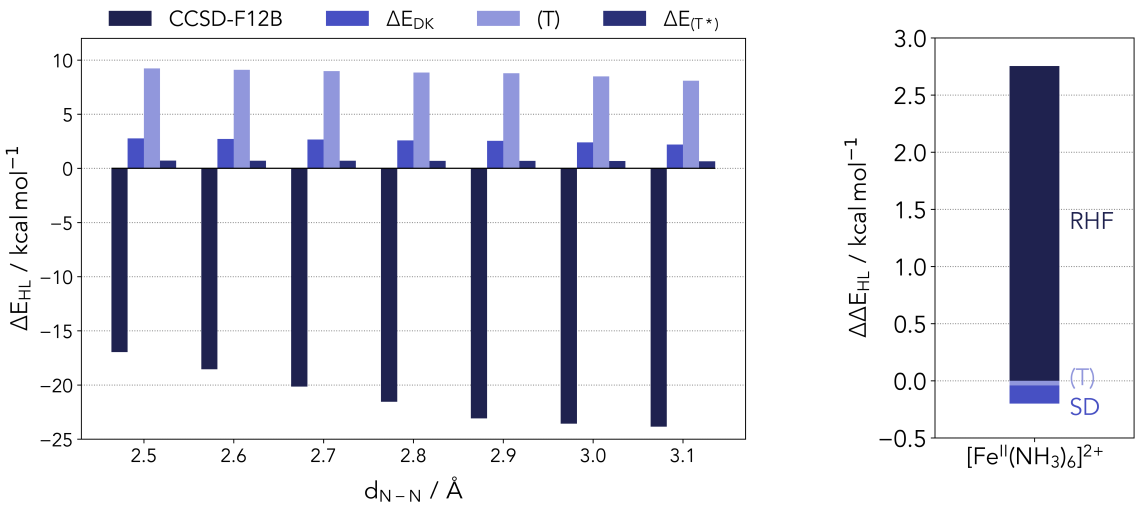

Figure 4.3: Left panel: different energy contributions to the UCCSD(T*)-F12B reference energy.
Right panel: energy difference between a relativistic and non-relativistic CCSD(T) calculation for the reference complex.

As shown in Fig. 4.3 (left panel), the primary trend of the reference energy in dependence of the nitrogen pair distance for distances shorter than 2.9 Å is mainly given by the CCSD energy. For larger distances the CCSD energy goes into saturation, and the overall trend is dominated by the decrease of the contribution of the perturbative triples excitation. The corrections for the perturbative triples and for the relativistic effects are largely independent of the geometry. The additivity of the scalar relativistic corrections to the HS-LS gap (ΔE_{DK}) can be observed as well. It amounts to 2.51 kcal/mol for the model system, and has only a small effect on the total computed correlation energies.

The right side of Fig. 4.3 illustrates the energy difference between a relativistic and a non-relativistic canonical CCSD(T) calculation of the $[Fe^{II}(NH_3)_6]^{2+}$ model system. The calculation was performed using a second-order Douglas-Kroll-Hess Hamiltonian (DKH2) [158, 159] and a cc-pwCVTZ-DK/cc-pwCVTZ [154] basis set

for the iron atom, as well as a cc-pVDZ-DK/cc-pVDZ [157] basis set for the ligand atoms. The energy difference indicates that the correlation energy is mostly unaffected by relativistic effects, while the reference energy is significantly influenced. It is therefore a reasonable approximation to recover the relativistic effects solely from the reference calculations. The scalar relativistic corrections were computed at the Hartree-Fock level and added to the non-relativistic CCSD(T) values.

The convergence of ΔE_{HL} for the relaxed geometry of the hexaamino complex at the coupled-cluster level has already been extensively addressed by Neese and coworkers [160]. A comparison to the results presented here shows only small deviations. The computed scalar relativistic corrections here amount to 2.51 kcal/mol, compared to 2.37 kcal/mol. Regarding the basis set correction, moving from triple-zeta to complete basis set (CBS) extrapolation or in this case using the F12B value as the limit, the deviations are quite small. The CBS[Q:5] correction of Flöser *et al.* amounts to -4.7 kcal/mol, while the F12B value is at -5.0 kcal/mol. For $[Fe^{II}(NH_3)_6]^{2+}$ a total value of $\Delta E_{\mathrm{HL}} = -13.37$ kcal/mol was obtained, compared to -11.3 kcal/mol by Flöser *et al.* The minor deviation between their ΔE_{HL} results and the values presented here is mostly due to differences in the geometry optimization.

A recent report by Radoń is also noteworthy, where various electronic structure methods are benchmarked against experimentally derived Fe^{II} spin-state energetics. CCSD(T) performs remarkably well [161] in these findings. Depending on the choice of reference orbitals the mean absolute error was about 1 kcal/mol when compared to the proposed back-corrected experimental data set. Other comparisons to experimental data have also been favorable to CCSD(T) [36, 41].

4.3.1 Multireference diagnostics

As mentioned in the Introduction 1, there is an ongoing debate regarding the single reference nature of both singlet and quintet states of the $[Fe^{II}(NH_3)_6]^{2+}$ complex. This issue is in line with the difficulties encountered in achieving convergence in the level of theory for non-heme iron complexes, as exemplified by ref. [162]. Song *et al.* [163] proposed that the system contains a significant amount of static correlation based on their analysis of single excitation amplitudes.

The two diagnostics used most often are the T1 diagnostic based on the Frobenius norm and the D1 diagnostic based on the matrix 2-norm [164]. The computed values vary between 0.049 and 0.087, depending on the spin state and basis set combination. This would exceed the threshold of 0.04 suggested to safely signify a single reference character [164], but such thresholds were derived from small molecule calculations without consideration for transition metals. Recent assessments [165] for 3-d transition metal compounds indicate that the threshold should be placed at D1$<$ 0.15. In practice it is best to combine several diagnostics for a more robust assessment. Wilson and coworkers recommended using a combination of D1 and T1 (which should remain below 0.05) as well as a computed percentage of the atomization energy.

Calculations were carried out to verify the multireference descriptors for the DFT optimized structure of the $[Fe^{II}(NH_3)_6]^{2+}$ model system. The results for the D1 diagnostic (with a triple-zeta quality basis set) are slightly higher (0.092 for the LS and 0.045 for the HS state) than those of Song *et al.*, but still well below the threshold of 0.15 suggested by Wilson and coworkers. The T1 values (0.02 for the LS and 0.013 for the HS state) are below the threshold as well, comparing to the suggested value of T1$<$ 0.05). Having fulfilled two out of three criteria, this supports the assessment made by Flöser *et al.* [160] that the multireference character of both states is amenable.

There were no significant changes in both T1 and D1 diagnostics over the studied range of different geometries.

4.4 Parameterization of hybrid functionals

Computational details

The ORCA 4.2.0 program package [126, 127] was used for all DFT calculations in this section.

The range of functionals included in this study were the GGAs PBE [60] and BP86 [61,62], the meta-GGAs TPSS [63] and M06-L [64], the hybrid GGAs PBE0 [67,68] and B3LYP [69] (both with varying amounts of exact exchange), and the range-separated hybrid functional CAM-B3LYP [73] (with variation in the amount of

initial exact exchange and in the distance parameter). The cc-pwCVQZ-DK [154] basis set was used for the Fe atom and cc-pVQZ-DK [157] for the ligand atoms. Relativistic effects are taken into account by using the second-order DKH2 [158, 159]. The RIJCOSX approximation [166] was used to speed up calculation time. Grimme's D3 method with Becke-Johnson damping [167,168] was used for dispersion correction, with the exception of M06-L. The convergence threshold was set to 10^{-9} H by using the 'verytightscf' keyword.

4.4.1 Overview

Every functional was used to carry out single-point energy calculations for the range of model complexes (meaning the structure was not re-optimized). From this the HS-LS gap could be calculated and compared to the benchmark values. The numerical values resulting from the calculations discussed in this and the following section are presented in the appendix B.

Figure 4.4 provides an overview of the results for the GGA and meta-GGA functionals, as well as the hybrid and range-separated hybrid functionals when used with default parameters. This will be discussed further in the next section.

The simpler GGA type functionals exhibit reasonable agreement with each other, but deviate from the benchmark values. As expected, these functionals assume the LS state to be highly stable, leading to a very large ΔE_{HL}. TPSS produces strongly divergent values as well, while the performance of M06-L is notably better.

However, it can be observed that the coupled-cluster values predict an almost linear relationship between ΔE_{HL} and $d_{\mathrm{N\text{-}N}}$. Almost all GGA and meta-GGA type functionals reproduce this behaviour quite well, except for M06-L, which flattened out by $d_{\mathrm{N\text{-}N}} \geq 3.0$ Å. Nonetheless, the comparison of SCO complexes on the basis of GGA is supported by the results, as the slope is almost the same as for the reference values. This, in turn, signals the possibility of reproducing trends across different ligands or distortions as well.

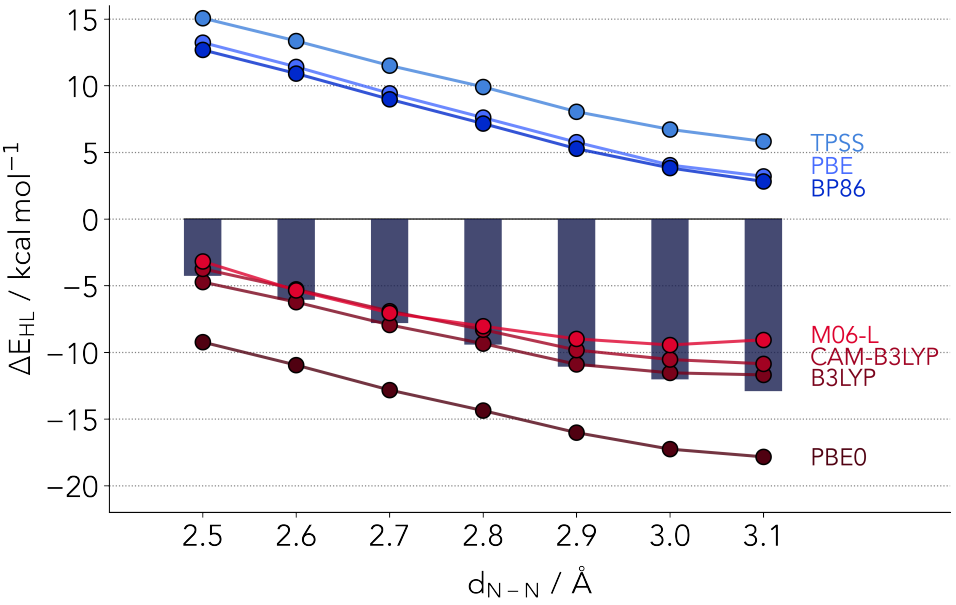

Figure 4.4: Overview of ΔE_{HL} from DFT calculations (lines) in relation to the coupled-cluster values (bars). In absolute values the hybrid functionals as well as M06-L outperform the remaining GGA and meta-GGA functionals. However, the slope evident in the coupled-cluster results is best reproduced by TPSS, BP86 and PBE0, while all other functionals level out too much at larger N-N distances.

4.4.2 Hybrid GGA type functionals

As described in 2.1.2, in hybrid GGA type functionals a certain percentage of the GGA exchange energy is replaced by the exact exchange energy calculated with HF. The replaced amount can vary, but the two functionals presented here have a relatively similar admixture in their default settings. For B3LYP it is $a = 0.2$ and for PBE0 it is $a = 0.25$. Especially of interest for this study was the behaviour of these functionals for varying amounts of HF exchange.

The results for ΔE_{HL} are provided in figure 4.5. Non-default admixture parameters are marked by placing the value in parenthesis, while the admixture with default parameteres is left unmarked. The B3LYP(0.15) variant is one exception, since it has been popularised by Reiher and coworkers [169], and it is marked here as B3LYP*, in line with the common literature nomenclature.

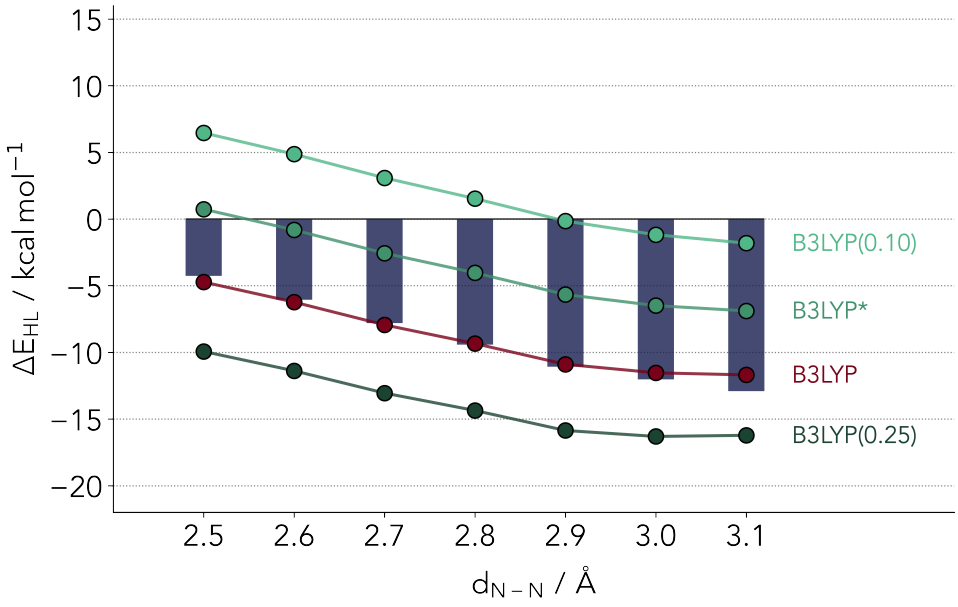

(a)

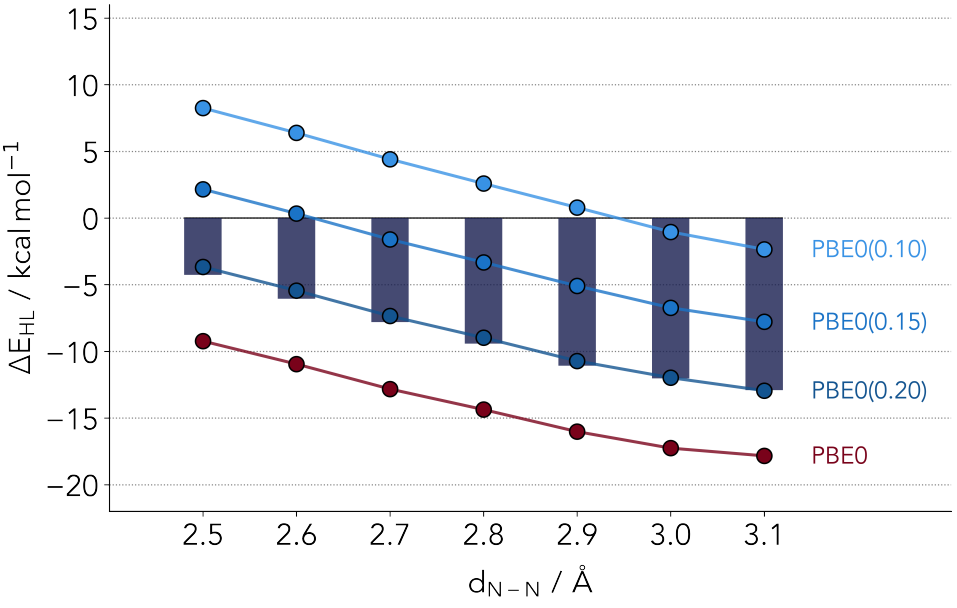

(b)

Figure 4.5: Comparison of ΔE_{HL} values for the $[\mathrm{Fe^{II}(NH_3)_6}]^{2+}$ model system computed with reparameterized (a) B3LYP and (b) PBE0 functionals. Values in parenthesis show non-default HF exchange parameters. The bars depict the coupled-cluster benchmark values.

The profiles for B3LYP and PBE0 look rather similar, with an optimal admixture observed at 20% exchange. It is unexpected to observe the same optimal range of admixture for two different functionals. Especially for B3LYP, one might expect a lower optimal value, as an admixture of 15% (e.g. B3LYP*) has been suggested for the energetics of Fe-S complexes [169]. This parameterization has also been validated for the first transition metal row [170]. Still, the overestimation of the LS state stability is evident. A nearly perfect linear relationship between ΔE_{HL} and the value of a can be observed, which several authors have suggested before but not confirmed for a fixed functional form [163, 171, 172].

When comparing the two functionals, it is noteworthy that the PBE0(0.20) variant performs slightly better than B3LYP. The slope is better represented by the parameterized PBE0, while B3LYP underestimates the relative stability of the HS state at larger distances. This deviation cannot be corrected by adjusting the parameter a. While smaller values of the parameter may improve the slope, the absolute values will diverge, reducing the overall overlap with the benchmark values.

4.4.3 Range-separated hybrid functionals

The CAM-B3LYP functional [73] was selected for this study, which has $\alpha = 0.19$, $\beta = 0.46$ and $\mu = 0.33$ for its default parameters. This type of functional has been developed with the calculation of electronically excited states and spectra in mind, and is regularly used for the calculation of spin energetics [42, 161, 173].

For this study β was left unchanged, while α and μ were varied between slightly lower ($\alpha_1 = 0.13, \mu_1 = 0.25$) and slightly higher ($\alpha_2 = 0.25, \mu_2 = 0.40$) values. Figure 4.6 illustrates the results obtained from calculations with the original set of parameters (α_0, μ_0) and the variations.

Similar to the case of B3LYP, the default CAM-B3LYP(α_0, μ_0) produces results in good agreement with the benchmark values, although the slope is not perfectly reproduced. The most significant deviation can be observed for distances exceeding 2.9 Å, with the HS state being too unstable. It was however not possible to correct this behaviour through the variations of the α and μ parameters, while maintaining a good accuracy for the absolute ΔE_{HL} values at the same time.

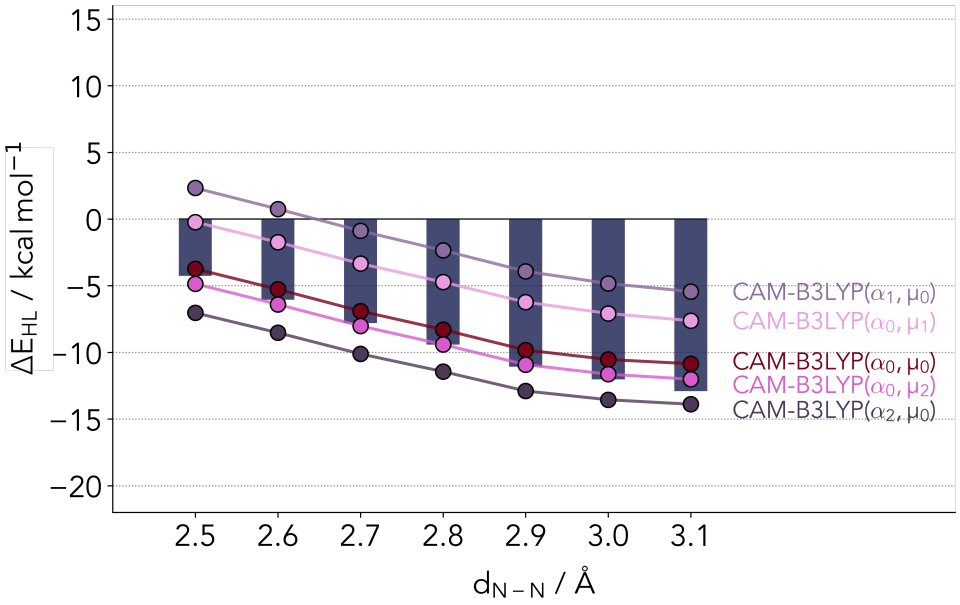

Figure 4.6: Comparison of ΔE_{HL} values for the $[\mathrm{Fe^{II}(NH_3)_6}]^{2+}$ model system computed with refitted CAM-B3LYP. The bars depict the coupled-cluster benchmark values. $\alpha_0 = 0.19, \mu_0 = 0.33$ are the original parameters. Varied parameteres are $\alpha_1 = 0.13, \alpha_2 = 0.25, \mu_1 = 0.25, \mu_2 = 0.40$

4.5 Parameterization of PBE0r

As mentioned in section 2.1.2, for the local hybrid functional PBE0r the hybrid terms are divided into atomic contributions, allowing for the adjustment of the admixture of the exact exchange separately for each atom species. For the $[Fe^{II}(NH_3)_6]^{2+}$ model system this offers 3 independent variables, though it can be demonstrated that the amount of HF exchange used for H atoms has only a small influence on the HS-LS gap, even for systems with a much higher number of H atoms (see also figure 6.7). Solving this 3-dimensional optimization problem of finding the ideal amount of Hartree-Fock exchange for iron, nitrogen and hydrogen was tackled with an automated BO procedure, which will be discussed in this section.

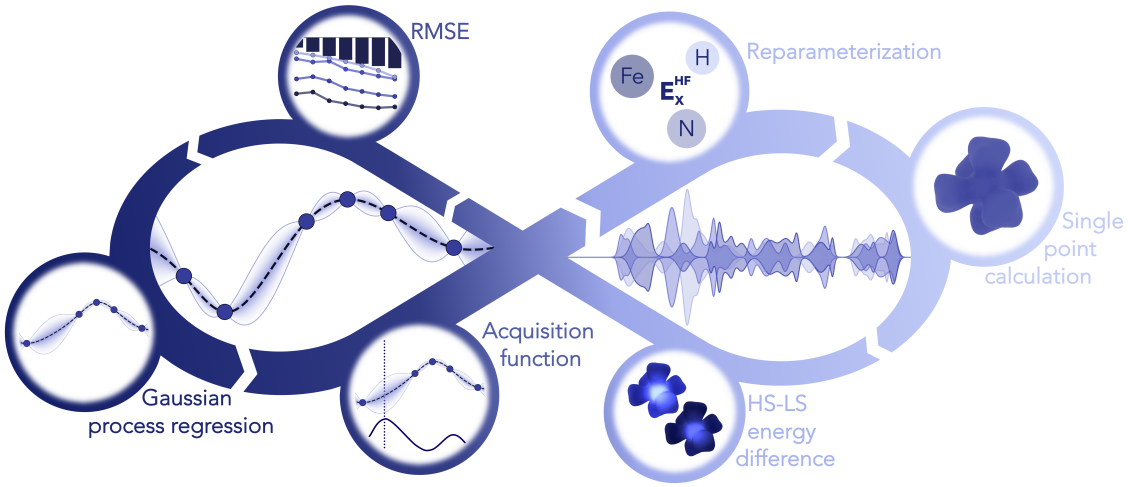

Figure 4.7: Diagram with an overview of the automated Bayesian optimization of PBE0r HF exchange parameters. The process starts by selecting a set of parameter values and computing ΔE_{HL} for the model systems, using the PBE0r functional. The RMSE is calculated by comparing the PBE0r results to the benchmark values, resulting in numerical value for the "quality" of the fit for this point in the sampling space. The Gaussian process regression produces values for the uncertainty between calculated points, letting the acquisition function choose the most promising next set of parameters, and the process is repeated. This figure has been graciously provided by Lukas Hasecke.

As discussed in section 2.5, the BO procedure is a machine learning tool, offering the opportunity to efficiently find the global minimum of a reference by varying a set of parameters [112, 113]. In this study, the root mean square error (RMSE) between the ΔE_{HL} values from the UCCSD(T*)-F12B benchmark and the values from the reparameterized PBE0r functional was used as the reference for the optimization. The parameters were the percentages of the element-specific HF exchange amounts. The Bayesian optimization was performed using a Gaussian process regression with a Matérn52 kernel and an expected improvement acquisition function, implemented in GPyOpt [174]. The HF exchange percentages were restricted to the range of 1-25%. In order to ensure effective optimization, the whole space was explored with 50 points determined by Latin hypercube sampling [175] prior to optimization. Subsequently, an additional 50 points were iteratively selected based on the acquisition function. Figure 4.7 offers an overview of the BO procedure, while the results from the acquisition function are presented in figure 4.8.

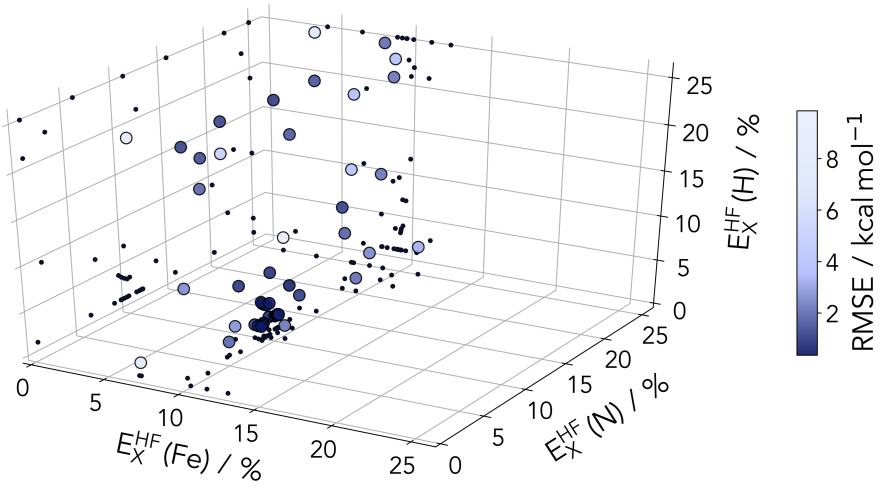

Figure 4.8: Sampled points during the Bayesian optimization process of the HF exchange percentages for the three atom species. The points are color coded according to the root mean-square error (RMSE) between the computed values and the coupled-cluster benchmark.

For the HF exchange factor of the Fe species the BO process clearly identifies 9% as the optimal value. This is found in a range consistent with several previous studies on various classes of transition metal compounds and materials, including a recent study on lithium manganese oxides (with the final value for Mn in this particular case also at 9%) [84] and DFT studies of perovskites [81, 176].

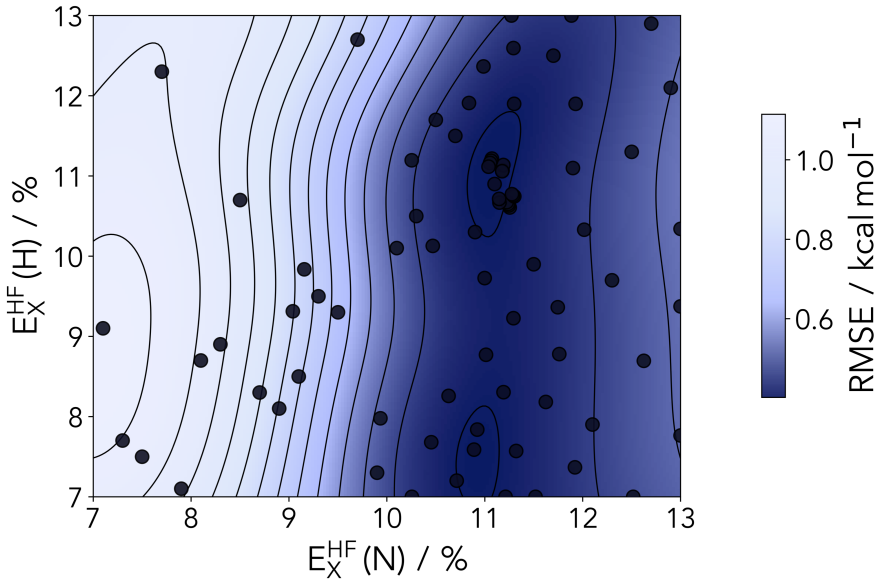

Figure 4.9: 2D-cut of the posterior distribution (at a fixed 9% HF-exchange for Fe) after 80 sampled points. A valley around 11% is clearly identifiable for the N atom scaling.

The HF exchange parameterization of PBE0r is most important for transition metal ions with partially filled d-shells such as Fe. The influence of the parameterization of hydrogen, on the other hand, can be expected to always be marginal. This is clearly demonstrated in figure 4.9, which shows a 2-dimensional cut of the sampled points at 9% HF exchange for iron. Varying the nitrogen HF exchange parameter in this region can change the RMSE of the fit by up to 1.0 kcal/mol, while the effect of varying the hydrogen parameter is an order of magnitude smaller. This indicates that particular attention must be paid to the description of the nitrogen species as well, especially considering the direct coordination to the metal.

Figure 4.10 shows a comparison of ΔE_{HL} computed with PBE0r for varying amounts of HF exchange, applied to all atom species. Unsurprisingly, using 9% HF exchange for all species yields the best agreement to the coupled-cluster benchmark values.

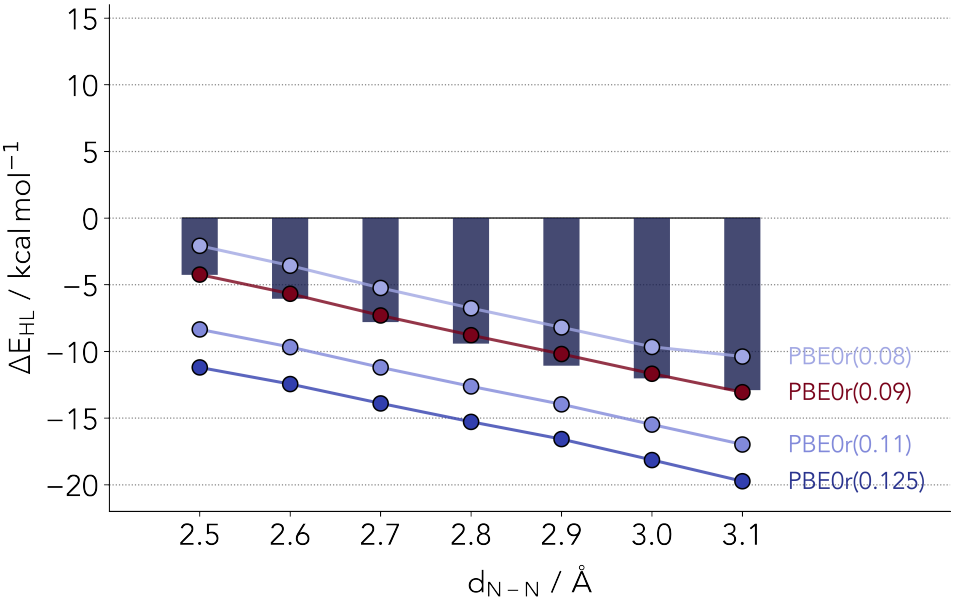

Figure 4.10: Comparison of ΔE_{HL} values computed with PBE0r. The numbers in parenthesis indicate the amount of HF exchange for all atom species. The bars depict the coupled-cluster benchmark values.

$[Fe^{II}(C_2H_4N_2)_3]^{2+}$ model system

A second model with ethane-1,2-diimine (with the chemical formula $C_2H_4N_2$) as the ligand was devised to observe whether the lack of dependence on the nitrogen HF-exchange fraction was maintained when considering more complex models of SCO complexes. This bidentate ligand should provide a better analogon for relevant SCO complexes.

In a new series of calculations, the percentage of HF exchange for the nitrogen species was varied while keeping every other species at 9%. The results, shown in figur 4.11, reveal that the dependence of ΔE_{HL} on the exchange admixture is larger than for the simple $[Fe^{II}(NH_3)_6]^{2+}$ model system. Although the reference data for the diimine model is not provided here, one can straightforwardly compare the dependence. Changes in the exchange functional for the local density located at

the nitrogen atoms will impact the charge distribution along the double bond to the carbon, which will affect the coordination to the metal. In the simpler $[Fe^{II}(NH_3)_6]^{2+}$ model, only protons were present, which took up little density.

The diimine model, among others, is discussed in more detail in chapter 5.

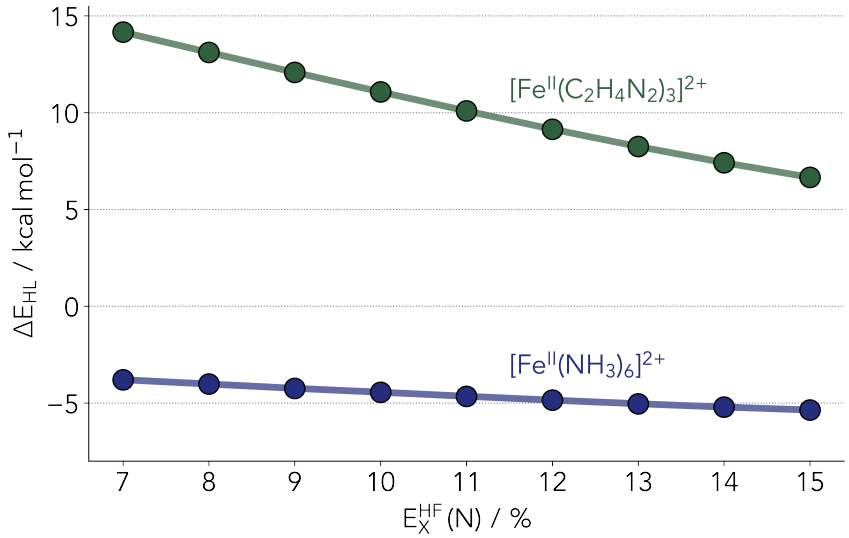

Figure 4.11: Comparison of the dependence of ΔE_{HL} on the exchange admixture for the simple model $[Fe^{II}(NH_3)_6]^{2+}$, and the more complex $[Fe^{II}(C_2H_4N_2)_3]^{2+}$.

4.6 Discussion

The primary focus of this study was to assess the feasibility of parameterizing hybrid density functionals to accurately reproduce the energy gap between the high-spin and low-spin state of N-coordinated Fe^{II} complexes, taking the $[Fe^{II}(NH_3)_6]^{2+}$ system as a reference. The set of model complexes with varying N-N distances was constructed (as described in section 4.2) in order to ensure that the approach is remains robust in the presence of changes to the complex structure. Essentially, a broad range of ligands was simulated using only a few reference calculations. Optimally, the obtained results should not be compromised by subtle variations in the coordination geometry. This is crucial for the precise modeling of the dynamics of SCO complexes and to ensure the predictive capability of the approach.

It has been reported repeatedly in the literature (for example [177]), that pure GGA type functionals tend to overestimate the stability of low-spin states. Despite this issue, many of the calculations on SCO complexes are still conducted at this level of theory due to the low computational cost and ease of implementation. Another factor is that using pure GGA type functionals also ensures that the ground-state is a LS state. The HS state is favored by entropy because of its longer bonds, so for actual SCO complexes where the transition occurs by heating up the system will require a small energy difference between the two, but with the LS state being lower in energy. The difficulties are especially pronounced for multicentered complexes, where benchmarks are much scarcer. In the case of the [2x2] Fe^{II} grid complexes synthesized at the Meyer group [30], a number of theoretical studies have accurately predicted that the LS states are indeed more stable [178,179], consistent with magnetic susceptibility measurements. However, the reported energy differences between the different spin states are generally too large for an SCO-capable complex. Theory has only provided a qualitative understanding of the process so far. The [2x2] Fe^{II} grid complex will be discussed further in chapter 6.

The results obtained from the wave function analysis strongly support the single-reference character of both singlet and quintet states in the $[Fe^{II}(NH_3)_6]^{2+}$ model. This suggests that coupled-cluster methods are an adequate benchmarking method for the discussion of the spin state energetics for these systems. The local coupled-cluster results of Flöser *et al.* [160] could be largely confirmed, though the approach for benchmarking DFT functionals presented here is different. The changes in coordination while keeping the same ligands provides insight into how the DFT method performs when structural changes occur in the complex, which is a fundamental issue in the theoretical description of SCO complexes.

The results demonstrate that while many functionals can be tuned to reproduce a reference singlet-quintet gap ΔE_{HL}, it is much more challenging to capture the trends occuring with structural changes. It is also observed that only the GGA functionals or hybrids with significantly reduced percentages of non-local exchange can match the coupled-cluster ΔE_{HL} slope, e.g. the energy gap as a function of the ligand structure. This observation validates the approach of Jakubikova [31], although it should to be noted that the model system used in this study is relatively small.

The hybrid GGA type functional PBE0(0.20) and the local hybrid PBE0r with an admixture of 9% for the Fe species were identified to be the best performing (parameterized) functionals. The latter offers reduced computational cost and can be readily employed for the simulation of larger systems, including oligo-nuclear SCO complexes such as the [2x2] Fe^{II} grid system mentioned earlier. However, some issues have to be addressed as well. It can be discerned from figure 4.11 that the $[Fe^{II}(NH_3)_6]^{2+}$ model system only provides part of the picture. To achieve results that are applicable to all Fe^{II} SCO complexes in general, the chemical diversity of the range of model systems would have to be expanded. This expansion should include important factors for common SCO complexes, such as the coordination to conjugated systems or the distortion of the octahedral geometry due to ligand constraints and steric effects. These more realistic models would also be more demanding in regard to the multidimensional tuning of the local hybrid functional. This extension of the model system set is discussed further in the next chapter 5.

Chapter 5

Extension of the Fe^{II} SCO model set

5.1 Introduction

As discussed in chapter 4, there is merit to the approach of parameterization of DFT functionals for an accurate but cost-effective description of Fe^{II} SCO complexes. To reiterate briefly, the initial approach involved constructing a set of small model complexes, computing benchmark values with a high level wavefunction method, and then fitting the DFT method to the benchmark with a Bayesian optimization procedure.

However, it has also been discussed that the first iteration of this approach was too simplistic, as it relied solely on a series of geometrically distorted $[Fe^{II}(NH_3)_6]^{2+}$ complexes for the model set. This lacks the chemical diversity of many of the Fe^{II} SCO complexes actually in existence, which often feature multidentate ligands and incorporate C atoms [13, 23, 31, 32, 146, 177, 180].

Presented in this chapter are efforts to improve the approach by extending the set of model systems, the results from these improvements, as well as the complications inherent to this approach.

5.2 Considerations for new model complexes

To be considered for the new set of model complexes, the systems obviously have to contain a Fe^{II} core. It was deemed appropriate to narrow the scope of this work to systems with the $Fe\{N\}_6$ motif, meaning that the first coordination sphere contains only six N atoms, in a roughly octahedral configuration. The rest of the systems should consist only of H, C and N atoms, as these are the most common species for the "backbones" of ligand structures associated with Fe^{II} SCO complexes. The ligands should connect to the Fe^{II} core in mono-, bi- or tridentate configurations, all of which are commonly observed in Fe SCO systems [13, 23, 31, 32, 146, 177, 180]. Additionally, there are restrictions imposed by the coupled-cluster benchmark method. As described in 4.3, it is possible to compute single point energies for a system like $[Fe^{II}(NH_3)_6]^{2+}$, but for much larger systems this becomes impractical. Another coupled-cluster variant was established to remedy this to a degree, which is described in 5.3. Even so, it was necessary to keep the model complexes as small as possible.

Apart from the well studied $[Fe^{II}(NH_3)_6]^{2+}$complex [34, 160, 163, 181, 182], there is alltogether not much research into systems conforming to all of these considerations, especially with the limitation of the system size. Some of the distorted $[Fe^{II}(NH_3)_6]^{2+}$ complexes from the previous model set (see chapter 4) were used again, specifically the one with the smallest (2.5 Å), the middle (2.8 Å), and the largest (3.1 Å) N-N pairwise distance. From here on these complexes are assigned as **B.01**, **B.02** and **B.03**, respectively. It was assumed that using more of the distorted $[Fe^{II}(NH_3)_6]^{2+}$ complexes would not add any more information to the model set.

The [2x2] Fe_4 grid complex synthesized by Meyer *et al.* [30] with its tridentate ligands gave inspiration toward the construction of **B.04** ($[Fe^{II}(N_3C_4H_6)_2]^0$), **B.05** ($[Fe^{II}(N_3C_4H_6)(N_3C_4H_7)]^{1+}$) and **B.06** ($[Fe^{II}(N_3C_4H_7)_2]^{2+}$). **B.07** ($[Fe^{II}(N_2C_2H_4)_2(NCH)_2]^{2+}$), **B.11** ($[Fe^{II}(N_4H_2)_3]^{2+}$) and **B.12** ($[Fe^{II}(N_6CH_4)_2]^{2+}$) are not directly based on literature, but try to mimic motifs found in other SCO complexes, while using a minimal amount of atoms. **B.08** ($[Fe^{II}(NCH)_6]^{2+}$) is an-

other well studied Fe^{II} SCO complex [160]. Both **B.09** ($[Fe^{II}(N_2C_2H_4)_3]^{2+}$) and **B.10** ($[Fe^{II}(N_2C_2H_8)_3]^{2+}$) are based upon structures found in another work benchmarking quantum chemistry methods for Fe^{II} complexes [161].

For systems where no structures from previous studies were available the initial guess was obtained by placing the atoms in the expected positions by hand. All of the structures were optimized with the CP-PAW code package [85, 86] using the PBE0r functional with 12.5% HF exchange, in the same manner as described in 4.1.

Figures 5.1 and 5.2 show all of the model systems in both HS and LS state constructed for this study. The structures are also presented in XYZ format in appendix C, except for the $[Fe^{II}(NH_3)_6]^{2+}$ variants (**B.01**, **B.02** and **B.03**), which are given in appendix B. Not all of the new model systems could be used in the end, for reasons that will be discussed in the next sections.

5.3 Coupled-cluster benchmark calculations

Even though the new model systems presented here are only slightly larger when compared to the $[Fe^{II}(NH_3)_6]^{2+}$complex, they are already too large to be effectively analysed with the canonical coupled cluster (CC) method discussed in 4.3. Instead, a local CC variant was applied, using the PNO-UCCSD(T)-F12b method [183] and the 3*A(LOC,FIX) ansatz [184, 185]. The other aspects of the calculations were kept identical, i.e. additional CABS singles correction and scaling of the perturbative triples were applied [152]. The method-specific cc-pVTZ-F12 basis sets were used for the ligands [153], while the aug-cc-pwCVTZ basis was chosen for iron [154] to allow for adequate recovery of the 3s3p correlation. Following the prior work on explicit correlation methods on transition metal complexes from Bross *et al.* [155], their aug-cc-pwCVTZ/MP2FIT was utilized as the density fitting basis and as the CABS for the resolution of identity. For the density fitting of the Fock matrices def2-QZVPP [156] was used. The Hartree-Fock calculations for the recovery of the relativistic contributions to the F12B energy were performed using a cc-pwCVQZ-DK/cc-pwCVQZ [154] basis for iron and cc-pVQZ-DK/cc-pVQZ [157] for the remainder.

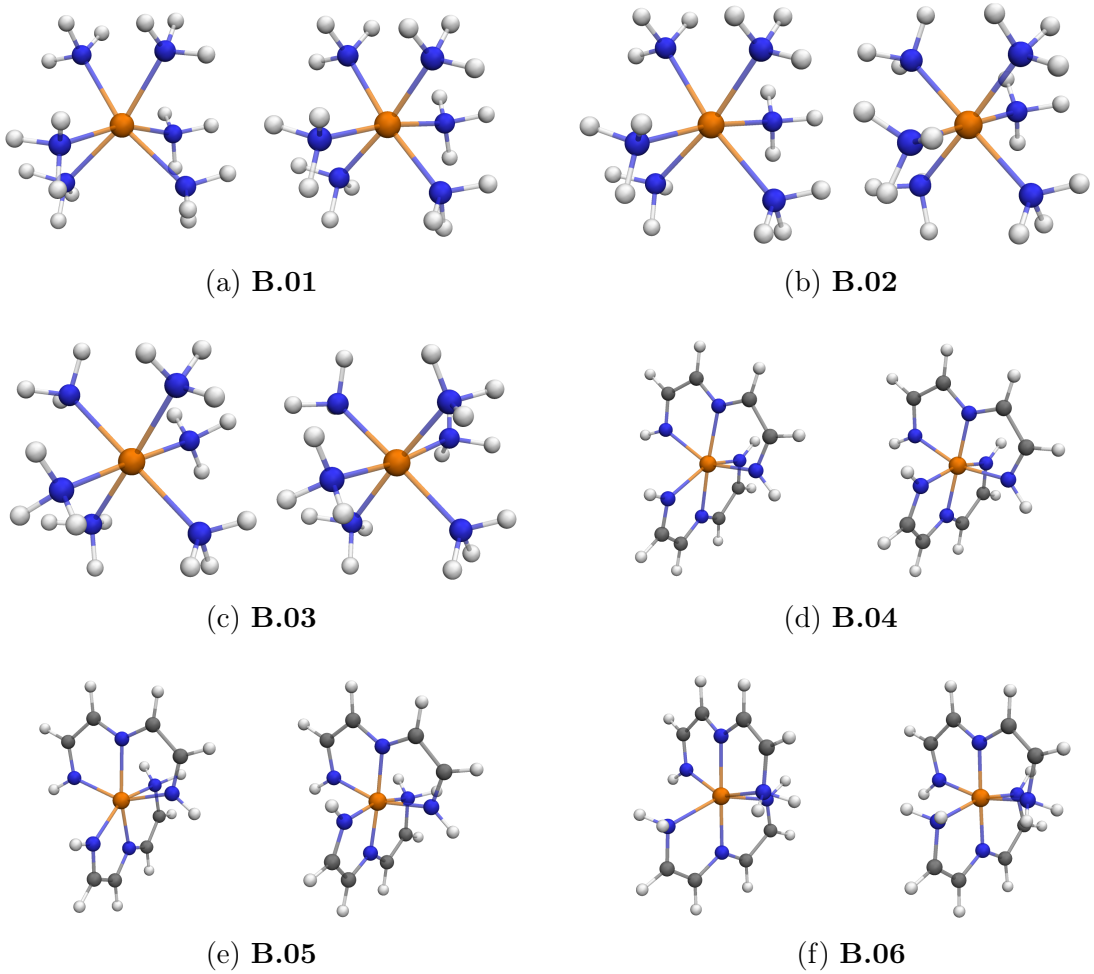

(a) **B.01** (b) **B.02**

(c) **B.03** (d) **B.04**

(e) **B.05** (f) **B.06**

Figure 5.1: First half of the DFT optimized molecular structures of the new model set. HS systems are on the left and LS systems on the right for each pair. Fe atoms are orange, C grey, H white, N blue. Visualized with PyMOL [27].

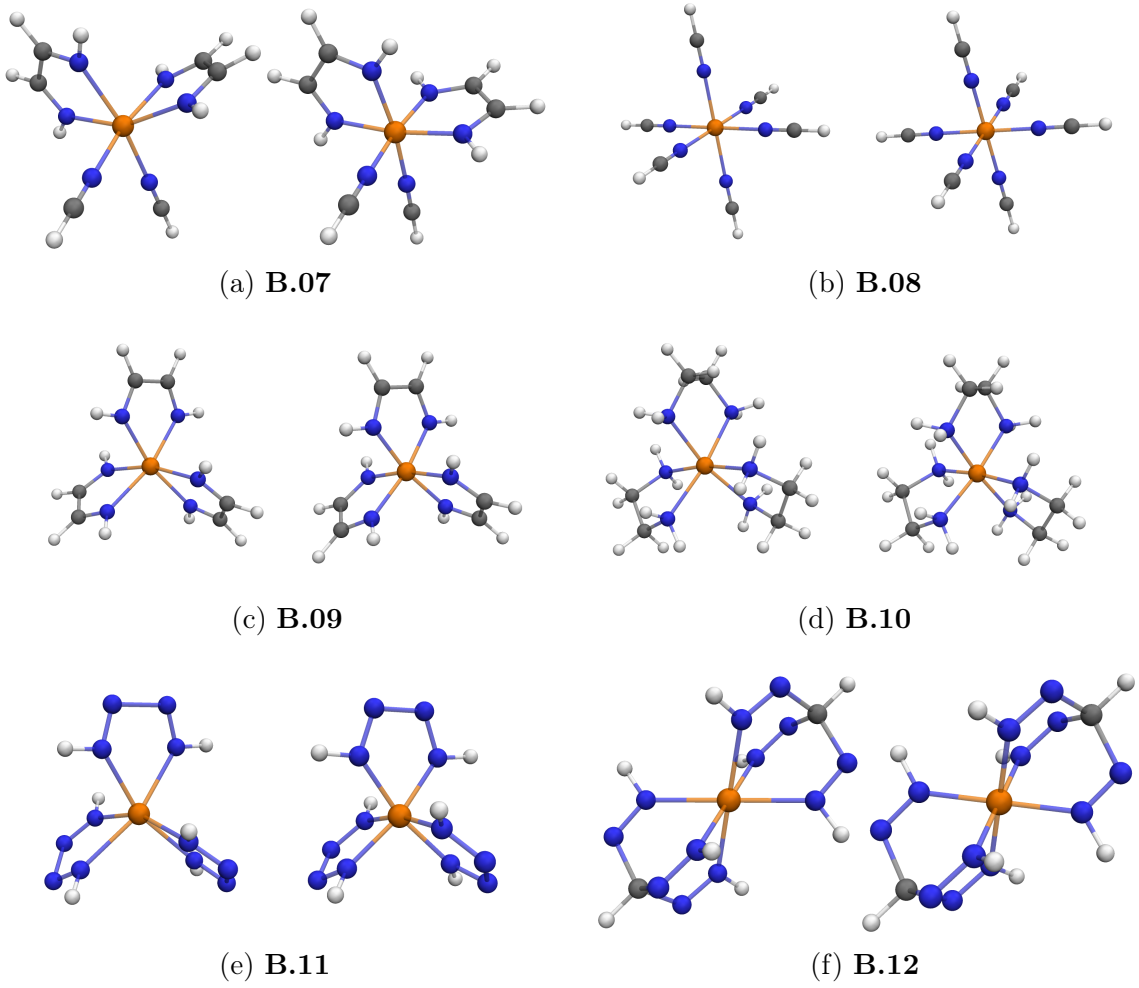

(a) **B.07** (b) **B.08**

(c) **B.09** (d) **B.10**

(e) **B.11** (f) **B.12**

Figure 5.2: Second half of the DFT optimized molecular structures of the new model set. HS systems are on the left and LS systems on the right for each pair. Fe atoms are orange, C grey, H white, N blue. Visualized with PyMOL [27].

For complexes **B.11** and **B.12** it was not possible to converge the benchmark calculations, making them unusable for the BO procedure. It can be noted that both complexes contain N-N double bonds, possible hinting at an issue in the local CC method for describing this specific kind of environment. For the purposes of this study it was deemed acceptable to disregard these two complexes, since multidentate ligands connected by N-N double bonds are a relatively rare motif. Aromatic motifs containing N-N bonds exist of course, but including such structures would make applying the local CC benchmark method impossible due to the extraneous number of electrons in the system.

The local CC benchmark method was applied to an unconstrained $[Fe^{II}(NH_3)_6]^{2+}$ system as well, the structure of which can be found in the appendix C. The ΔE_{HL} results from the benchmark calculations for all new systems are presented in table 5.1. The values from the canonical CC calculations will continue to be used as a benchmark for **B.01**, **B.02** and **B.03**.

		LCCSD(T*)-F12	RHF-DK	RHF	CABS	$\Delta E_{\mathrm{HL}}^{CC}$ (kcal/mol)
$[Fe^{II}(NH_3)_6]^{2+}$	HS (Eh)	-1601.826259	-1608.509538	-1599.458712	-0.005658	-13.334787
	LS (Eh)	-1601.800598	-1608.386071	-1599.331218	-0.006042	
	ΔDK (kcal/mol)		-77.476347	-80.003598		
	ΔE_{HL} (kcal/mol)	-16.102745	2.527251		0.240707	
B.04	HS (Eh)	-1902.968391	-1908.452693	-1899.283187	-0.005661	6.263247
	LS (Eh)	-1902.972485	-1908.312563	-1899.137561	-0.006052	
	ΔDK (kcal/mol)		-87.932959	-91.381567		
	ΔE_{HL} (kcal/mol)	2.569346	3.448608		0.245293	
B.05	HS (Eh)	-1903.368902	-1908.862096	-1899.691886	-0.005919	13.638622
	LS (Eh)	-1903.385002	-1908.731506	-1899.556034	-0.006292	
	ΔDK (kcal/mol)		-81.946745	-85.248581		
	ΔE_{HL} (kcal/mol)	10.102891	3.301836		0.233896	
B.06	HS (Eh)	-1903.642238	-1909.176740	-1900.007368	-0.006199	6.494444
	LS (Eh)	-1903.646506	-1909.032461	-1899.857358	-0.006550	
	ΔDK (kcal/mol)		-90.536697	-94.132559		
	ΔE_{HL} (kcal/mol)	2.678452	3.595862		0.220130	
B.07	HS (Eh)	-1825.117842	-1831.076651	-1821.936227	-0.005060	0.969483
	LS (Eh)	-1825.112716	-1830.924102	-1821.777390	-0.005443	
	ΔDK (kcal/mol)		-95.725659	-99.671715		
	ΔE_{HL} (kcal/mol)	-3.216887	3.946056		0.240314	
B.08	HS (Eh)	-1822.648883	-1828.735697	-1819.594664	-0.004270	-10.115045
	LS (Eh)	-1822.625844	-1828.577184	-1819.429608	-0.004646	
	ΔDK (kcal/mol)		-99.468370	-103.574342		
	ΔE_{HL} (kcal/mol)	-14.456795	4.105972		0.235778	
B.09	HS (Eh)	-1826.345118	-1832.244308	-1823.104186	-0.005457	10.944690
	LS (Eh)	-1826.356049	-1832.095464	-1822.949223	-0.005849	
	ΔDK (kcal/mol)		-93.400993	-97.240574		
	ΔE_{HL} (kcal/mol)	6.859455	3.839582		0.245653	
B.10	HS (Eh)	-1833.702527	-1839.342058	-1830.203211	-0.007130	-4.986031
	LS (Eh)	-1833.690037	-1839.223389	-1830.080331	-0.007464	
	ΔDK (kcal/mol)		-74.466064	-77.108233		
	ΔE_{HL} (kcal/mol)	-7.837831	2.642169		0.209630	
B.11	HS (Eh)	-1922.195052	-1927.877520	-1918.650616	-0.006288	29.892710
	LS (Eh)	-1922.235034	-1927.764655	-1918.530904	-0.007096	
	ΔDK (kcal/mol)		-70.823850	-75.120488		
	ΔE_{HL} (kcal/mol)	25.089071	4.296638		0.507001	
B.12	HS (Eh)	-1999.570517	-2004.247369	-1994.994416	-0.006983	38.078849
	LS (Eh)	-1999.621822	-2004.809083	-1995.547150	-0.007380	
	ΔDK (kcal/mol)		352.480961	346.845433		
	ΔE_{HL} (kcal/mol)	32.194219	5.635528		0.249102	

Table 5.1: Detailed breakdown of energy composition from local CCSD(T*)-F12B calculations for $[Fe^{II}(NH_3)_6]^{2+}$ and the extended model set.

5.4 Bayesian optimization

No major changes were made to the BO procedure as it has been presented in 4.5. However, the HF exchange factor regarding H atoms was permanently set to 12.5% to reduce the dimensionality of the fitting problem to only 3 parameters, i.e. the Fe, N and C HF exchange percentages. As discussed previously, the H HF exchange percentage is found to have a negligible contribution to the total effect on the ΔE_{HL}.

5.4.1 Results for complete model set

The result from the Bayesian optimization procedure for the complete extended model set is shown in figure 5.3. Each point reflects an iteration of the procedure, with a unique set of parameters and resulting RMSE. The color gradient is derived from the mean of the Gaussian process regression, reflecting the predicted RMSE values inbetween sampled points, with the darkest hue corresponding to the best result. While the parameter for the HF exchange of the C atoms was part of the fitting procedure, it became apparent that it had little influence on the quality of the fit. The distribution of the sampled points also becomes much easier to evaluate when reduced to two dimensions, which is why the results from the Bayesian optimizations will be presented in this manner.

The best performing iteration had an RMSE of 10.47 kcal/mol and used HF exchange factors of 10.4% for Fe, 6.4% for N and 5.0% for C. Using these factors to evaluate the ΔE_{HL} of the (unconstrained) $[Fe^{II}(NH_3)_6]^{2+}$ yielded a result of -14.42 kcal/mol. These values are shown and reviewed in table 5.4 in the discussion 5.5.

Cross-validation

To evaluate the performance of the procedure and specifically the extended model set, a cross-validation was carried out. In this approach, also referred to as "leave-one-out" validation, the model set is divided into training and test sets. The training set contains all model systems except for one, which is instead contained in the test set. Using only the training set, the Bayesian optimization procedure is carried out. The resulting set of HF exchange parameters, optimal for this specific training set, can then be used to compute the $\Delta E_{\mathrm{HL}}^{\mathrm{BO}}$ of the test set complex. Comparing the

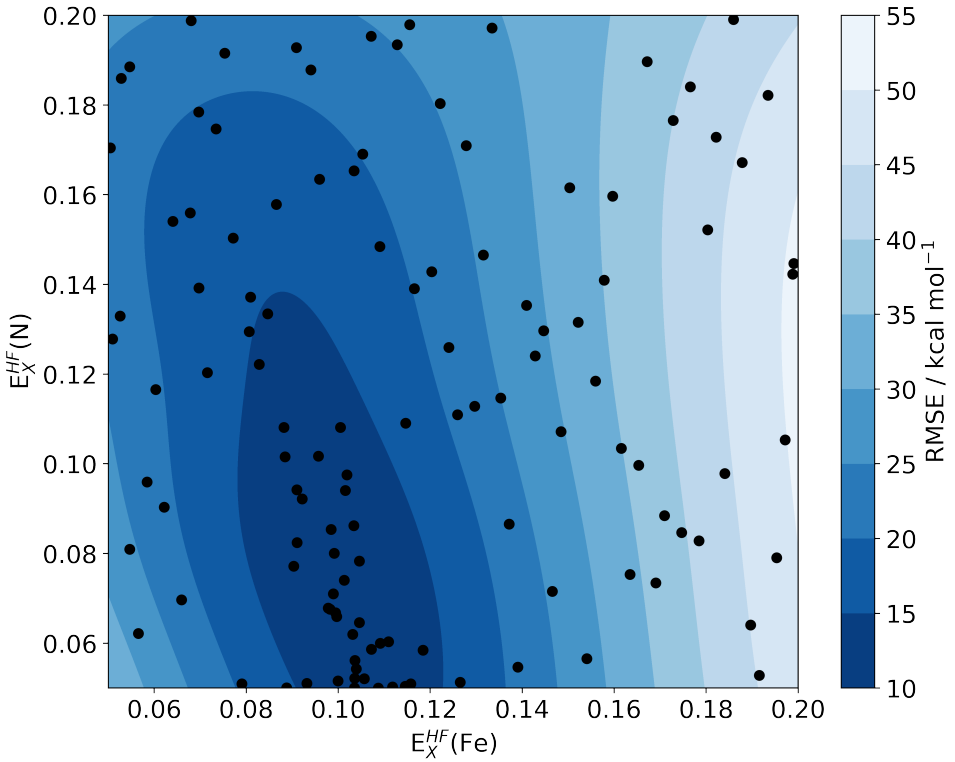

Figure 5.3: 2D representation of the result of the BO procedure using the extended (10) model set. Each point reflects an iteration, with a unique set of HF exchange parameters and resulting RMSE. The color gradient is derived from the mean of the Gaussian process regression, reflecting the predicted RMSE values inbetween sampled points.

result can to $\Delta E_{\mathrm{HL}}^{\mathrm{CC}}$ (from the CC benchmark) provides insight into the whether the fit based on this subset of model complex would be useful for the description of the complex placed in the test set. This was repeated for all 10 systems of the extended model set, placing each of them in the test set in turn. The results are presented in table 5.2.

Test set system	RMSE (kcal/mol)	E_X^{HF}(Fe)	E_X^{HF}(N)	E_X^{HF}(C)	$\Delta E_{\mathrm{HL}}^{\mathrm{BO}}$ (kcal/mol)	$\Delta E_{\mathrm{HL}}^{\mathrm{CC}}$ (kcal/mol)	$\Delta\Delta E_{\mathrm{HL}}$ (kcal/mol)
B.01	10.18	0.106	0.053	0.050	-7.40	-4.27	-3.13
B.02	10.25	0.105	0.050	0.050	-11.98	-9.42	-2.56
B.03	10.22	0.104	0.055	0.050	-15.46	-12.91	-2.55
B.04	10.02	0.106	0.058	0.050	2.02	6.26	-4.25
B.05	8.79	0.105	0.069	0.050	5.23	13.64	-8.41
B.06	10.39	0.102	0.060	0.050	7.47	6.49	0.98
B.07	9.50	0.098	0.064	0.050	7.75	0.97	6.78
B.08	7.50	0.100	0.057	0.050	0.53	-10.12	10.65
B.09	10.32	0.104	0.050	0.050	13.40	10.94	2.45
B.10	10.33	0.106	0.050	0.051	-7.06	-4.99	-2.07

Table 5.2: Results from Bayesian optimization procedures (as described in 4.5) in the attempt to cross-validate the extended model set. The "Test set system" column denotes the system left out of the training set. The RMSE is the discrepancy between BO and CC benchmark ΔE_{HL} values for the best iteration, and can be taken as the measure of quality of the fit. E_X^{HF} are the corresponding HF exchange parameters. $\Delta E_{\mathrm{HL}}^{\mathrm{BO}}$ values are the ΔE_{HL} for the test set system, computed with the HF factors derived from the Bayesian optimization of the training set. $\Delta E_{\mathrm{HL}}^{\mathrm{CC}}$ values are the ΔE_{HL} for the test set system, computed with the CC benchmark method. $\Delta\Delta E_{\mathrm{HL}}$ values are the difference between $\Delta E_{\mathrm{HL}}^{\mathrm{BO}}$ and $\Delta E_{\mathrm{HL}}^{\mathrm{CC}}$.

The RMSE values are for the most part consistent, with notable exceptions for **B.05**, **B.08**, and **B.07** to a lesser degree. The HF exchange parameter varies by less than 1% for Fe atoms and less than 2% for N atoms. For C it is almost completely consistent at 5%, the lower bound of the parameterization. The $\Delta\Delta E_{\mathrm{HL}}$ values show that for most systems of the extended model set, they are quite well represented by their respective training set. There is a discrepancy of less than 5 kcal/mol between values from coupled-cluster calculations and from the DFT calculations, parameterized with the results from the BO procedure. The notable exceptions are again **B.05**, **B.08**, and **B.07**.

5.4.2 Reduced model set

Since the exclusion of **B.05** and **B.08** yielded the largest reduction of the RMSE, another BO procedure was carried out with the remaining 8 model systems. The results are shown in figure 5.4. The best performing iteration had an RMSE of 5.64 kcal/mol and used HF exchange factors of 9.5% for Fe, 8.4% for N and 5.0% for C. Using these factors to evaluate the ΔE_{HL} of the (unconstrained) $[\mathrm{Fe^{II}(NH_3)_6}]^{2+}$ yielded a result of -12.52 kcal/mol. These values are shown and discussed further in table 5.4. The cross-validation was repeated for this reduced model set as well, with the results presented in table 5.3.

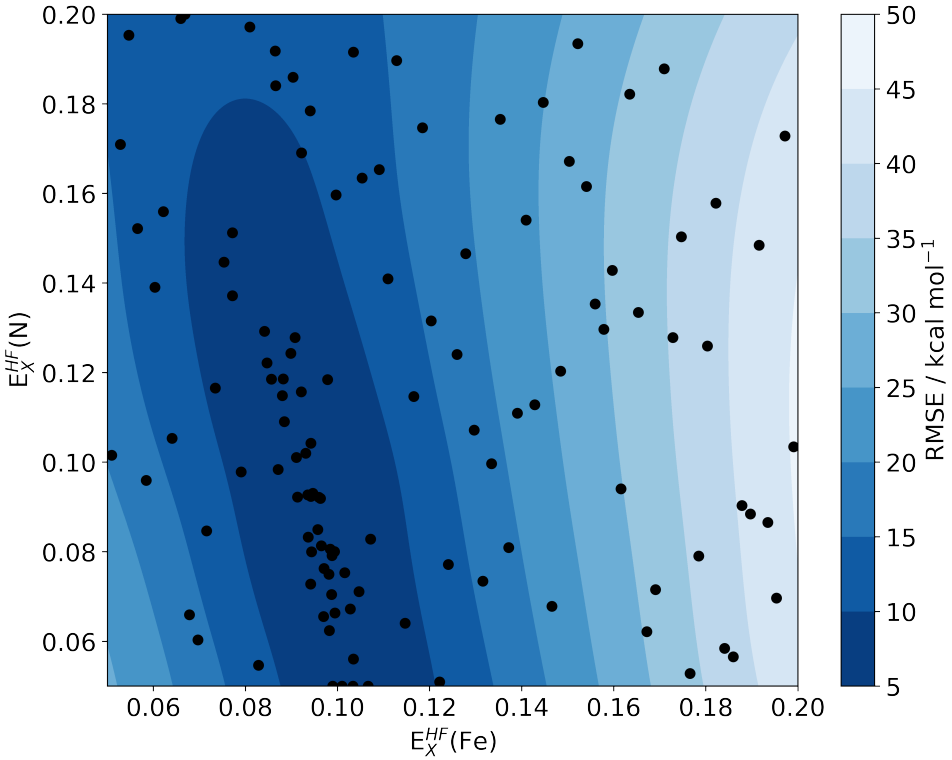

Figure 5.4: 2D representation of the result of the BO procedure using the reduced (8) model set. Each point reflects an iteration, with a unique set of HF exchange parameters and resulting RMSE. The color gradient is derived from the mean of the Gaussian process regression, reflecting the predicted RMSE values inbetween sampled points.

Test set system	RMSE (kcal/mol)	E_X^{HF}(Fe)	E_X^{HF}(N)	E_X^{HF}(C)	$\Delta E_{\mathrm{HL}}^{\mathrm{BO}}$ (kcal/mol)	$\Delta E_{\mathrm{HL}}^{\mathrm{CC}}$ (kcal/mol)	$\Delta\Delta E_{\mathrm{HL}}$ (kcal/mol)
B.01	5.477	0.098	0.078	0.054	-6.345	-4.268	-2.078
B.02	5.544	0.098	0.079	0.05	-10.980	-9.422	-1.558
B.03	5.560	0.098	0.077	0.066	-14.922	-12.910	-2.012
B.04	4.624	0.092	0.104	0.052	1.503	6.263	-4.760
B.06	5.608	0.095	0.086	0.05	7.391	6.494	0.897
B.07	2.690	0.091	0.087	0.192	10.069	0.970	9.100
B.09	5.606	0.094	0.086	0.05	12.292	10.945	1.347
B.10	5.640	0.095	0.089	0.05	-5.082	-4.986	-0.096

Table 5.3: Results from Bayesian optimization procedures (as described in 4.5) in the attempt to cross-validate the reduced model set. The "Test set system" column denotes the system left out of the training set. The RMSE is the discrepancy between BO and CC benchmark ΔE_{HL} values for the best iteration, and can be taken as the measure of quality of the fit. E_X^{HF} are the corresponding HF exchange parameters. $\Delta E_{\mathrm{HL}}^{\mathrm{BO}}$ values are the ΔE_{HL} for the test set system, computed with the HF factors derived from the Bayesian optimization of the training set. $\Delta E_{\mathrm{HL}}^{\mathrm{CC}}$ values are the ΔE_{HL} for the test set system, computed with the CC benchmark method. $\Delta\Delta E_{\mathrm{HL}}$ values are the difference between $\Delta E_{\mathrm{HL}}^{\mathrm{BO}}$ and $\Delta E_{\mathrm{HL}}^{\mathrm{CC}}$.

Eliminating **B.05** and **B.08** significantly reduces the RMSE for all training sets. The RMSE and exchange parameters are quite consistent, with the exception of **B.07**, which was to be expected. The reduction of the RMSE when moving **B.07** to the test set is even bigger than before (as shown in table 5.2), meaning that the relative discrepancy of **B.07** to the training set is bigger. It is also the only system for which $\Delta\Delta E_{\mathrm{HL}}$ has significantly increased relative to the values from the cross-validation of the complete extended set.

Since the training set without **B.07** had such a significant reduction of the RMSE, the HF exchange parameters of the best iteration (9.1% for Fe atoms, 8.7% for N atoms and 19.2% for C atoms) were used to compute the ΔE_{HL} of the (unconstrained) $[Fe^{II}(NH_3)_6]^{2+}$ once more. This yielded a result of $\Delta E_{\mathrm{HL}} = -11.75$ kcal/mol. These values are shown and discussed further in table 5.4.

Figures with 2D representations of the result of the BO procedures for all cross-validation training sets, for both extended and reduced model set, can be found in the appendix C.

5.5 Discussion

The previously mentioned results for the BO procedure applied to the "extended", the "reduced" and the "minimized" model set are summarized in table 5.4 for the sake of comparison.

Model set	RMSE (kcal/mol)	E_X^{HF}(Fe)	E_X^{HF}(N)	E_X^{HF}(C)	$\Delta E_{\mathrm{HL}}^{\mathrm{BO}}$ (kcal/mol)
Extended (10 systems)	10.47	0.104	0.064	0.050	-14.42
Reduced (8 systems)	5.64	0.095	0.084	0.050	-12.52
Minimized (7 systems)	2.69	0.091	0.087	0.192	-11.75

Table 5.4: Results from the BO procedure for the different model sets. Shown are the RMSE as a measure of the quality of the fit, the predicted optimal exchange parameters E_X^{HF} for each atom species, and the ΔE_{HL} for $[Fe^{II}(NH_3)_6]^{2+}$ when computed by the PBE0r functional using the respective E_X^{HF}.

These results can now be compared to the $\Delta E_{\mathrm{HL}}^{\mathrm{CC}}$ of the unconstrained $[\mathrm{Fe^{II}(NH_3)_6}]^{2+}$ system computed with the local CC variant, which amounts to -13.33 kcal/mol (see 5.1). Removing **B.05** and **B.08** from the extended set not only lowers the RMSE significantly, but also produces a $\Delta E_{\mathrm{HL}}^{\mathrm{BO}}$ in better agreement to the benchmark $\Delta E_{\mathrm{HL}}^{\mathrm{CC}}$. It has to be said that the difference in agreement is rather small, with $\Delta\Delta E_{\mathrm{HL}} = 1.09$ kcal/mol for the extended set, and $\Delta\Delta E_{\mathrm{HL}} = -0.81$ kcal/mol for the reduced set. Removing **B.07** lowers the RMSE again, but the deviation to $\Delta E_{\mathrm{HL}}^{\mathrm{CC}}$ of the unconstrained $[\mathrm{Fe^{II}(NH_3)_6}]^{2+}$ is increased, with $\Delta\Delta E_{\mathrm{HL}} = -1.58$ kcal/mol. This demonstrates that the RMSE can only be taken as measure of the internal cohesion of a given model set, and not necessarily be relied upon to mark the quality of the end result. It can be noted that Neese and coworkers reported a result of -11.3 kcal/mol for the ΔE_{HL} of $[\mathrm{Fe^{II}(NH_3)_6}]^{2+}$, though this was achieved with a DLPNO-CCSD(T) coupled-cluster variant [160].

These results demonstrate that it is possible to achieve a deviation smaller than 1.0 kcal/mol to the coupled-cluster benchmark values, but that the correct choice of model systems is of utmost importance. While it is possible to improve the model set by "pruning" systems which contribute to a bad fit, this improvement is not entirely self-reliant. Without knowledge of the desired $\Delta E_{\mathrm{HL}}^{\mathrm{CC}}$ of the unconstrained $[\mathrm{Fe^{II}(NH_3)_6}]^{2+}$ it would be hard to tell whether the reduced set or the minimized set produced better results. It also has to be noted that this result, and the respective HF exchange factors, are only optimal for $[\mathrm{Fe^{II}(NH_3)_6}]^{2+}$, and not necessarily for $\mathrm{Fe^{II}}$ SCO complexes in general. This will become evident in the following chapter 6, which aims to describe the spin states of a [2x2] $\mathrm{Fe^{II}}$ grid complex.

Regardless, as already discussed in chapter 4, the vast majority of commonly used DFT functionals yield results with much greater deviation to those of coupled-cluster level of theory. For this reason, the Bayesian optimization procedure can be considered a significant improvement, which is also transferable to target systems with different charges, ligand structures, or transition metal centers.

Chapter 6

Application toward the [2x2] Fe^{II} grid complex

6.1 Introduction

This chapter aims to use the Bayesian optimization procedure, which was established in chapter 4 and improved upon in chapter 5, to describe the spin states of a [2x2] Fe^{II} grid complex, already mentioned briefly in the introduction 1, and depicted in figure 6.1. This complex has been first synthesized by Meyer and coworkers in 2010 [30] and extensively characterized with experimental methods [186–188]. Especially useful for this investigation is a measurement of the dependence of the magnetic susceptibility on the temperature, reported by Benjamin Schneider and shown in figure 6.2. It clearly demonstrates the complex going through multiple successive SCO events upon cooling down from room temperature. Knowledge of this temperature dependency also enables some thermodynamic considerations. Since $\chi_M T$ can be correlated to the fraction of Fe cores in the HS state, 6.2 allows for an assessment of the equilibrium temperature $T_{1/2}$ for the first two spin transition events. From this the complete ΔH for the transition from $(Fe_{HS})_4$ to $(Fe_{LS})_4$ can be estimated at 6 kcal/mol [189].

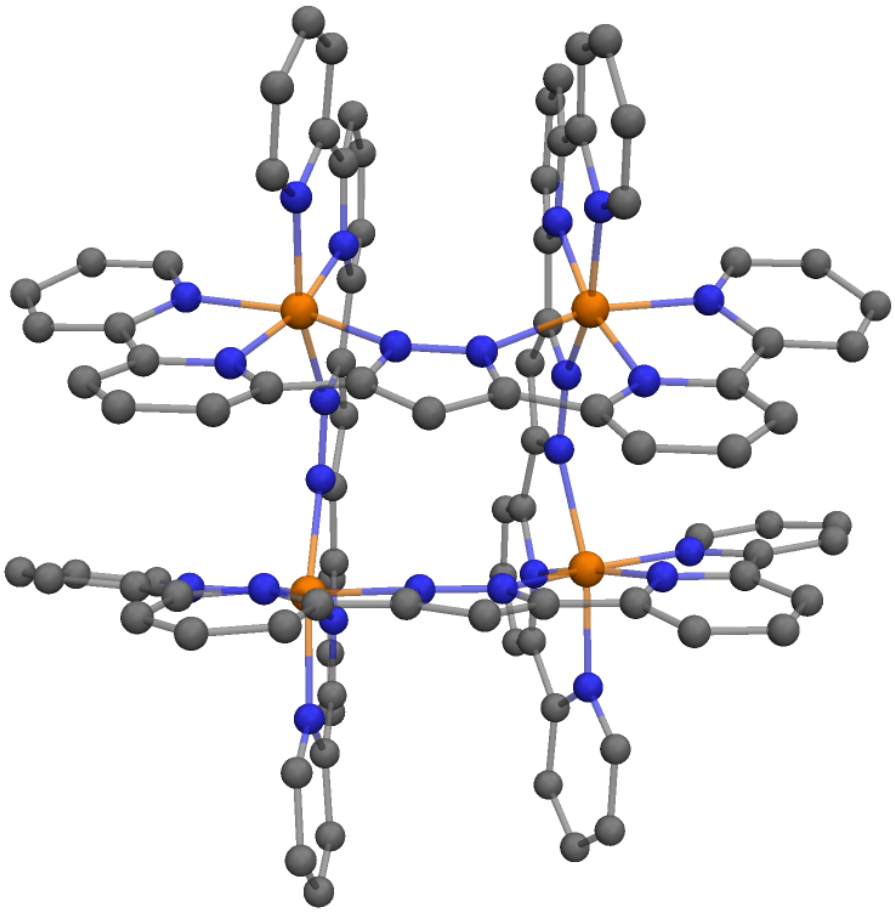

Figure 6.1: Molecular structure of the [2x2] Fe^{II} grid complex. Fe atoms are orange, C grey, N blue. H atoms are omitted for clarity. Visualized with PyMOL [27].

Theoretical studies of this complex [178] and of similar ones [190] have been less extensive so far. This is not surprising, since the size of the system and the intricacies of SCO capable transition metals complicate any approach aiming to calculate energetic states to a reasonable degree of accuracy.

As shown in figure 6.1, the complex consists of four Fe^{II} atoms in arranged in a square-shaped configuration, which are bridged by four pyrazolate-based ligands. Each ligand coordinates to two Fe^{II} atoms simultaneously through its tridentate binding pockets, such that every Fe atom is surrounded by a roughly octahedral $\{N\}_6$ environment. When discussing the separate Fe cores of the [2x2] Fe^{II} grid complex, they are noted as Fe_1, Fe_2, Fe_3 and Fe_4. For this investigation these cores

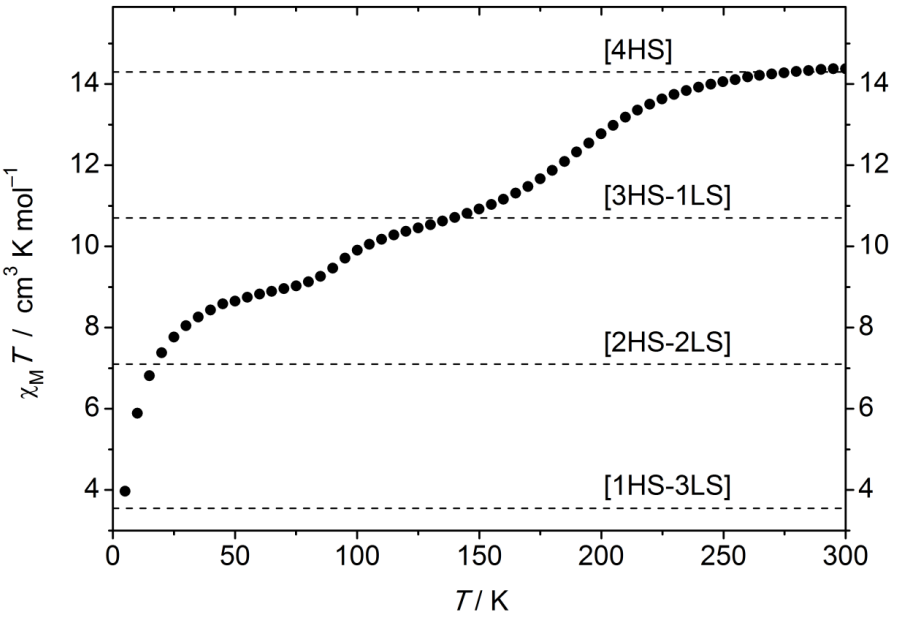

Figure 6.2: Temperature dependence of $\chi_M T$ for the [2x2] Fe^{II} grid complex. Expected values for the different spin states are marked with the dotted lines. Reported by Benjamin Schneider [188].

are assumed to be interchangeable, and their absolute position irrelevant. However, Fe_1 always is positioned across from Fe_3, and adjacent to Fe_2 and Fe_4. The total charge of the complex is 4+, since each pyrazolate-based ligand carries a charge of 1−. Stepwise oxidation of the Fe^{II} cores has been achieved as well, leading to mixed-valent and even a fully oxidized [2x2] Fe^{III} grid complex [30, 186]. Since only Fe^{II} states are considered in this work, the total charge of 4+ for the complex is dropped throughout.

6.2 Preparation of the grid complex structures

The basic structure of the grid complex was taken from earlier studies by Ingolf Harden, under the supervisison of Peter Blöchl. It was then re-optimized, using the latest CP-PAW code version at that time [1], and taking dispersion forces into

[1]Development version, revision 1216, latest changes at 19.01.2019

account. The PBE0r functional was employed for these optimizations, using 6% HF exchange for all atom types. 6% HF exchange can be considered a roughly correct amount, which is sufficient for the structural optimization, since the influence of the exchange factor on the geometries is negligible. An example for the input file of such an optimization can be found in the appendix D.

Because the spin state of the Fe atom has a significant impact on the surrounding structure (see 1), each spin state permutation has to be considered a unique system, and its structure optimized separately. It is assumed that for a given spin state all variants are interchangeable, e.g. for $(Fe_{HS})_1(Fe_{LS})_3$ it is irrelevant whether it is the Fe_1, Fe_2, Fe_3 or Fe_4 in the HS state. However, for $(Fe_{HS})_2(Fe_{LS})_2$ there are two distinguishable configurations: *cis*, where the two Fe cores in the HS state are next to each other, and *trans*, where the two cores are apart. Thus there are 6 systems under consideration in this work: $(Fe_{LS})_4$, $(Fe_{HS})_1(Fe_{LS})_3$, *cis*-$(Fe_{HS})_2(Fe_{LS})_2$, *trans*-$(Fe_{HS})_2(Fe_{LS})_2$, $(Fe_{HS})_3(Fe_{LS})_1$ and $(Fe_{HS})_4$.

Converging the systems to the intended spin state is non-trivial. As can be seen in the appendix D, the input file includes the total spin S of the system (in $\hbar$). Each LS Fe^{II} core contributes 0.0 to this value, while each HS$\uparrow$ Fe^{II} core raises the value by 2.0 $\hbar$. However, an HS$\downarrow$ Fe^{II} core would also lower this value by 2.0 $\hbar$, and while the $\uparrow/\downarrow$ designation is arbitrary, the two spin directions cancel each other out in regard to the total spin S. This has the effect that, for example, while trying to converge the electronic structure of $(Fe_{LS})_4$ with total S=0.0 $\hbar$, one might instead converge upon a state like $(Fe_{HS\downarrow})(Fe_{HS\uparrow})(Fe_{HS\downarrow})(Fe_{HS\uparrow})$, which is also a (local) minimum. Even though $(Fe_{LS})_4$ is energetically more stable, converging from a state like $(Fe_{HS\downarrow})(Fe_{HS\uparrow})(Fe_{HS\downarrow})(Fe_{HS\uparrow})$ to $(Fe_{LS})_4$ is highly improbable, since it would entail the simultaneous spin crossover event on all 4 Fe cores, changing from their HS states to LS. This issue can be somewhat alleviated by placing an external potential upon all Fe d-orbitals, orientating them in the same spin direction before the structure optimization. This reduces the likelihood of the occurrence of unintended spin states, but it is still a possibility, as can be observed below.

Density of states visualization

The electronic structure obtained from the optimizations can be visualized by the Kohn-Sham density of states (DOS), which provide information about the orbital occupations. This can be qualitatively compared to experimental observations. Since the DOS is quite unique to the system and its spin state, it can also be used as a "fingerprint". By comparing the results from a calculation with another it is possible to make sure that the intended spin state has been converged upon. The two extreme cases, $(Fe_{LS})_4$ and $(Fe_{HS})_4$, can serve as a benchmark. For the sake of completion their total DOS is depicted in 6.3.

The Fermi level (i.e. the HOMO energy) can be observed here, at -12.14 eV for $(Fe_{LS})_4$, and -11.77 eV for $(Fe_{HS})_4$. The DOS at this level is almost exclusively constructed from Fe d-states. The band gap can also be observed, separating the occupied (valence) states from the unoccupied (conduction) states. For $(Fe_{HS})_4$ the band gap amounts to 0.86 eV, while for $(Fe_{LS})_4$ it is 1.77 eV. It can be noted that for $(Fe_{LS})_4$, the d-orbitals contribute little to the unoccupied states, being eclipsed by contributions from the ligand structure. For $(Fe_{HS})_4$ the opposite is true, with the Fe d-orbitals contributing much more density. Separating the contributions from t_{2g} and e_g orbitals, as shown in the following figures (6.4-6.6a), demonstrates that specifically the t_{2g} orbitals (in green) are mainly responsible.

Plotting only the DOS of the Fe d-orbitals makes it easier to distinguish the spin states, visualizing the unique shapes of the HS states (figure 6.4a) and the LS states (figure 6.4b) of the Fe cores. It can also be observed that for $(Fe_{HS})_4$ all states have the same spin-direction ($\uparrow$).

These "fingerprints" can now be compared to the d-electron DOS of the intermediate states $(Fe_{HS})_1(Fe_{LS})_3$ (figure 6.5a), *cis*-$(Fe_{HS})_2(Fe_{LS})_2$ (figure 6.5b), *trans*-$(Fe_{HS})_2(Fe_{LS})_2$ (figure 6.5c) and $(Fe_{HS})_3(Fe_{LS})_1$ (figure 6.5d).

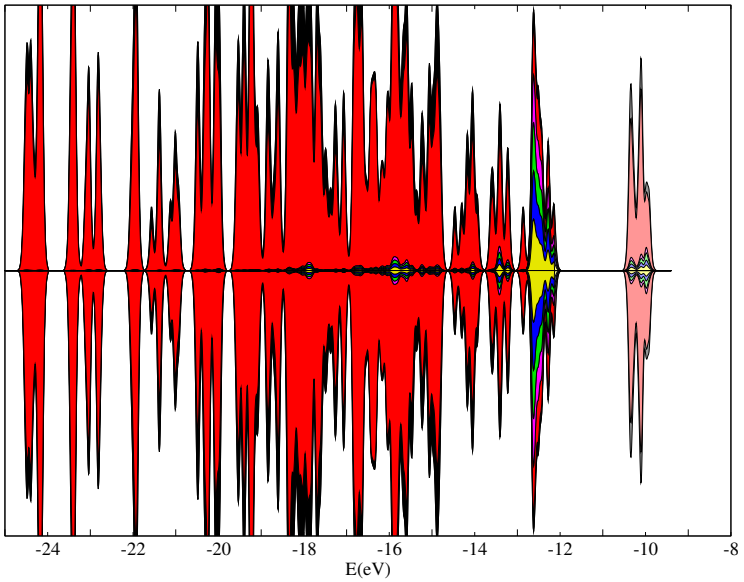

(a) $(Fe_{LS})_4$

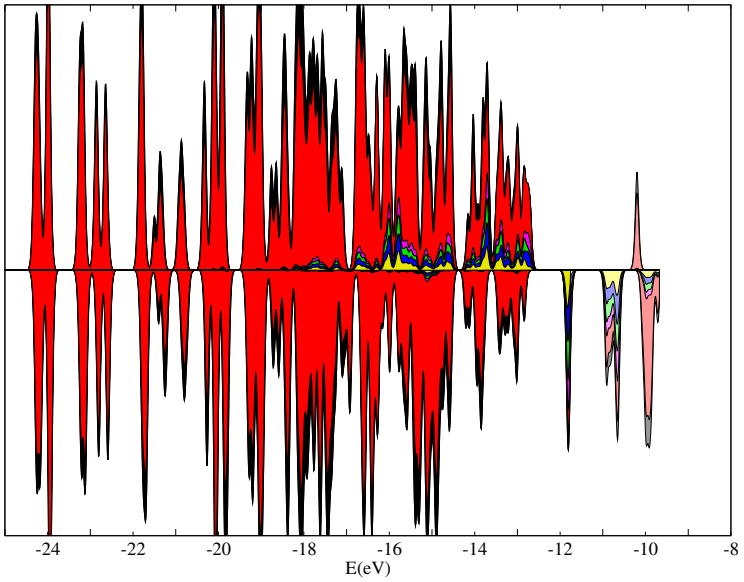

(b) $(Fe_{HS})_4$

Figure 6.3: Visualization of the DOS in the optimized (a) $(Fe_{HS})_4$ and (b) $(Fe_{LS})_4$ structure. The total DOS are colored black. The ligand DOS are colored red, while the DOS of the d-orbitals of the Fe atoms are colored yellow (Fe_1), blue (Fe_2), green (Fe_3) and magenta (Fe_4). The partial DOS plots are stacked, so that their contributions can be distinguished. Lighter colors represent unoccupied orbitals.

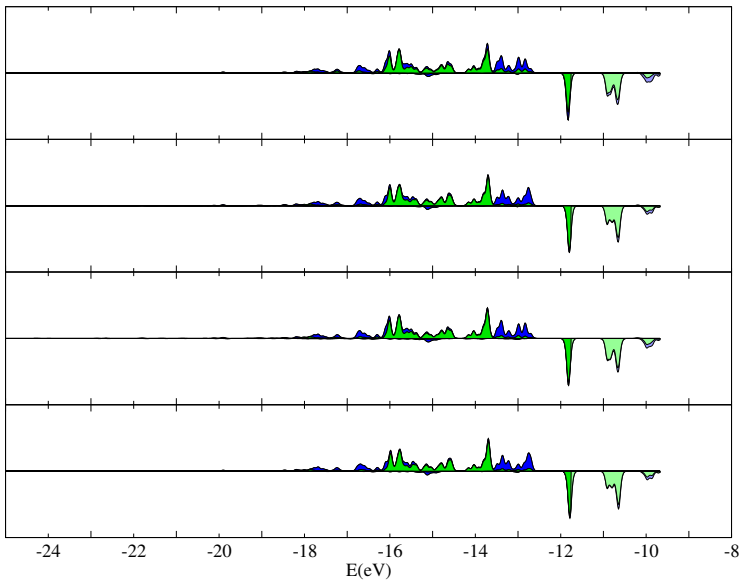

(a) $(Fe_{LS})_4$

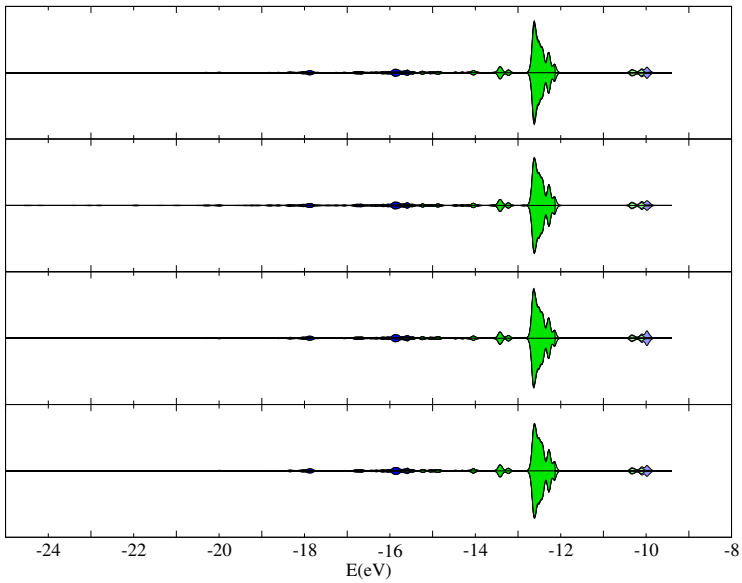

(b) $(Fe_{HS})_4$

Figure 6.4: Visualization of the DOS of the d-orbitals of the Fe atoms in the optimized (a) $(Fe_{HS})_4$ and (b) $(Fe_{LS})_4$ structure. (Fe_1) is represented by the first graph from the top, (Fe_2) by the second, (Fe_3) by the third, (Fe_4) by the last. The contributions from t_{2g} are shown in green and those from e_g in blue. Lighter colors represent unoccupied orbitals.

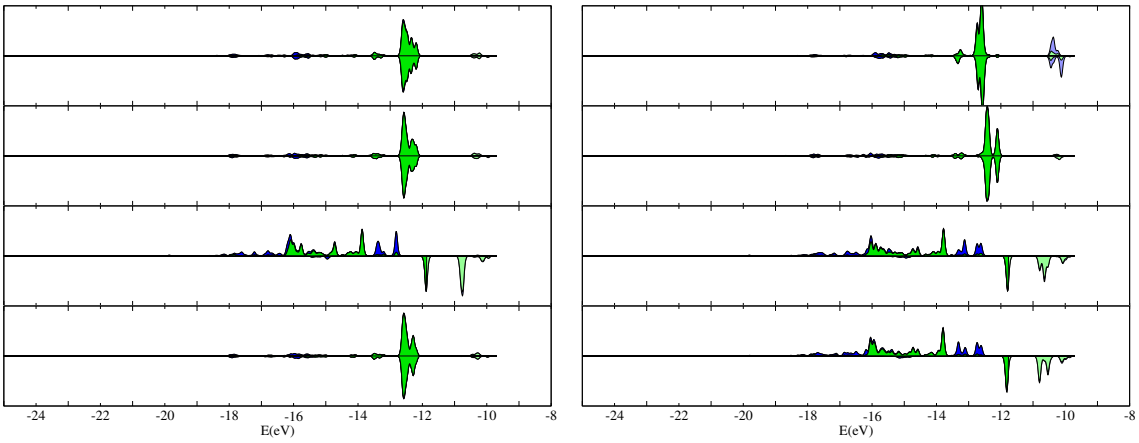

(a) $(Fe_{HS})_1(Fe_{LS})_3$

(b) *cis*-$(Fe_{HS})_2(Fe_{LS})_2$

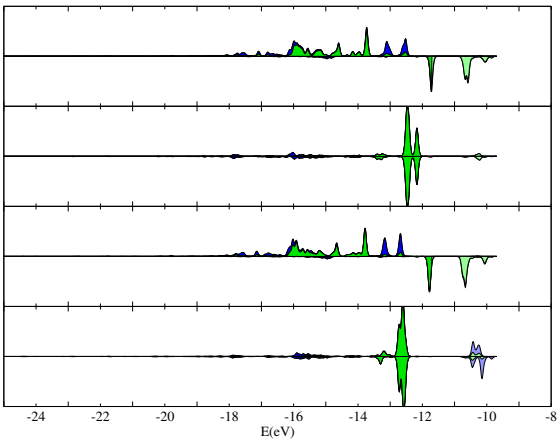

(c) *trans*-$(Fe_{HS})_2(Fe_{LS})_2$

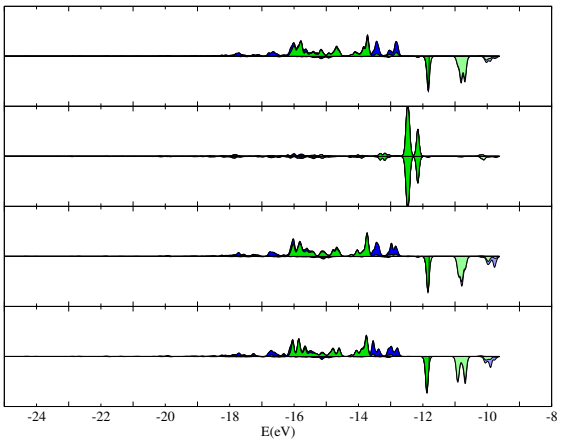

(d) $(Fe_{HS})_3(Fe_{LS})_1$

Figure 6.5: Visualization of the DOS of the d-orbitals of the Fe atoms in the optimized (a) $(Fe_{HS})_1(Fe_{LS})_3$, (b) *cis*-$(Fe_{HS})_2(Fe_{LS})_2$, (c) *trans*-$(Fe_{HS})_2(Fe_{LS})_2$ and (d) $(Fe_{HS})_3(Fe_{LS})_1$ structure. (Fe_1) is represented by the first graph from the top, (Fe_2) by the second, (Fe_3) by the third, (Fe_4) by the last. The contributions from t_{2g} are shown in green and those from e_g in blue. Lighter colors represent unoccupied orbitals.

For (6.5a) $(Fe_{HS})_1(Fe_{LS})_3$ and (6.5d) $(Fe_{HS})_3(Fe_{LS})_1$ it can be concluded that the structure optimization indeed converged upon the intended spin states. The DOS of the Fe d-orbitals look identical to those of $(Fe_{HS})_4$ and $(Fe_{LS})_4$ when it comes to HS and LS states, respectively. For (6.5a) $(Fe_{HS})_1(Fe_{LS})_3$, the single HS state is located at Fe_3, while the rest of the Fe atoms are in the LS state. For (6.5d) $(Fe_{HS})_3(Fe_{LS})_1$, the single LS state is located at Fe_3, while the rest of the Fe atoms are in the HS(↑) state.

Unfortunately, the same cannot be concluded for (6.5b) *cis*-$(Fe_{HS})_2(Fe_{LS})_2$ and (6.5c) *trans*-$(Fe_{HS})_2(Fe_{LS})_2$. Upon close inspection it can be observed that for (6.5b) *cis*-$(Fe_{HS})_2(Fe_{LS})_2$ the Fe_1 exhibits a DOS that is different from the intended LS state. The same holds for Fe_4 of (6.5c) *trans*-$(Fe_{HS})_2(Fe_{LS})_2$, which seems to have converged upon the same state, judging from the shape of the DOS. It can also be noted that both systems are significantly higher in energy than all other systems computed in this section, in contrast to experimental observations, which locate an $(Fe_{HS})_2(Fe_{LS})_2$ state between $(Fe_{HS})_3(Fe_{LS})_1$ and $(Fe_{HS})_1(Fe_{LS})_3$. From this it has to be concluded that it was not possible to converge correctly to the intended state for both *cis*-$(Fe_{HS})_2(Fe_{LS})_2$ and *trans*-$(Fe_{HS})_2(Fe_{LS})_2$. The converged structures for $(Fe_{LS})_4$, $(Fe_{HS})_1(Fe_{LS})_3$, $(Fe_{HS})_3(Fe_{LS})_1$ and $(Fe_{HS})_4$ however are presented in XYZ format in appendix D.

Figure 6.6a depicts the DOS of the Fe d-orbitals for another unsuccessful attempt at converging on the intended spin state for *trans*-$(Fe_{HS})_2(Fe_{LS})_2$, for curiosities sake. In this case, while Fe_1 and Fe_3 have converged correctly to a LS and HS state, respectively, Fe_2 and Fe_4 have again not converged to the target states. The states of these two Fe atoms are markedly different from those shown in figure 6.5b and figure 6.5c, but identical to one another.

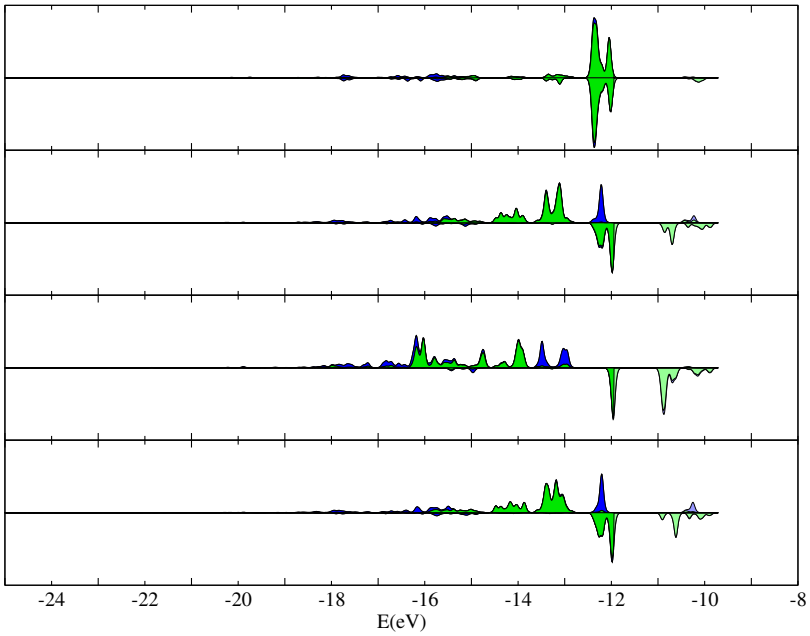

(a) *trans*-$(Fe_{HS})_2(Fe_{LS})_2$

Figure 6.6: Visualization of the DOS of the d-orbitals of the Fe atoms in a failed structure optimization of *trans*-$(Fe_{HS})_2(Fe_{LS})_2$. (Fe_1) is represented by the first graph from the top, (Fe_2) by the second, (Fe_3) by the third, (Fe_4) by the last. The contributions from t_{2g} are shown in green and those from e_g in blue. Lighter colors represent unoccupied orbitals.

Estimating $(Fe_{HS})_2(Fe_{LS})_2$

In a previous study by Borshch and Zueva [178], the relative energies of the spin states were calculated as presented in table 6.1. These values will be shown again in the discussion 6.5

Though calculated using the GGA type functional PBE, the relative ordering of the spin states is in agreement with the experimental observations [188]. Taking the magnetic susceptibility measurements 6.2 into account, it seems reasonable to assume that *trans*-$(Fe_{HS})_2(Fe_{LS})_2$ can be located energetically roughly halfway between $(Fe_{LS})_4$ and $(Fe_{HS})_3(Fe_{LS})_1$, with *cis*-$(Fe_{HS})_2(Fe_{LS})_2$ being somewhat higher in energy. *trans*-$(Fe_{HS})_2(Fe_{LS})_2$ will be included at this position in the tables in section 6.4.3 to aid in visual clarity, though marked with a *.

Spin state	ΔE_{PBE}
$(Fe_{LS})_4$	0.0
$(Fe_{HS})_1(Fe_{LS})_3$	11.2
cis-$(Fe_{HS})_2(Fe_{LS})_2$	27.0
trans-$(Fe_{HS})_2(Fe_{LS})_2$	22.8
$(Fe_{HS})_3(Fe_{LS})_1$	43.1
$(Fe_{HS})_4$	64.5

Table 6.1: Energies of the spin states of the [2x2] Fe^{II} grid complex relative to the total energy of $(Fe_{LS})_4$, calculated by Borshch and Zueva [178] using PBE. All energy values in kcal/mol.

6.3 Influence of ZPVE

So far, all observations on the various Fe^{II} SCO systems have taken only electronic energies at 0 K into account. Computing the multitudes of frequencies for the grid complexes to a relevant degree of accuracy was not possible, but an estimation can still be made by a comparison to the model systems. Table 6.2 shows the ZPVE for both HS and LS state for $[Fe^{II}(NH_3)_6]^{2+}$ and for **B.05**, computed with a selection of commonly used functionals. Out of all the model systems **B.05** can be assumed to provide the ligand environment that is the most similar to that of the grid complexes. It is identical both in the charge of the ligand per Fe core ($^{1-}$ for **B.05** and $^{4-}$ in the grid complex) and in the octahedral environment being heavily distorted by the tridentate ligands. The ZPVE were calculated using the ORCA 4.2.0 program package [126,127], using various functionals with a DKH-def2-TZVPP basis set [128], including sarc/J auxiliary basis set [129] and Grimme's D3 dispersion correction with Becke-Johnson damping [130,131]. Relativistic effects are taken into account by using the second-order DKH2 [158, 159]. An example of the input file can be found in the appendix D.

Regardless of model system and of functional, the ZPVE is higher for LS state than for the HS state. This is to be expected, because of the on average shorter bond length in the LS complexes (see 1). For $[Fe^{II}(NH_3)_6]^{2+}$, with a negative ΔE_{HL}, this results in a widening of the gap. For **B.05** and the [2x2] grid complex on the other

		BP86	M06-L	B3LYP	PBE0
$[Fe^{II}(NH_3)_6]^{2+}$	$ZPVE_{HS}$	140.09	145.02	143.79	144.70
	$ZPVE_{LS}$	144.00	148.82	148.09	149.48
	$\Delta ZPVE_{HL}$	-3.91	-3.80	-4.30	-4.78
B.05	$ZPVE_{HS}$	134.84	139.33	139.22	140.44
	$ZPVE_{LS}$	138.25	141.89	139.99	143.63
	$\Delta ZPVE_{HL}$	-3.42	-2.56	-0.77	-3.19

Table 6.2: ZPVE of HS and LS states of $[Fe^{II}(NH_3)_6]^{2+}$and **B.05**, computed with various functionals. $\Delta ZPVE_{HL}$ is calculated by subtracting the ZPVE of the LS state from the ZPVE of the HS state. All energy values in kcal/mol.

hand, ΔE_{HL}becomes smaller. The amount of $\Delta ZPVE_{HL}$ seems also large unaffected by model system and functional, the only outlier being B3LYP on **B.05**.

It seems reasonable to use the result from the PBE0 calculation on the **B.05** model system, since it is closest in both system and method to the grid complex, and it is in good agreement with most other $\Delta ZPVE_{HL}$ results as well. The $\Delta ZPVE_{HL}$ for the grid complex can in this manner be estimated at around -3 kcal/mol per Fe core, i.e. -12 kcal/mol in total when applied to the ΔE_{HL} between $(Fe_{HS})_4$ and $(Fe_{LS})_4$.

6.4 Application of model system parameterization

6.4.1 Influence of HF exchange factor per atom type

It has been stated previously that the effect of the HF exchange factor on the ΔE_{HL} of the studied Fe^{II} SCO systems is negligible when it comes to H atoms, and rather small when it comes to C atoms. Also, when it comes to the amount of HF exchange in regard to Fe and N atoms, it can be seen, for example from the 2D representations of the results from the BO of the extended model set (see 5.3), that it is to some degree interchangeable. Lowering the amount of HF exchange for Fe atoms can be compensated up to a point by increasing the amount of HF exchange for N atoms, and vice versa.

To investigate these aspects further, the ΔE_{HL} between $(Fe_{HS})_4$ and $(Fe_{LS})_4$ was determined with single-point energy calculations, using a range of different HF ex-

change parameters. The parameter for a given atom type was varied between 10% and 3%, while the parameters for all other types were kept fixed at 10%. The results are depicted in figure 6.7.

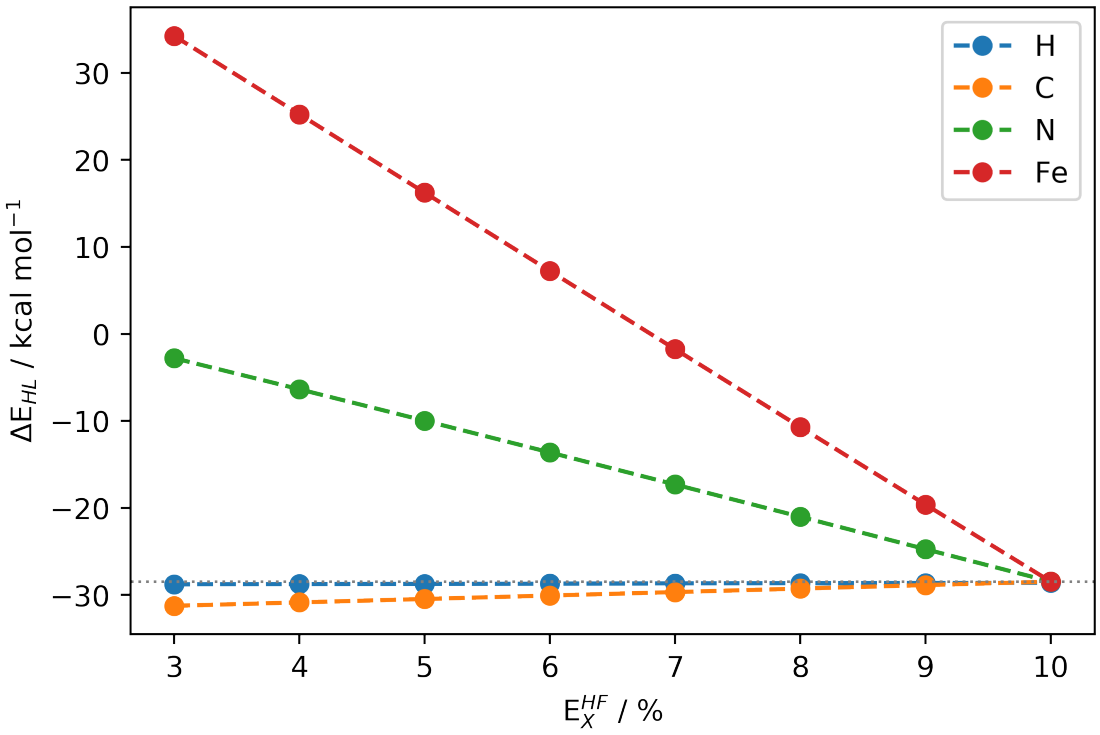

Figure 6.7: Results from single-point energy calculations for the ΔE_{HL} between $(\mathrm{Fe_{HS}})_4$ and $(\mathrm{Fe_{LS}})_4$. The HF exchange factor E_X^{HF} is varied only for the given atom type, while E_X^{HF} for all other types is kept fixed at 10%. The dotted grey line is drawn as a visual aid at ΔE_{HL}=28.5 kcal/mol, which is the size of ΔE_{HL} when computed with all HF exchange factors at 10%.

This aptly demonstrates how much smaller the influence of the HF exchange factor is for H and C atoms. When varying between 10% and 3%, the ΔE_{HL} only changes by -0.2 kcal/mol for the H atom factor, and -2.8 kcal/mol for the C atom factor. Contrary to this, varying the N atom factor between 10% and 3% changes the ΔE_{HL} by 25.7 kcal/mol, and varying the Fe atom factor changes the ΔE_{HL} by 62.7 kcal/mol. It is interesting to note that the H and C HF exchange factors not only have a significantly smaller influence on the ΔE_{HL}, but also lead to smaller (i.e. more negative) values for the ΔE_{HL}. This runs somewhat contrary to the commonly

held belief that GGA type functionals always and without exception over-stabilize the LS state for SCO systems [177].

6.4.2 Brute force approach

A comparison of the quality of these results can also be made to an approach using "brute force", where instead of a directed search the entirety of the available sampling space is probed uniformly. Using the structures of $(Fe_{HS})_4$ and $(Fe_{LS})_4$, the ΔE_{HL} was determined with single-point energy calculations. The HF exchange factors for Fe, N and C atoms were varied each between 3.0% and 10.5% in steps of 0.5%, for all possible combinations of factors. The complete results with all 4096 ΔE_{HL} values are depicted in figure 6.8, though a 2D horizontal slice at a fixed C atom HF exchange factor of 10% offers a clearer representation in figure 6.9.

From this it is evident that there are many combinations of the Fe/N HF exchange factors for which the correct ΔE_{HL} between $(Fe_{HS})_4$ and $(Fe_{LS})_4$ can be reproduced. If ΔE_{HL} is assumed to be around 20 kcal/mol, Fe/N HF exchange factors of 4.5%/10.0%, 6.0%/7.0% and 7.5%/3.5% all fulfill this condition, for example. The merits of this approach are discussed further in chapter 7.

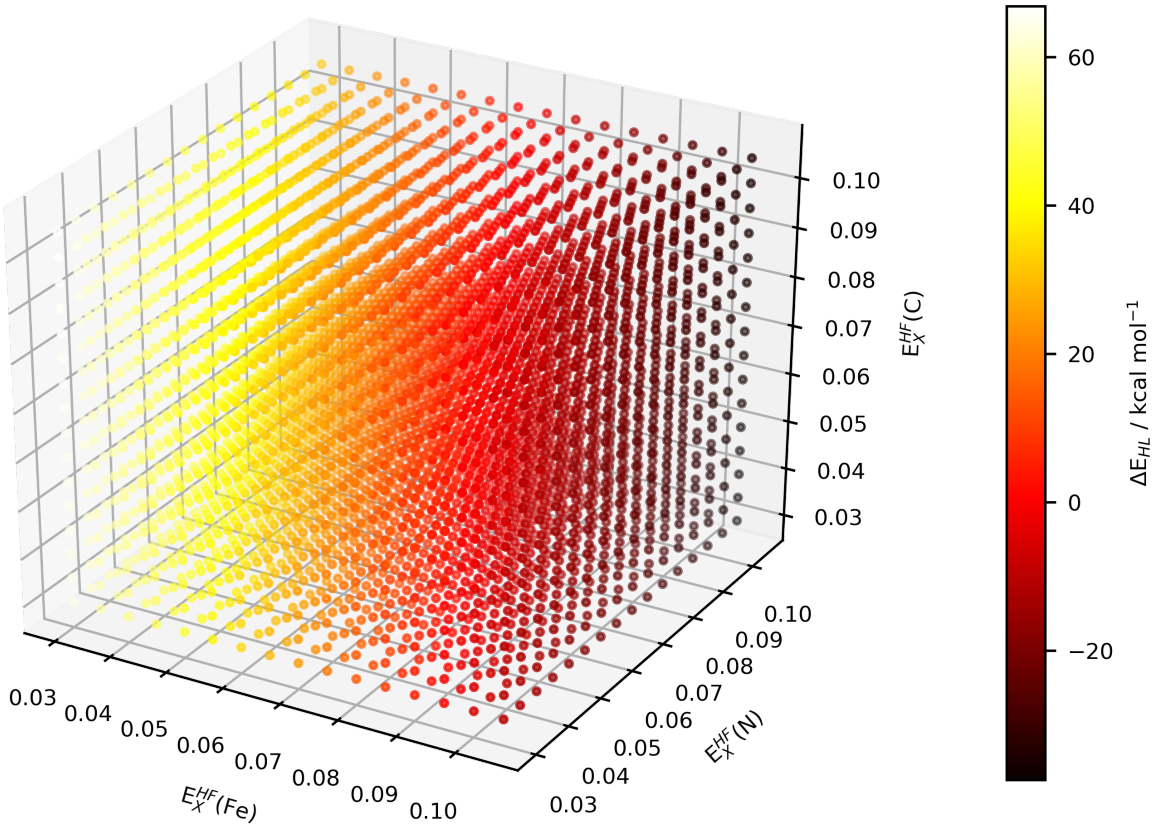

Figure 6.8: Results from single-point energy calculations for the ΔE_{HL} between $(\mathrm{Fe_{HS}})_4$ and $(\mathrm{Fe_{LS}})_4$. The HF exchange factor E_X^{HF} is varied for Fe, N and C atoms between 3.0% and 10.5% in steps of 0.5%, for all possible combinations of factors.

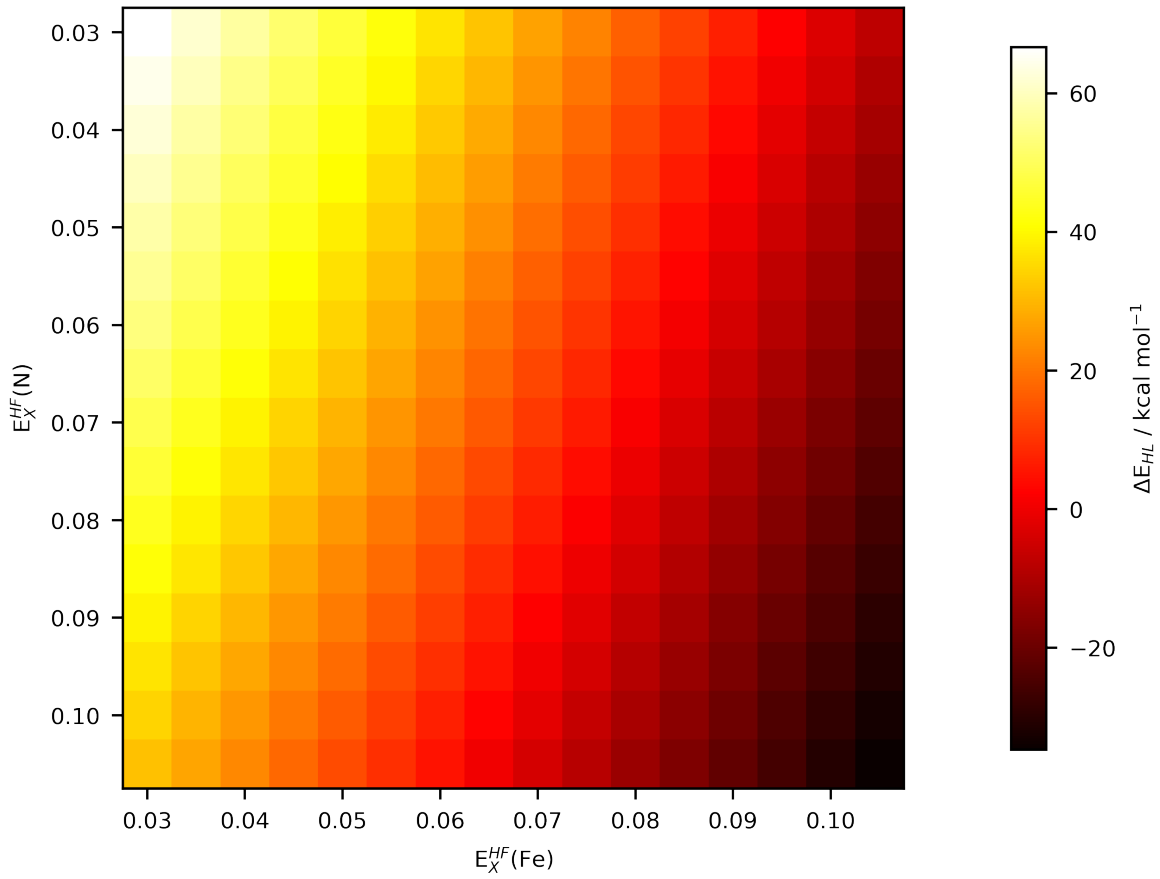

Figure 6.9: Results from single-point energy calculations for the ΔE_{HL} between $(\mathrm{Fe_{HS}})_4$ and $(\mathrm{Fe_{LS}})_4$. The HF exchange factor E_X^{HF} is fixed at 10% for C atoms, and varied for Fe and N atoms between 3.0% and 10.5% in steps of 0.5%.

6.4.3 Application of parameterization

When comparing the results from the BO procedure (see 5.4) to the viable Fe/N HF exchange factor combinations from the brute force approach, it becomes apparent that the former cannot be relied upon to produce sensible results in regard to the [2x2] Fe^{II} grid complex. Even the latest iteration with the "minimized" model set predicts 9.1%/8.7% as optimal for the Fe/N HF exchange factors. For the ΔE_{HL} between $(Fe_{HS})_4$ and $(Fe_{LS})_4$ this combination will produce a negative ΔE_{HL}, in contrast to the experimental observations.

However, an additional BO procedure was carried out, in the same manner as described in 5.4, but using solely the **B.05** model system. By using only a single system, the BO procedure is sure to produce HF exchange factors that are optimal for the representation of exactly this system. The results for **B.05** are presented in figure 6.10

For the **B.05** model system, the predicted optimal HF exchange parameters are 5.0% for Fe atoms, 10.5% for N atoms and 20.0% for C atoms (while H remained fixed at 12.5%). Using these parameters, single-point energy calculations were carried out, using the converged [2x2] Fe^{II} grid structures. These values can then be corrected by the $\Delta ZPVE_{HL}$ per Fe^{II} core in the LS state, as estimated previously. The results for the electronic energies ΔE_{el} as well as the corrected energies ΔH_0, relative to the total energy of $(Fe_{LS})_4$, are presented in table 6.3.

As a point of comparison, the energy gap between $(Fe_{HS})_4$ and $(Fe_{LS})_4$ was calculated once more, using an HF exchange factor of 25% for all atom types, as is the default setting for the PBE0 functional. The result, $\Delta_{\mathrm{HL}}^{default} = -109.3$ kcal/mol, is discussed in the following section.

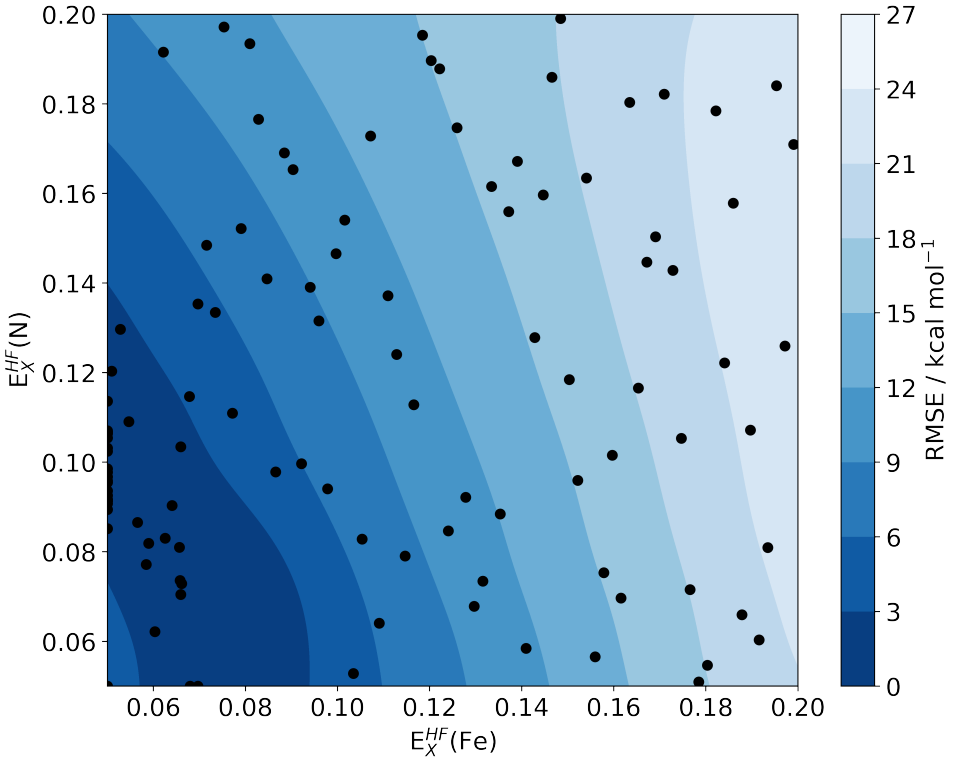

Figure 6.10: 2D representation of the result of the BO procedure using only the **B.05** model system. Each point reflects an iteration, with a unique set of HF exchange parameters and resulting RMSE. The color gradient is derived from the mean of the Gaussian process regression, reflecting the predicted RMSE values inbetween sampled points.

Spin state	ΔE_{el}	ΔH_0
$(Fe_{LS})_4$	0.0	0.0
$(Fe_{HS})_1(Fe_{LS})_3$	0.1	-2.9
trans-$(Fe_{HS})_2(Fe_{LS})_2$	4.3*	—
$(Fe_{HS})_3(Fe_{LS})_1$	8.6	-0.4
$(Fe_{HS})_4$	18.3	6.3

Table 6.3: Energies of the spin states of the [2x2] Fe^{II} grid complex relative to $(Fe_{LS})_4$, calculated using HF exchange parameters of 5.0% for Fe atoms, 10.5% for N atoms, 20.0% for C atoms and 12.5% for H atoms. The value of ΔH_0 is computed by adding $\Delta ZPVE_{HL}$ per Fe^{II} core in the LS state to ΔE_{el}. The value for *trans*-$(Fe_{HS})_2(Fe_{LS})_2$ was interpolated at half the value of $(Fe_{HS})_3(Fe_{LS})_1$. All energy values in kcal/mol.

6.5 Discussion

The previously reported values ΔE_{el} from the DFT calculations parameterized with the results from the BO applied to the **B.05** model system are presented once more in table 6.4, as are the values ΔH_0, corrected by the ZPVE estimation. For the sake of comparison, the values ΔE_{PBE} reported by Borshch and Zueva [178] are shown once more as well.

Spin state	ΔE_{el}	ΔH_0	ΔE_{PBE}
$(\mathrm{Fe_{LS}})_4$	0.0	0.0	0.0
$(\mathrm{Fe_{HS}})_1(\mathrm{Fe_{LS}})_3$	0.1	-2.9	11.2
trans-$(\mathrm{Fe_{HS}})_2(\mathrm{Fe_{LS}})_2$	4.3*	—	22.8
$(\mathrm{Fe_{HS}})_3(\mathrm{Fe_{LS}})_1$	8.6	-0.4	43.1
$(\mathrm{Fe_{HS}})_4$	18.3	6.3	64.5

Table 6.4: Energies of the spin states of the [2x2] $\mathrm{Fe^{II}}$ grid complex relative to $(\mathrm{Fe_{LS}})_4$. ΔE_{el} has been calculated using HF exchange parameters of 5.0% for Fe atoms, 10.5% for N atoms, 20.0% for C atoms and 12.5% for H atoms. The value of ΔH_0 is computed by adding $\Delta\mathrm{ZPVE_{HL}}$ per $\mathrm{Fe^{II}}$ core in the LS state to ΔE_{el}. ΔE_{PBE} are the values reported by Borshch and Zueva [178]. The values for *trans*-$(\mathrm{Fe_{HS}})_2(\mathrm{Fe_{LS}})_2$ marked with * were interpolated at half the value of $(\mathrm{Fe_{HS}})_3(\mathrm{Fe_{LS}})_1$. All energy values in kcal/mol.

When computing ΔE_{el} for the spin crossover events of the [2x2] $\mathrm{Fe^{II}}$ grid complex by using the HF exchange parameters obtained from the BO procedure applied to the **B.05** model system, the results conform rather well to the experimental observations (see 6.2). A total ΔE_{HL} of 18.3 kcal/mol for the difference between $(\mathrm{Fe_{HS}})_4$ and $(\mathrm{Fe_{LS}})_4$ is a reasonable value, considering that at room temperature the total spin state is exclusively $(\mathrm{Fe_{HS}})_4$ [188]. Upon cooling down the spin crossover events to $(\mathrm{Fe_{HS}})_3(\mathrm{Fe_{LS}})_1$ and $\mathrm{Fe_{HS}})_2(\mathrm{Fe_{LS}})_2$ could be observed (though whether this species is *cis*-$(\mathrm{Fe_{HS}})_2(\mathrm{Fe_{LS}})_2$ or *trans*-$(\mathrm{Fe_{HS}})_2(\mathrm{Fe_{LS}})_2$ could not be clearly determined). The observations upon cooling below 20 K are less clear, and $(\mathrm{Fe_{HS}})_1(\mathrm{Fe_{LS}})_3$ and $(\mathrm{Fe_{LS}})_4$ could not be observed separately. This conforms to the calculated values for ΔE_{el}, which place these two states at almost the same level in energy.

Adding the estimated ZPVE changes the relative energies significantly. Since the ZPVE has a stronger effects on Fe atoms in the LS state, the amount of the energetic difference depends on the total spin state of the system. With the correction, $(Fe_{HS})_1(Fe_{LS})_3$ can be found at a slightly lower level in energy than $(Fe_{LS})_4$, which still matches the experimental observations. At first glance, placing $(Fe_{HS})_3(Fe_{LS})_1$ at a similar level in energy as $(Fe_{LS})_4$ seems contrary to the observations, which can clearly differentiate the $(Fe_{HS})_3(Fe_{LS})_1$ state. However, the relaxation from $(Fe_{HS})_4$ to $(Fe_{LS})_4$ would include simultaneous transitions of all four Fe centers, making it much less likely than the relaxation to $(Fe_{HS})_3(Fe_{LS})_1$. Finally, the ΔH_0 for $(Fe_{HS})_4$ seems somewhat too low to match the stability of $(Fe_{HS})_4$ at room temperature. It can be concluded that this method of estimating the ZPVE might have been too superficial. On the other hand, a ΔH_0 of 6.3 kcal/mol concurs very well with the thermodynamic estimation.

The values reported by Borshch and Zueva [178] are demonstrating once again the overstabilization of LS states by GGA type functionals [177]. The general trends of the experimental observations are reproduced, except for the energy level of $(Fe_{HS})_1(Fe_{LS})_3$. If correct, a difference in energy of 11.2 kcal/mol should have been observable.

On the other hand, calculating $\Delta_{HL}^{default}$ with an HF exchange factor of 25%, which is the commonly used default setting for PBE0 [67, 68], clearly demonstrates why hybrid functionals cannot be used for the description of the energy levels of SCO complexes, without first considering the parameters. $(Fe_{HS})_4$ is calculated at a much lower level on energy than $(Fe_{LS})_4$, at an absurd $\Delta_{HL}^{default} = -109.3$ kcal/mol, in stark contrast to the experimental observations. The [2x2] Fe^{II} grid complex could not be counted as a SCO complex, were this result even remotely accurate.

The complex exhibits an inverse cooperativity in regard to the spin crossover events. When starting from $(Fe_{LS})_4$, the first SCO is essentially free, but every successive one needs to cross a higher energetic threshold. This is explained by the changes to the ligand structure upon SCO, as mentioned in 1. After the first SCO, the changes are communicated through the ligand backbone, distorting the environment of the adjacent Fe cores in a manner that is unfavorable for the next SCO. This also explains why Borshch and Zueva [178] found the *trans*-$(Fe_{HS})_2(Fe_{LS})_2$ to be more stable in energy than its *cis*-$(Fe_{HS})_2(Fe_{LS})_2$ counterpart. Influences of fixed ligand structures upon the ΔE_{HL} of SCO complexes in general have already been widely reported [14–16, 188, 191].

Chapter 7

Summary and Outlook

To summarize, the general usefulness of a range of DFT techniques, which are currently in everyday use for the validation and explanation of experimental observations, has been demonstrated in chapter 3. Chapter 4 reviewed the the recurrent issues of DFT methods when it comes to the description of transition metal SCO complexes. Also presented are the initial attempts at the development of a procedure to alleviate these issues. This was done by reparameterizing the HF exchange factors through the use of the Bayesian optimization machine learning tool, on the basis of benchmark values computed with a coupled-cluster method. This approach was then refined, as described in chapter 5. A local CC variant allowed for the inclusion of a broader range of systems into the model set, leading to broader applicability and increased accuracy in the results. It has been demonstrated that the BO procedure is quite capable of finding an optimal set of HF exchange parameters for the calculation of the HS-LS energy gap for small Fe^{II} SCO systems, such as $[Fe^{II}(NH_3)_6]^{2+}$. However, this is dependent on finding a range of model systems that are structurally similar to the target system. As demonstrated in chapter 6, for a [2x2] Fe^{II} grid complex this approach does not work as well. On the other hand, using only the HF exchange parameters from the model system **B.05**, which is structurally the most similar model to the grid complex, resulted in energies in very good agreement to experimental observations. This leads to the conclusion that the BO procedure is still valid and can be a useful tool for the parameterization of hybrid functionals, as long as the correct model systems are chosen.

It could be stated that the "brute force" approach as discussed in chapter 6.4.2 can produce results on par with those of the developed BO procedure. While not wrong, it has to be noted that evaluating those results is only possible based on the knowledge gained from experimental observations. It would contribute little to no value to a purely *in silico*-driven methodology, which could be seen as the ultimate goal of these studies. Furthermore, the "brute force" approach required an excessive 8192 separate calculations, the energy cost of which can be estimated at around 1,400 kWh. The cost of the Bayesian optimization procedure is somewhat harder to estimate, but amounts to roughly 10%. This includes the coupled-cluster benchmark calculations, which are the most expensive part. Later modifications to the procedure, such as the "pruning" discussed in 5.5, are much less costly.

From a conceptual perspective, the BO procedure can also be compared to a neural network approach, such as the HDNNP championed by Jörg Behler *et al.* [192–195]. In both methods a training set is used to parameterize a posterior function, with the goal of being able to use the less costly functional afterwards, which should have a degree of accuracy approaching that of the benchmarking method. While the basic idea is the same, there are some important differences to note. As opposed to the BO procedure, neural networks are a "black box". Fitting a training set to the neural network optimizes a series of weights and biases, influencing the equations by which the energies are computed for a given configuration. These weights and biases have no physical meaning by themselves, as they are purely mathematical constructs. Systematic improvements are still possible, but they often rely on statistical methods for the search of outliers or poorly defined configurational spaces. Consequently the number of data points in the training set has to be much higher. Another key difference lies in the ability to extrapolate away from data covered by the training set. Neural network potentials are not able to do so with any degree of accuracy, whereas a parameterized functional should have fewer issues in this regard.

By trying to approximate the spin transitions for $[Fe^{II}(NH_3)_6]^{2+}$ and for the [2x2] Fe^{II} grid complex as discussed in chapter 4, 5 and 6, it has become apparent that there are strict limitations to the types of model systems that should be included. Specifically, this approach works best for models systems that are structurally as similar to the target complex as possible. Recent works in our group by Rafael Machleid have started taking this factor into account. Here the local Fe environment is

expressed through the use of descriptor called "local many-body tensor representation" (LMBTR) [196, 197], making it possible to assign a quantitative value to the structural similarity between any two complexes. When applied to a target complex and the model systems in its respective training set, this standardized similarity model (SSM) can be used to assign separate weights to the contribution of each model. The higher the structural similarity to the target complex is, the more influence the model system has on the predicted parameterization, significantly lowering the deviations between HS-LS energy gaps computed with the benchmark coupled-cluster method and with the parameterized DFT. The works of Rafael Machleid investigated Fe^{III} SCO complexes, but the methodology should be easily transferable to Fe^{II} or even other transition metals such as Co or Mn [15–18, 198].

An issue remains with the benchmark calculation of the model system. It is desirable to expand the diversity of available model systems as far as possible, possibly including aromatic and charged ligand systems, or highly distorted geometries [14, 22, 26, 199, 200]. However, being able to only compute systems of rather small sizes with the coupled-cluster method is a starkly limiting factor. Trade-offs can be made between accuracy and available system size [35, 36, 40–42], as has been done with the local CC variant to a small degree. But this in turn limits the potential accuracy of the end result. After all, a parameterized method can only ever be as accurate as its benchmark method [193].

This problem can be alleviated through the development of more efficient benchmarking methods, advances in raw computing power, or ideally both. Looking at recent efforts in these fields [160, 183, 201–203] can provide confidence that these solutions will be coming sooner rather than later.

List of Abbreviations

BOA	Born-Oppenheimer approximation
BO	Bayesian optimization
CASPT2	complete active space second-order perturbation
CASSCF	complete active space self-consistent field
CABS	complementary auxiliary basis set
CBS	complete basis set
CC	coupled cluster
CCSD(T)	coupled cluster with single, double and perturbative triple excitations
CP-PAW	Car-Parinello Projector Augmented Wave
CPCM	conductor-like polarizable continuum model
DFT	density functional theory
DOS	density of states
DKH2	Douglas-Kroll-Hess Hamiltonian
GGA	generalized gradient approximation
GPR	Gaussian process regression
HF	Hartree-Fock
HS	high-spin

LDA	local density approximation
LS	low-spin
MD	molecular dynamics
MEP	minimum energy path
NEB	nudged elastic band
NEVPT2	N-electron valence state perturbation theory
PES	potential energy surface
RASPT2	restricted active space second-order perturbation
RASSCF	restricted active space self-consistent field
RMSE	root mean square error
SCO	spin crossover
SORCI	spectroscopy oriented configuration interaction
ZPVE	zero-point vibrational energy

Bibliography

[1] G. A. Lawrance. *Introduction to Coordination Chemistry*. Wiley, 2010. doi:10.1002/9780470687123.fmatter.

[2] F. A. Cotton and G. Wilkinson. *Advanced Inorganic Chemistry*. Wiley, 5th edition, 1989.

[3] R. K. Sodhi and S. Paul. Metal Complexes in Medicine: An Overview and Update from Drug Design Perspective. *Canc Therapy & Oncol Int J.*, 14:555883, 2019. doi:10.19080/CTOIJ.2019.14.555883.

[4] F. Cavani, G. Centi, S. Perathoner, and F. Trifiró. *Sustainable Industrial Chemistry: Principles, Tools and Industrial Examples*. Wiley, 2009.

[5] T. Rauchfuss. *Inorganic Syntheses, Volume 35*. Wiley, 2010.

[6] R. A. Sheldon and H. van Bekkum. *Fine Chemicals through Heterogeneous Catalysis*. Wiley, 2008.

[7] L. Cambi and A. Cagnasso. Atti accad. naz. lincei, cl. *Sci. Fis., Mat. Nat., Rend*, 13(254):809, 1931.

[8] N. Amin, S. Said, M. Salleh, A. Afifi, N. Ibrahim, M. Hasnan, M. Tahir, and N. Hashim. Review of fe-based spin crossover metal complexes in multiscale device architectures. *Inorg. Chim. Acta*, 544:121168, 2023. doi:10.1016/j.ica.2022.121168.

[9] G. Molnár, L. Salmon, W. Nicolazzi, F. Terki, and A. Bousseksou. Emerging properties and applications of spin crossover nanomaterials. *J. Mater. Chem. C*, 2:1360–1366, 2014. doi:10.1039/C3TC31750A.

[10] S. Brooker. Spin crossover with thermal hysteresis: practicalities and lessons learnt. *Chem. Soc. Rev.*, 44:2880–2892, 2015. doi:10.1039/C4CS00376D.

[11] A. Bousseksou, G. Molnár, L. Salmon, and W. Nicolazzi. Molecular spin crossover phenomenon: recent achievements and prospects. *Chem. Soc. Rev.*, 40:3313–3335, 2011. doi:10.1039/C1CS15042A.

[12] J. R. Galán-Mascarós, E. Coronado, A. Forment-Aliaga, M. Monrabal-Capilla, E. Pinilla-Cienfuegos, and M. Ceolin. Tuning Size and Thermal Hysteresis in Bistable Spin Crossover Nanoparticles. *Inorg. Chem.*, 49(12):5706–5714, 2010. doi:10.1021/ic100751a.

[13] K. Senthil Kumar and M. Ruben. Emerging trends in spin crossover (SCO) based functional materials and devices. *Coord. Chem. Rev.*, 346:176–205, 2017. doi:10.1016/j.ccr.2017.03.024.

[14] U. Rastetter, A. Jacobi von Wangelin, and C. Herrmann. Redox-active ligands as a challenge for electronic structure methods. *J. Comput. Chem.*, 44(3):468–479, 2023. doi:10.1002/jcc.27013.

[15] R. Akiyoshi, Y. Komatsumaru, M. Donoshita, S. Dekura, Y. Yoshida, H. Kitagawa, Y. Kitagawa, L. F. Lindoy, and S. Hayami. Ferroelectric and Spin Crossover Behavior in a Cobalt(II) Compound Induced by Polar-Ligand-Substituent Motion. *Angew. Chem. Int. Ed.*, 60(23):12717–12722, 2021. doi:10.1002/anie.202015322.

[16] S.-Y. Zhang, H.-Y. Sun, R.-G. Wang, Y.-S. Meng, T. Liu, and Y.-Y. Zhu. Construction of spin-crossover dinuclear cobalt(ii) compounds based on complementary terpyridine ligand pairing. *Dalton Trans.*, 51:9888–9893, 2022. doi:10.1039/D2DT00436D.

[17] D. Villaman, C. J. McMonagle, M. R. Probert, O. Peña, Y. Moreno, and M. Fuentealba. Structural studies of a manganese(iii) complex with spin-crossover and thermochromic properties. *CrystEngComm*, 22:3221–3233, 2020. doi:10.1039/C9CE01962F.

[18] Z. Liu, S. Liang, X. Di, and J. Zhang. A manganese(iii) complex that exhibits spin crossover behavior. *Inorg. Chem. Comm.*, 11(7):783–786, 2008. doi:

10.1016/j.inoche.2008.03.030.

[19] D. M. Halepoto, D. G. L. Holt, L. F. Larkworthy, G. J. Leigh, D. C. Povey, and G. W. Smith. Spin crossover in chromium(II) complexes and the crystal and molecular structure of the high spin form of bis[1,2-bis(diethylphosphino)ethane]di-iodochromium(II). *J. Chem. Soc., Chem. Commun.*, pages 1322–1323, 1989. doi:10.1039/C39890001322.

[20] L. F. Lindoy and S. E. Livingstone. Complexes of iron(II),cobalt(II) and nickel(II) with α-diimines and related bidentate ligands. *Coord. Chem. Rev.*, 2(2):173–193, 1967. doi:10.1016/S0010-8545(00)80204-0.

[21] P. Gütlich, Y. Garcia, and H. A. Goodwin. Spin crossover phenomena in Fe(II) complexes. *Chem. Soc. Rev.*, 29:419–427, 2000. doi:10.1039/B003504L.

[22] C. Cook, F. Habib, T. Aharen, R. Clérac, A. Hu, and M. Murugesu. High-Temperature Spin Crossover Behavior in a Nitrogen-Rich FeIII-Based System. *Inorg. Chem.*, 52(4):1825–1831, 2013. doi:10.1021/ic301864d.

[23] P. Gütlich, A. B. Gaspar, V. Ksenofontov, and Y. Garcia. Pressure effect studies in molecular magnetism. *J. Phys. Condens. Matter*, 16(14):S1087, 2004. doi:10.1088/0953-8984/16/14/019.

[24] V. N. Raj M., K. Bhar, T. A. Khan, S. Jain, F. Perdih, P. Mitra, and A. K. Sharma. Temperature induced spin crossover behaviour in mononuclear cobalt(ii) bis terpyridine complexes. *MRS Advances*, 4(28-29):1597–1610, 2019. doi:10.1557/adv.2019.166.

[25] J.-F. Létard. Photomagnetism of iron(ii) spin crossover complexes—the T(LIESST) approach. *J. Mater. Chem.*, 16:2550–2559, 2006. doi:10.1039/B603473J.

[26] D. J. Harding, P. Harding, and W. Phonsri. Spin crossover in iron(III) complexes. *Coord. Chem. Rev.*, 313:38–61, 2016. doi:10.1016/j.ccr.2016.01.006.

[27] Schrödinger, LLC. The PyMOL molecular graphics system, version 2.3. February 2019.

[28] R. W. Hogue, S. Singh, and S. Brooker. Spin crossover in discrete polynuclear iron(II) complexes. *Chem. Soc. Rev.*, 47:7303–7338, 2018. doi:10.1039/C7CS00835J.

[29] M. Ruben, J. Rojo, F. J. Romero-Salguero, L. H. Uppadine, and J.-M. Lehn. Grid-Type Metal Ion Architectures: Functional Metallosupramolecular Arrays. *Angew. Chem. Int. Edit.*, 43(28):3644–3662, 2004. doi:10.1002/anie.200300636.

[30] B. Schneider, S. Demeshko, S. Dechert, and F. Meyer. A Double-Switching Multistable Fe4 Grid Complex with Stepwise Spin-Crossover and Redox Transitions. *Angew. Chem. Int. Edit.*, 49(48):9274–9277, 2010. doi:10.1002/anie.201001536.

[31] D. N. Bowman and E. Jakubikova. Low-Spin versus High-Spin Ground State in Pseudo-Octahedral Iron Complexes. *Inorg. Chem.*, 51(11):6011–6019, 2012. doi:10.1021/ic202344w.

[32] D. N. Bowman, A. Bondarev, S. Mukherjee, and E. Jakubikova. Tuning the Electronic Structure of Fe(II) Polypyridines via Donor Atom and Ligand Scaffold Modifications: A Computational Study. *Inorg. Chem.*, 54(17):8786–8793, 2015. doi:10.1021/acs.inorgchem.5b01409.

[33] R. A. Mata and M. A. Suhm. Benchmarking Quantum Chemical Methods: Are We Heading in the Right Direction? *Angew. Chem. Int. Edit.*, 56(37):11011–11018, 2017. doi:10.1002/anie.201611308.

[34] A. Fouqueau, M. E. Casida, L. M. L. Daku, A. Hauser, and F. Neese. Comparison of density functionals for energy and structural differences between the high- [5T2g:(t2g)4(eg)2] and low- [1A1g:(t2g)6(eg)0] spin states of iron(II) coordination compounds. II. More functionals and the hexaminoferrous cation, [Fe(NH3)6]2+. *J. Chem. Phys.*, 122(4):044110, 2005. doi:10.1063/1.1839854.

[35] M. Kepenekian, V. Robert, B. Le Guennic, and C. De Graaf. Energetics of [Fe(NCH)6]2+ via CASPT2 calculations: A spin-crossover perspective. *J. Comput. Chem.*, 30(14):2327–2333, 2009. doi:10.1002/jcc.21236.

[36] K. Pierloot, Q. M. Phung, and A. Domingo. Spin State Energetics in First-Row Transition Metal Complexes: Contribution of (3s3p) Correlation and Its Description by Second-Order Perturbation Theory. *J. Chem. Theory Comput.*, 13(2):537–553, 2017. doi:10.1021/acs.jctc.6b01005.

[37] M. Radoń, E. Broclawik, and K. Pierloot. Electronic Structure of Selected FeNO7 Complexes in Heme and Non-Heme Architectures: A Density Functional and Multireference ab Initio Study. *J. Phys. Chem. B*, 114(3):1518–1528, 2010. doi:10.1021/jp910220r.

[38] S. Vancoillie, H. Zhao, M. Radoń, and K. Pierloot. Performance of CASPT2 and DFT for Relative Spin-State Energetics of Heme Models. *J. Chem. Theory Comput.*, 6(2):576–582, 2010. doi:10.1021/ct900567c.

[39] M. Radoń, E. Broclawik, and K. Pierloot. DFT and Ab Initio Study of Iron-Oxo Porphyrins: May They Have a Low-Lying Iron(V)-Oxo Electromer? *J. Chem. Theory Comput.*, 7(4):898–908, 2011. doi:10.1021/ct1006168.

[40] A. Domingo, M. Àngels Carvajal, and C. de Graaf. Spin crossover in Fe(II) complexes: An ab initio study of ligand σ-donation. *Int. J. Quantum Chem.*, 110(2):331–337, 2010. doi:10.1002/qua.22105.

[41] M. Radoń. Spin-State Energetics of Heme-Related Models from DFT and Coupled Cluster Calculations. *J. Chem. Theory Comput.*, 10(6):2306–2321, 2014. doi:10.1021/ct500103h.

[42] L. M. Lawson Daku, F. Aquilante, T. W. Robinson, and A. Hauser. Accurate Spin-State Energetics of Transition Metal Complexes. 1. CCSD(T), CASPT2, and DFT Study of [M(NCH)6]2+ (M = Fe, Co). *J. Chem. Theory Comput.*, 8(11):4216–4231, 2012. doi:10.1021/ct300592w.

[43] M. Radoń. Revisiting the role of exact exchange in DFT spin-state energetics of transition metal complexes. *Phys. Chem. Chem. Phys.*, 16:14479–14488, 2014. doi:10.1039/C3CP55506B.

[44] W. Kohn. Nobel Lecture: Electronic structure of matter—wave functions and density functionals. *Rev. Mod. Phys.*, 71:1253–1266, 1999. doi:10.1103/RevModPhys.71.1253.

[45] E. Schrödinger. Quantisierung als Eigenwertproblem, Erste Mitteilung. *Ann. Phys.*, 384(4):361–376, 1926. doi:10.1002/andp.19263840404.

[46] E. Schrödinger. Quantisierung als Eigenwertproblem, Zweite Mitteilung. *Ann. Phys.*, 384(6):489–527, 1926. doi:10.1002/andp.19263840602.

[47] E. Schrödinger. An Undulatory Theory of the Mechanics of Atoms and Molecules. *Phys. Rev.*, 28(6):1049–1070, 1926. doi:10.1103/PhysRev.28.1049.

[48] M. Born and W. Heisenberg. Zur Quantentheorie der Molekeln. *Ann. Phys.*, 379(9):1–31, 1924. doi:10.1002/andp.19243790902.

[49] M. Born and R. Oppenheimer. Zur Quantentheorie der Molekeln. *Ann. Phys.*, 389(20):457–484, 1927. doi:10.1002/andp.19273892002.

[50] D. R. Hartree. The Wave Mechanics of an Atom with a Non-Coulomb Central Field. Part I. Theory and Methods. *Math. Proc. Camb. Philos. Soc.*, 24(1):89–110, 1928. doi:10.1017/S0305004100011919.

[51] V. Fock. Näherungsmethode zur Lösung des quantenmechanischen Mehrkörperproblems. *Z. Physik*, 61(1):126–148, 1930. doi:10.1007/BF01340294.

[52] P. Hohenberg and W. Kohn. Inhomogeneous Electron Gas. *Phys. Rev.*, 136:B864–B871, 1964. doi:10.1103/PhysRev.136.B864.

[53] W. Ritz. Über eine neue Methode zur Lösung gewisser Variationsprobleme der mathematischen Physik. *J. Reine Angew. Math.*, 1909(135):1–61, 1909. doi:doi:10.1515/crll.1909.135.1.

[54] W. Kohn and L. J. Sham. Self-Consistent Equations Including Exchange and Correlation Effects. *Phys. Rev.*, 140:A1133–A1138, 1965. doi:10.1103/PhysRev.140.A1133.

[55] J. C. Slater. The Theory of Complex Spectra. *Phys. Rev.*, 34:1293–1322, 1929. doi:10.1103/PhysRev.34.1293.

[56] K. Burke. Perspective on density functional theory. *J. Chem. Phys.*, 136(15):150901, 2012. doi:10.1063/1.4704546.

[57] R. Peverati and D. G. Truhlar. Quest for a universal density functional: the accuracy of density functionals across a broad spectrum of databases in chemistry and physics. *Phil. Trans. R. Soc. A*, 372(2011):20120476, 2014. doi:10.1098/rsta.2012.0476.

[58] J. P. Perdew and K. Schmidt. Jacob's ladder of density functional approximations for the exchange-correlation energy. *AIP Conf. Proc.*, 577(1):1–20, 2001. doi:10.1063/1.1390175.

[59] S. H. Vosko, L. Wilk, and M. Nusair. Accurate spin-dependent electron liquid correlation energies for local spin density calculations: a critical analysis. *Can. J. Phys.*, 58(8):1200–1211, 1980. doi:10.1139/p80-159.

[60] J. P. Perdew, K. Burke, and M. Ernzerhof. Generalized Gradient Approximation Made Simple. *Phys. Rev. Lett.*, 77:3865–3868, 1996. doi:10.1103/PhysRevLett.77.3865.

[61] J. P. Perdew. Density-functional approximation for the correlation energy of the inhomogeneous electron gas. *Phys. Rev. B*, 33:8822–8824, 1986. doi:10.1103/PhysRevB.33.8822.

[62] A. D. Becke. Density-functional exchange-energy approximation with correct asymptotic behavior. *Phys. Rev. A*, 38:3098–3100, 1988. doi:10.1103/PhysRevA.38.3098.

[63] J. Tao, J. P. Perdew, V. N. Staroverov, and G. E. Scuseria. Climbing the Density Functional Ladder: Nonempirical Meta–Generalized Gradient Approximation Designed for Molecules and Solids. *Phys. Rev. Lett.*, 91:146401, 2003. doi:10.1103/PhysRevLett.91.146401.

[64] Y. Zhao and D. G. Truhlar. A new local density functional for main-group thermochemistry, transition metal bonding, thermochemical kinetics, and noncovalent interactions. *J. Chem. Phys.*, 125(19):194101, 2006. doi:10.1063/1.2370993.

[65] A. D. Becke. A new mixing of Hartree–Fock and local density-functional theories. *J. Chem. Phys.*, 98(2):1372–1377, 1993. doi:10.1063/1.464304.

[66] A. V. Arbuznikov. Hybrid exchange correlation functionals and potentials: Concept elaboration. *J. Struct. Chem.*, 48(1):1–31, 2007. doi:10.1021/acs.jpclett.9b01983.

[67] C. Adamo and V. Barone. Toward reliable density functional methods without adjustable parameters: The PBE0 model. *J. Chem. Phys.*, 110(13):6158–6170, 1999. doi:10.1063/1.478522.

[68] M. Ernzerhof and G. E. Scuseria. Assessment of the Perdew–Burke–Ernzerhof exchange-correlation functional. *J. Chem. Phys.*, 110(11):5029–5036, 1999. doi:10.1063/1.478401.

[69] P. J. Stephens, F. J. Devlin, C. F. Chabalowski, and M. J. Frisch. Ab Initio Calculation of Vibrational Absorption and Circular Dichroism Spectra Using Density Functional Force Fields. *J. Phys. Chem.*, 98(45):11623–11627, 1994. doi:10.1021/j100096a001.

[70] P. Borlido, J. Schmidt, A. W. Huran, F. Tran, M. A. L. Marques, and S. Botti. Exchange-correlation functionals for band gaps of solids: benchmark, reparametrization and machine learning. *Npj Comput. Mater.*, 6(1):96, 2020. doi:10.1038/s41524-020-00360-0.

[71] T. Ohto, M. Dodia, J. Xu, S. Imoto, F. Tang, F. Zysk, T. D. Kühne, Y. Shigeta, M. Bonn, X. Wu, and Y. Nagata. Accessing the Accuracy of Density Functional Theory through Structure and Dynamics of the Water–Air Interface. *J. Phys. Chem. Lett.*, 10(17):4914–4919, 2019. doi:10.1021/acs.jpclett.9b01983.

[72] H. Iikura, T. Tsuneda, T. Yanai, and K. Hirao. A long-range correction scheme for generalized-gradient-approximation exchange functionals. *J. Chem. Phys.*, 115(8):3540–3544, 2001. doi:10.1063/1.1383587.

[73] T. Yanai, D. P. Tew, and N. C. Handy. A new hybrid exchange–correlation functional using the Coulomb-attenuating method (CAM-B3LYP). *Chem. Phys. Lett.*, 393(1):51 – 57, 2004. doi:10.1016/j.cplett.2004.06.011.

[74] M. Marsman, J. Paier, A. Stroppa, and G. Kresse. Hybrid functionals applied to extended systems. *J. Phys.: Condens. Matter*, 20(6):064201, 2008. doi:10.1088/0953-8984/20/6/064201.

[75] J.-D. Chai and M. Head-Gordon. Long-range corrected hybrid density functionals with damped atom–atom dispersion corrections. *Phys. Chem. Chem. Phys.*, 10:6615–6620, 2008. doi:10.1039/B810189B.

[76] T. M. Maier, A. V. Arbuznikov, and M. Kaupp. Local hybrid functionals: Theory, implementation, and performance of an emerging new tool in quantum chemistry and beyond. *WIREs Comput. Mol. Sc.*, 9(1):e1378, 2019. doi:10.1002/wcms.1378.

[77] Grotjahn, Robin and Furche, Filipp and Kaupp, Martin. Development and Implementation of Excited-State Gradients for Local Hybrid Functionals. *J. Chem. Theory Comput.*, 15(10):5508–5522, 2019. doi:10.1021/acs.jctc.9b00659.

[78] M. Haasler, T. M. Maier, R. Grotjahn, S. Gückel, A. V. Arbuznikov, and M. Kaupp. A Local Hybrid Functional with Wide Applicability and Good Balance between (De)Localization and Left–Right Correlation. *J. Chem. Theory Comput.*, 16(9):5645–5657, 2020. doi:10.1021/acs.jctc.0c00498.

[79] P. E. Blöchl, C. F. J. Walther, and T. Pruschke. Method to include explicit correlations into density-functional calculations based on density-matrix functional theory. *Phys. Rev. B*, 84:205101, 2011. doi:10.1103/PhysRevB.84.205101.

[80] P. E. Blöchl, T. Pruschke, and M. Potthoff. Density-matrix functionals from Green's functions. *Phys. Rev. B*, 88:205139, 2013. doi:10.1103/PhysRevB.88.205139.

[81] J. He and C. Franchini. Screened hybrid functional applied to $3d^0 \rightarrow 3d^8$ transition-metal perovskites LaMO$_3$ (M = Sc–Cu): Influence of the exchange mixing parameter on the structural, electronic, and magnetic properties. *Phys. Rev. B*, 86:235117, 2012. doi:10.1103/PhysRevB.86.235117.

[82] A. Alkauskas, P. Broqvist, and A. Pasquarello. Defect levels through hybrid density functionals: Insights and applications. *Phys. Status Solidi B*, 248(4):775–789, 2011. doi:10.1002/pssb.201046195.

[83] J. H. Skone, M. Govoni, and G. Galli. Self-consistent hybrid functional for condensed systems. *Phys. Rev. B*, 89:195112, 2014. doi:10.1103/PhysRevB.89.195112.

[84] M. Eckhoff, P. E. Blöchl, and J. Behler. Hybrid density functional theory benchmark study on lithium manganese oxides. *Phys. Rev. B*, 101:205113, 2020. doi:10.1103/PhysRevB.101.205113.

[85] P. E. Blöchl. Projector augmented-wave method. *Phys. Rev. B*, 50:17953–17979, 1994. doi:10.1103/PhysRevB.50.17953.

[86] P. E. Blöchl and J. Schimpl. Projector augmented wave method: *ab initio* molecular dynamics with full wave functions. *Bull. Mater. Sci.*, 26:33–41, 2003. doi:10.1007/BF02712785.

[87] F. Coester and Kümmel. Short-range correlations in nuclear wave functions. *Nucl. Phys.*, 17:477, 1960.

[88] J. Čížek. On the Correlation Problem in Atomic and Molecular Systems. Calculation of Wavefunction Components in Ursell-Type Expansion Using Quantum-Field Theoretical Methods. *J. Chem. Phys.*, 45:4256, 1966.

[89] G. D. Purvis and R. J. Bartlett. A full coupled-cluster singles and doubles model: The inclusion of disconnected triples. *J. Chem. Phys.*, 76:1910–1918, 1982.

[90] R. J. Bartlett and M. Musiał. Coupled-cluster theory in quantum chemistry. *Rev. Mod. Phys.*, 79:291–352, 2007.

[91] J. Noga and R. J. Bartlett. The full CCSDT model for molecular electronic structure. *J. Chem. Phys.*, 86:7041–7050, 1987.

[92] G. E. Scuseria and H. F. Schaefer. A new implementation of the full CCSDT model for molecular electronic structure. *Chemi. Phys. Lett.*, 152:382–386, 1988.

[93] K. Raghavachari, G. W. Trucks, J. A. Pople, and M. Head-Gordon. A fifth-order perturbation comparison of electron correlation theories. *Chem. Phys. Lett.*, 157:479–483, 1989.

[94] J. Řezáč and P. Hobza. Describing Noncovalent Interactions beyond the Common Approximations: How Accurate Is the "Gold Standard," CCSD(T) at the Complete Basis Set Limit? *J. Chem. Theory Comput.*, 9:2151–2155, 2013.

[95] G. Mills, H. Jónsson, and G. K. Schenter. Reversible work transition state theory: application to dissociative adsorption of hydrogen. *Surface Science*, 324(2):305–337, 1995. doi:10.1016/0039-6028(94)00731-4.

[96] G. Henkelman and H. Jónsson. Improved tangent estimate in the nudged elastic band method for finding minimum energy paths and saddle points. *J. Chem. Phys.*, 113(22):9978–9985, 2000. doi:10.1063/1.1323224.

[97] H. Jónsson, G. Mills, and K. W. Jacobsen. *Nudged elastic band method for finding minimum energy paths of transitions*, pages 385–404. World Scientific, 1998. doi:10.1142/9789812839664_0016.

[98] S. Smidstrup, A. Pedersen, K. Stokbro, and H. Jónsson. Improved initial guess for minimum energy path calculations. *J. Chem. Phys.*, 140(21):214106, 2014. doi:10.1063/1.4878664.

[99] O. Weser, B. Hein-Janke, and R. A. Mata. Automated handling of complex chemical structures in z-matrix coordinates—the chemcoord library. *J. Comput. Chem.*, 44(5):710–726, 2023. doi:10.1002/jcc.27029.

[100] G. Henkelman, B. P. Uberuaga, and H. Jónsson. A climbing image nudged elastic band method for finding saddle points and minimum energy paths. *J. Chem. Phys.*, 113(22):9901–9904, 2000. doi:10.1063/1.1329672.

[101] B. J. Alder and T. E. Wainwright. Phase Transition for a Hard Sphere System. *J. Chem. Phys.*, 27(5):1208–1209, 1957. doi:10.1063/1.1743957.

[102] B. J. Alder and T. E. Wainwright. Studies in Molecular Dynamics. I. General Method. *J. Chem. Phys.*, 31(2):459–466, 1959. doi:10.1063/1.1730376.

[103] L. Verlet. Computer "Experiments" on Classical Fluids. I. Thermodynamical Properties of Lennard-Jones Molecules. *Phys. Rev.*, 159:98–103, 1967. doi:10.1103/PhysRev.159.98.

[104] W. C. Swope, H. C. Andersen, P. H. Berens, and K. R. Wilson. A computer simulation method for the calculation of equilibrium constants for the formation of physical clusters of molecules: Application to small water clusters. *J. Chem. Phys.*, 76(1):637–649, 1982. doi:10.1063/1.442716.

[105] R. Hockney, S. Goel, and J. Eastwood. Quiet high-resolution computer models of a plasma. *J. Comput. Phys.*, 14(2):148–158, 1974. doi:10.1016/0021-9991(74)90010-2.

[106] P. H. Hünenberger. *Thermostat Algorithms for Molecular Dynamics Simulations*, pages 105–149. Springer Berlin Heidelberg, 2005. doi:10.1007/b99427.

[107] H. C. Andersen. Molecular dynamics simulations at constant pressure and/or temperature. *J. Chem. Phys.*, 72(4):2384–2393, 1980. doi:10.1063/1.439486.

[108] H. J. C. Berendsen, J. P. M. Postma, W. F. van Gunsteren, A. DiNola, and J. R. Haak. Molecular dynamics with coupling to an external bath. *J. Chem. Phys.*, 81(8):3684–3690, 1984. doi:10.1063/1.448118.

[109] S. Nosé. A molecular dynamics method for simulations in the canonical ensemble. *Molecular Physics*, 52(2):255–268, 1984. doi:10.1080/00268978400101201.

[110] S. Nosé. A unified formulation of the constant temperature molecular dynamics methods. *J. Chem. Phys.*, 81(1):511–519, 1984. doi:10.1063/1.447334.

[111] W. G. Hoover. Canonical dynamics: Equilibrium phase-space distributions. *Phys. Rev. A*, 31:1695–1697, 1985. doi:10.1103/PhysRevA.31.1695.

[112] J. Snoek, H. Larochelle, and R. P. Adams. Practical Bayesian Optimization of Machine Learning Algorithms. In F. Pereira, C. J. C. Burges, L. Bottou, and K. Q. Weinberger, editors, *Advances in Neural Information Processing Systems 25*, pages 2951–2959. Curran Associates, Inc., 2012. URL: http://papers.nips.cc/paper/4522-practical-bayesian-optimization-of-machine-learning-algorithms.pdf.

[113] P. I. Frazier. A tutorial on bayesian optimization. http://arxiv.org/abs/1807.02811, 2018.

[114] C. E. Rasmussen and C. K. I. Williams. *Gaussian Processes for Machine Learning*. The MIT Press, 2005. doi:10.7551/mitpress/3206.001.0001.

[115] J. Joyce. Bayes' Theorem. In E. N. Zalta, editor, *The Stanford Encyclopedia of Philosophy*. Metaphysics Research Lab, Stanford University, Fall 2021 edition, 2021.

[116] J. Močkus. *Optimization Techniques IFIP Technical Conference Novosibirsk, July 1–7, 1974*, pages 400–404. Springer Berlin Heidelberg, 1975. doi:10.1007/3-540-07165-2_55.

[117] E. Brochu, V. M. Cora, and N. de Freitas. A Tutorial on Bayesian Optimization of Expensive Cost Functions, with Application to Active User Modeling and Hierarchical Reinforcement Learning, 2010. arXiv:1012.2599.

[118] J. Močkus, V. Tiesis, and A. Zilinskas. The Application of Bayesian Methods for Seeking the Extremum. *Towards Global Optimization*, 2(117-129):2, 1978.

[119] R. A. Schulz. *Activation and transformation of small molecules at a bimetallic β-diketiminato nickel platform*. Georg-August-Universität Göttingen, 2022.

[120] J. Magano and J. R. Dunetz. Large-Scale Applications of Transition Metal-Catalyzed Couplings for the Synthesis of Pharmaceuticals. *Chem. Rev.*, 111(3):2177–2250, 2011. doi:10.1021/cr100346g.

[121] D. V. Gutsulyak, W. E. Piers, J. Borau-Garcia, and M. Parvez. Activation of Water, Ammonia, and Other Small Molecules by PC(carbene)P Nickel Pincer Complexes. *J. Am. Chem. Soc.*, 135(32):11776–11779, 2013. doi:10.1021/ja406742n.

[122] M.-C. Chang, K. A. Jesse, A. S. Filatov, and J. S. Anderson. Reversible homolytic activation of water via metal–ligand cooperativity in a T-shaped Ni(ii) complex. *Chem. Sci.*, 10:1360–1367, 2019. doi:10.1039/C8SC03719A.

[123] O. V. Ozerov. Oxidative addition of water to transition metal complexes. *Chem. Soc. Rev.*, 38:83–88, 2009. doi:10.1039/B802420K.

[124] D.-H. Manz, P.-C. Duan, S. Dechert, S. Demeshko, R. Oswald, M. John, R. A. Mata, and F. Meyer. Pairwise H2/D2 Exchange and H2 Substitution at a Bimetallic Dinickel(II) Complex Featuring Two Terminal Hydrides. *J. Am. Chem. Soc.*, 139(46):16720–16731, 2017. doi:10.1021/jacs.7b08629.

[125] P.-C. Duan, R. A. Schulz, A. Römer, B. E. Van Kuiken, S. Dechert, S. Demeshko, G. E. Cutsail III, S. DeBeer, R. A. Mata, and F. Meyer. Ligand Protonation Triggers H2 Release from a Dinickel Dihydride Complex to Give a Doubly "T"-Shaped Dinickel(I) Metallodiradical. *Angew. Chem.*, 60(4):1891–1896, 2021. doi:10.1002/anie.202011494.

[126] F. Neese. The ORCA program system. *WIREs Comput. Mol. Sci.*, 2(1):73–78, 2012. doi:10.1002/wcms.81.

[127] F. Neese. Software update: the ORCA program system, version 4.0. *WIREs Comput. Mol. Sci.*, 8(1):e1327, 2018. doi:10.1002/wcms.1327.

[128] F. Weigend and R. Ahlrichs. Balanced basis sets of split valence, triple zeta valence and quadruple zeta valence quality for H to Rn: Design and assessment of accuracy. *Phys. Chem. Chem. Phys.*, 7:3297–3305, 2005. doi:10.1039/B508541A.

[129] F. Weigend. Accurate Coulomb-fitting basis sets for H to Rn. *Phys. Chem. Chem. Phys.*, 8:1057–1065, 2006. doi:10.1039/B515623H.

[130] S. Grimme, J. Antony, S. Ehrlich, and H. Krieg. A consistent and accurate ab initio parametrization of density functional dispersion correction (DFT-D) for the 94 elements H-Pu. *J. Chem. Phys.*, 132(15):154104, 2010. doi:10.1063/1.3382344.

[131] S. Grimme, S. Ehrlich, and L. Goerigk. Effect of the damping function in dispersion corrected density functional theory. *J. Comput. Chem.*, 32(7):1456–1465, 2011. doi:10.1002/jcc.21759.

[132] H. Hirao. Which DFT Functional Performs Well in the Calculation of Methylcobalamin? Comparison of the B3LYP and BP86 Functionals and Evaluation of the Impact of Empirical Dispersion Correction. *J. Phys. Chem. A*, 115(33):9308–9313, 2011. doi:10.1021/jp2052807.

[133] T. Weymuth, E. P. A. Couzijn, P. Chen, and M. Reiher. New Benchmark Set of Transition-Metal Coordination Reactions for the Assessment of Density Functionals. *J. Chem. Theory Comput.*, 10(8):3092–3103, 2014. doi:10.1021/ct500248h.

[134] W. Koch and M. C. Holthausen. *A Chemist's Guide to Density Functional Theory*. Wiley-VCH, 2nd edition, 2001. doi:10.1002/3527600043.ch8.

[135] K. J. Laidler and M. C. King. Development of transition-state theory. *J. Phys. Chem.*, 87(15):2657–2664, 1983. doi:10.1021/j100238a002.

[136] V. Barone and M. Cossi. Quantum Calculation of Molecular Energies and Energy Gradients in Solution by a Conductor Solvent Model. *J. Phys. Chem. A*, 102(11):1995–2001, 1998. doi:10.1021/jp9716997.

[137] H. Eyring and M. Polanyi. On Simple Gas Reactions. *Z. Phys. Chem. Abt. B*, 12:279–311, 1931. doi:doi:10.1524/zpch.2013.9023.

[138] H. Eyring. The Activated Complex in Chemical Reactions. *J. Chem. Phys.*, 3(2):107–115, 1935. doi:10.1063/1.1749604.

[139] M. G. Evans and M. Polanyi. Some applications of the transition state method to the calculation of reaction velocities, especially in solution. *Trans. Faraday Soc.*, 31:875–894, 1935. doi:10.1039/TF9353100875.

[140] S. Grimme, J. G. Brandenburg, C. Bannwarth, and A. Hansen. Consistent structures and interactions by density functional theory with small atomic orbital basis sets. *J. Chem. Phys.*, 143(5):054107, 2015. doi:10.1063/1.4927476.

[141] G. Savasci, M. Borges-Martínez, R. Berger, C. Ochsenfeld, and R. Mera-Adasme. A comparison of computational methodologies for the structural modelling of biologically relevant zinc complexes. *J. Mol. Model.*, 25(9):258, 2019. doi:10.1007/s00894-019-4139-8.

[142] N. V. Belkova, L. M. Epstein, O. A. Filippov, and E. S. Shubina. Hydrogen and Dihydrogen Bonds in the Reactions of Metal Hydrides. *Chem. Rev.*, 116(15):8545–8587, 2016. doi:10.1021/acs.chemrev.6b00091.

[143] M. K. Kesharwani, B. Brauer, and J. M. L. Martin. Frequency and Zero-Point Vibrational Energy Scale Factors for Double-Hybrid Density Functionals (and Other Selected Methods): Can Anharmonic Force Fields Be Avoided? *J. Phys. Chem. A*, 119(9):1701–1714, 2015. doi:10.1021/jp508422u.

[144] A. K. Chandra and T. Uchimaru. A DFT Study on the C-H Bond Dissociation Enthalpies of Haloalkanes: Correlation between the Bond Dissociation Enthalpies and Activation Energies for Hydrogen Abstraction. *J. Phys. Chem. A*, 104(40):9244–9249, 2000. doi:10.1021/jp001815x.

[145] A. Römer, L. Hasecke, P. Blöchl, and R. A. Mata. A Review of Density Functional Models for the Description of Fe(II) Spin-Crossover Complexes. *Molecules*, 25(21), 2020. doi:10.3390/molecules25215176.

[146] H. Phan, J. J. Hrudka, D. Igimbayeva, L. M. Lawson Daku, and M. Shatruk. A Simple Approach for Predicting the Spin State of Homoleptic Fe(II) Tris-diimine Complexes. *J. Am. Chem. Soc.*, 139(18):6437–6447, 2017. doi:10.1021/jacs.7b02098.

[147] M. Sotoudeh, S. Rajpurohit, P. Blöchl, D. Mierwaldt, J. Norpoth, V. Roddatis, S. Mildner, B. Kressdorf, B. Ifland, and C. Jooss. Electronic structure of $Pr_{1-x}Ca_xMnO_3$. *Phys. Rev. B*, 95:235150, 2017. doi:10.1103/PhysRevB.95.235150.

[148] L. Kong, F. A. Bischoff, and E. F. Valeev. Explicitly Correlated R12/F12 Methods for Electronic Structure. *Chem. Rev.*, 112(1):75–107, 2012. doi:10.1021/cr200204r.

[149] T. B. Adler, G. Knizia, and H.-J. Werner. A simple and efficient CCSD(T)-F12 approximation. *J. Chem. Phys.*, 127(22):221106, 2007. doi:10.1063/1.2817618.

[150] G. Knizia and H.-J. Werner. Explicitly correlated RMP2 for high-spin open-shell reference states. *J. Chem. Phys.*, 128(15):154103, 2008. doi:10.1063/1.2889388.

[151] H.-J. Werner, P. J. Knowles, G. Knizia, F. R. Manby, M. Schütz, P. Celani, W. Györffy, D. Kats, T. Korona, R. Lindh, A. Mitrushenkov, G. Rauhut,

K. R. Shamasundar, T. B. Adler, R. D. Amos, S. J. Bennie, A. Bernhardsson, A. Berning, D. L. Cooper, M. J. O. Deegan, A. J. Dobbyn, F. Eckert, E. Goll, C. Hampel, A. Hesselmann, G. Hetzer, T. Hrenar, G. Jansen, C. Köppl, S. J. R. Lee, Y. Liu, A. W. Lloyd, Q. Ma, R. A. Mata, A. J. May, S. J. McNicholas, W. Meyer, T. F. Miller III, M. E. Mura, A. Nicklass, D. P. O'Neill, P. Palmieri, D. Peng, K. Pflüger, R. Pitzer, M. Reiher, T. Shiozaki, H. Stoll, A. J. Stone, R. Tarroni, T. Thorsteinsson, M. Wang, and M. Welborn. Molpro, version 2019.2, a package of ab initio programs, 2019.

[152] G. Knizia, T. B. Adler, and H.-J. Werner. Simplified CCSD(T)-F12 methods: Theory and benchmarks. *J. Chem. Phys.*, 130(5):054104, 2009. doi:10.1063/1.3054300.

[153] K. A. Peterson, T. B. Adler, and H.-J. Werner. Systematically convergent basis sets for explicitly correlated wavefunctions: The atoms H, He, B–Ne, and Al–Ar. *J. Chem. Phys.*, 128(8):084102, 2008. doi:10.1063/1.2831537.

[154] N. B. Balabanov and K. A. Peterson. Systematically convergent basis sets for transition metals. I. All-electron correlation consistent basis sets for the 3d elements Sc–Zn. *J. Chem. Phys.*, 123(6):064107, 2005. doi:10.1063/1.1998907.

[155] D. H. Bross, J. G. Hill, H.-J. Werner, and K. A. Peterson. Explicitly correlated composite thermochemistry of transition metal species. *J. Chem. Phys.*, 139(9):094302, 2013. doi:10.1063/1.4818725.

[156] F. Weigend. Hartree–Fock exchange fitting basis sets for H to Rn. *J. Comput. Chem.*, 29(2):167–175, 2008. doi:10.1002/jcc.20702.

[157] T. H. Dunning. Gaussian basis sets for use in correlated molecular calculations. I. The atoms boron through neon and hydrogen. *J. Chem. Phys.*, 90(2):1007–1023, 1989. doi:10.1063/1.456153.

[158] A. Wolf, M. Reiher, and B. A. Hess. The generalized Douglas–Kroll transformation. *J. Chem. Phys.*, 117(20):9215–9226, 2002. doi:10.1063/1.1515314.

[159] B. A. Heß. Relativistic Effects in Heavy-Element Chemistry. *Ber. Bunsenges. Phys. Chem.*, 101(1):1–10, 1997. doi:10.1002/bbpc.19971010102.

[160] B. M. Flöser, Y. Guo, C. Riplinger, F. Tuczek, and F. Neese. Detailed Pair Natural Orbital-Based Coupled Cluster Studies of Spin Crossover Energetics. *J. Chem. Theory Comput.*, 16(4):2224–2235, 2020. doi:10.1021/acs.jctc.9b01109.

[161] M. Radoń. Benchmarking quantum chemistry methods for spin-state energetics of iron complexes against quantitative experimental data. *Phys. Chem. Chem. Phys.*, 21:4854–4870, 2019. doi:10.1039/C9CP00105K.

[162] M. Feldt, Q. M. Phung, K. Pierloot, R. A. Mata, and J. N. Harvey. Limits of Coupled-Cluster Calculations for Non-Heme Iron Complexes. *J. Chem. Theory Comput.*, 15(2):922–937, 2019. doi:10.1021/acs.jctc.8b00963.

[163] S. Song, M.-C. Kim, E. Sim, A. Benali, O. Heinonen, and K. Burke. Benchmarks and Reliable DFT Results for Spin Gaps of Small Ligand Fe(II) Complexes. *J. Chem. Theory Comput.*, 14(5):2304–2311, 2018. doi:10.1021/acs.jctc.7b01196.

[164] C. L. Janssen and I. M. B. Nielsen. New diagnostics for coupled-cluster and Møller–Plesset perturbation theory. *Chem. Phys. Lett.*, 290(4):423 – 430, 1998. doi:10.1016/S0009-2614(98)00504-1.

[165] W. Jiang, N. J. DeYonker, and A. K. Wilson. Multireference Character for 3d Transition-Metal-Containing Molecules. *J. Chem. Theory Comput.*, 8(2):460–468, 2012. doi:10.1021/ct2006852.

[166] F. Neese, F. Wennmohs, A. Hansen, and U. Becker. Efficient, approximate and parallel Hartree-Fock and hybrid DFT calculations. A 'chain-of-spheres' algorithm for the Hartree-Fock exchange. *Chem. Phys.*, 356(1-3):98–109, 2009. doi:10.1016/j.chemphys.2008.10.036.

[167] S. Grimme, J. Antony, S. Ehrlich, and H. Krieg. A consistent and accurate ab initio parametrization of density functional dispersion correction (DFT-D) for the 94 elements H-Pu. *J. Chem. Phys.*, 132(15):154104, 2010. doi:10.1063/1.3382344.

[168] S. Grimme, S. Ehrlich, and L. Goerigk. Effect of the damping function in dispersion corrected density functional theory. *J. Comput. Chem.*, 32(7):1456–

1465, 2011. doi:10.1002/jcc.21759.

[169] M. Reiher, O. Salomon, and B. Artur Hess. Reparameterization of hybrid functionals based on energy differences of states of different multiplicity. *Theor. Chem. Acc.*, 107(1):48–55, 2001. doi:10.1007/s00214-001-0300-3.

[170] O. Salomon, M. Reiher, and B. A. Hess. Assertion and validation of the performance of the B3LYP* functional for the first transition metal row and the G2 test set. *J. Chem. Phys.*, 117(10):4729–4737, 2002. doi:10.1063/1.1493179.

[171] E. I. Ioannidis and H. J. Kulik. Towards quantifying the role of exact exchange in predictions of transition metal complex properties. *J. Chem. Phys.*, 143(3):034104, 2015. doi:10.1063/1.4926836.

[172] G. Ganzenmüller, N. Berkaïne, A. Fouqueau, M. E. Casida, and M. Reiher. Comparison of density functionals for differences between the high- (T2g5) and low- (A1g1) spin states of iron(II) compounds. IV. Results for the ferrous complexes [Fe(L)('NHS4')]. *J. Chem. Phys.*, 122(23):234321, 2005. doi:10.1063/1.1927081.

[173] O. S. Siig and K. P. Kepp. Iron(II) and Iron(III) Spin Crossover: Toward an Optimal Density Functional. *J. Phys. Chem. A*, 122(16):4208–4217, 2018. doi:10.1021/acs.jpca.8b02027.

[174] The GPyOpt authors. Gpyopt: A bayesian optimization framework in python. http://github.com/SheffieldML/GPyOpt, 2016.

[175] W.-L. Loh. On Latin hypercube sampling. *Ann. Statist.*, 24(5):2058–2080, 1996. doi:10.1214/aos/1069362310.

[176] M. Sotoudeh, S. Rajpurohit, P. Blöchl, D. Mierwaldt, J. Norpoth, V. Roddatis, S. Mildner, B. Kressdorf, B. Ifland, and C. Jooss. Electronic structure of $Pr_{1-x}Ca_xMnO_3$. *Phys. Rev. B*, 95:235150, 2017. doi:10.1103/PhysRevB.95.235150.

[177] M. Swart, A. R. Groenhof, A. W. Ehlers, and K. Lammertsma. Validation of Exchange-Correlation Functionals for Spin States of Iron Complexes. *J. Phys. Chem. A*, 108(25):5479–5483, 2004. doi:10.1021/jp049043i.

[178] S. A. Borshch and E. M. Zueva. Theoretical Study of Spin-State and Redox Multistability in an Iron [2×2] Grid Complex. *Eur. J. Inorg. Chem.*, 2013(5-6):1009–1014, 2013. doi:10.1002/ejic.201201074.

[179] M. A. Naumova, A. Kalinko, J. W. L. Wong, S. Alvarez Gutierrez, J. Meng, M. Liang, M. Abdellah, H. Geng, W. Lin, K. Kubicek, M. Biednov, F. Lima, A. Galler, P. Zalden, S. Checchia, P.-A. Mante, J. Zimara, D. Schwarzer, S. Demeshko, V. Murzin, D. Gosztola, M. Jarenmark, J. Zhang, M. Bauer, M. L. Lawson Daku, D. Khakhulin, W. Gawelda, C. Bressler, F. Meyer, K. Zheng, and S. E. Canton. Exploring the light-induced dynamics in solvated metallogrid complexes with femtosecond pulses across the electromagnetic spectrum. *J. Chem. Phys.*, 152(21):214301, 2020. doi:10.1063/1.5138641.

[180] Y. Sunatsuki, H. Ohta, M. Kojima, Y. Ikuta, Y. Goto, N. Matsumoto, S. Iijima, H. Akashi, S. Kaizaki, F. Dahan, and J.-P. Tuchagues. Supramolecular Spin-Crossover Iron Complexes Based on Imidazole-Imidazolate Hydrogen Bonds. *Inorg. Chem.*, 43(14):4154–4171, 2004. doi:10.1021/ic0498384.

[181] K. Pierloot and S. Vancoillie. Relative energy of the high-(T2g5) and low-(A1g1) spin states of [Fe(H2O)6]2+, [Fe(NH3)6]2+, and [Fe(bpy)3]2+: CASPT2 versus density functional theory. *J. Chem. Phys.*, 125(12):124303, 2006. doi:10.1063/1.2353829.

[182] L. Wilbraham, P. Verma, D. G. Truhlar, L. Gagliardi, and I. Ciofini. Multiconfiguration Pair-Density Functional Theory Predicts Spin-State Ordering in Iron Complexes with the Same Accuracy as Complete Active Space Second-Order Perturbation Theory at a Significantly Reduced Computational Cost. *J. Phys. Chem. Lett.*, 8(9):2026–2030, 2017. doi:10.1021/acs.jpclett.7b00570.

[183] Q. Ma and H.-J. Werner. Scalable Electron Correlation Methods. 8. Explicitly Correlated Open-Shell Coupled-Cluster with Pair Natural Orbitals PNO-RCCSD(T)-F12 and PNO-UCCSD(T)-F12. *J. Chem. Theory Comput.*, 17(2):902–926, 2021. doi:10.1021/acs.jctc.0c01129.

[184] W. Klopper and C. C. M. Samson. Explicitly correlated second-order Møller–Plesset methods with auxiliary basis sets. *J. Chem. Phys.*,

116(15):6397–6410, 2002. doi:10.1063/1.1461814.

[185] H.-J. Werner, T. B. Adler, and F. R. Manby. General orbital invariant MP2-F12 theory. *J. Chem. Phys.*, 126(16), 2007. doi:10.1063/1.2712434.

[186] M. Steinert, B. Schneider, S. Dechert, S. Demeshko, and F. Meyer. Spin-State Versatility in a Series of Fe4 [2 × 2] Grid Complexes: Effects of Counteranions, Lattice Solvent, and Intramolecular Cooperativity. *Inorg. Chem.*, 55(5):2363–2373, 2016. doi:10.1021/acs.inorgchem.5b02762.

[187] E. Breuning, M. Ruben, J.-M. Lehn, F. Renz, Y. Garcia, V. Ksenofontov, P. Gütlich, E. Wegelius, and K. Rissanen. Spin Crossover in a Supramolecular Fe_4II [2×2] Grid Triggered by Temperature, Pressure, and Light. *Angew. Chem. Int. Ed.*, 39(14):2504–2507, 2000. doi:10.1002/1521-3773(20000717)39:14<2504::AID-ANIE2504>3.0.CO;2-B.

[188] B. Schneider. *Multistabile Gitterkomplexe*. Georg-August-Universität Göttingen, 2012.

[189] W. Nicolazzi and A. Bousseksou. Thermodynamical aspects of the spin crossover phenomenon. *C. R. Chim.*, 21(12):1060–1074, 2018. Spin crossover phenomenon / Phénomène de transition de spin. doi:10.1016/j.crci.2018.10.003.

[190] E. M. Zueva, E. R. Ryabikh, and S. A. Borshch. Theoretical Analysis of Spin Crossover in Iron(II) [2 × 2] Molecular Grids. *Inorg. Chem.*, 50(21):11143–11151, 2011. doi:10.1021/ic2016929.

[191] Y. Pan, Y.-S. Meng, Q. Liu, W.-Q. Gao, C.-H. Liu, T. Liu, and Y.-Y. Zhu. Construction of SCO-Active Fe(II) Mononuclear Complexes from the Thiopybox Ligand. *Inorg. Chem.*, 59(11):7398–7407, 2020. doi:10.1021/acs.inorgchem.9b03506.

[192] J. Behler. Representing potential energy surfaces by high-dimensional neural network potentials. *J. Phys. Condens.*, 26(18):183001, 2014. doi:10.1088/0953-8984/26/18/183001.

[193] J. Behler. Constructing high-dimensional neural network potentials: A tutorial review. *Int. J. Quantum Chem.*, 115(16):1032–1050, 2015. doi:10.1002/qua.24890.

[194] J. Behler. First Principles Neural Network Potentials for Reactive Simulations of Large Molecular and Condensed Systems. *Angew. Chem. Int. Edit.*, 56(42):12828–12840, 2017. doi:10.1002/anie.201703114.

[195] J. Behler. Four Generations of High-Dimensional Neural Network Potentials. *Chem. Rev.*, 121(16):10037–10072, 2021. doi:10.1021/acs.chemrev.0c00868.

[196] H. Huo and M. Rupp. Unified representation of molecules and crystals for machine learning. *Mach. learn.: sci. technol.*, 3(4):045017, 2022. doi:10.1088/2632-2153/aca005.

[197] L. Himanen, M. O. Jäger, E. V. Morooka, F. F. Canova, Y. S. Ranawat, D. Z. Gao, P. Rinke, and A. S. Foster. Dscribe: Library of descriptors for machine learning in materials science. *Comput. Phys. Commun.*, 247:106949, 2020. doi:10.1016/j.cpc.2019.106949.

[198] J. I. van der Vlugt, S. Demeshko, S. Dechert, and F. Meyer. Tetranuclear CoII, MnII, and CuII Complexes of a Novel Binucleating Pyrazolate Ligand Preorganized for the Self-Assembly of Compact [2 × 2]-Grid Structures. *Inorg. Chem.*, 47(5):1576–1585, 2008. doi:10.1021/ic701951a.

[199] M. Kaneko and S. Nakashima. Computational Study on Thermal Spin-Crossover Behavior for Coordination Polymers Possessing trans - Fe(NCS)2(pyridine)4 Unit. *Bull. Chem. Soc. Jpn.*, 88:1164, 2015. doi:10.1246/bcsj.20150026.

[200] K. Senthil Kumar, Y. Bayeh, T. Gebretsadik, F. Elemo, M. Gebrezgiabher, M. Thomas, and M. Ruben. Spin-crossover in iron(ii)-Schiff base complexes. *Dalton T.*, 48:15321–15337, 2019. doi:10.1039/C9DT02085C.

[201] A. Nowak and K. Boguslawski. A configuration interaction correction on top of pair coupled cluster doubles. *Phys. Chem. Chem. Phys.*, 25:7289–7301, 2023. doi:10.1039/D2CP05171K.

[202] Y. Sherry and N. C. Thompson. How Fast Do Algorithms Improve? [Point of View]. *Proc. IEEE*, 109(11):1768–1777, 2021. doi:10.1109/JPROC.2021.3107219.

[203] A. Chiolerio, T. C. Draper, C. Jost, and A. Adamatzky. Electrical properties of solvated tectomers: Toward zettascale computing. *Adv. Electron. Mater.*, 5(12):1900202, 2019. doi:10.1002/aelm.201900202.

Appendix A

Supplemental material for Chapter 3

A.1 ORCA input files

Optimization of **A.2**

```
!BP86 def2-SVP def2/J D3BJ Opt PAL8 tightscf tightopt slowconv
%scf
BrokenSym 1,1
MaxIter 600
DIISMaxEq 20
directresetfreq 10
end
*xyzfile 0 3 *.xyz
```

NEB with **A.4** as reactant and **A.3** product

```
!BP86 def2-SVP def2/J D3BJ NEB-TS PAL8 slowconv
%neb
NEB_End_XYZFile "g3.xyz"
Nimages 8
end
%scf
BrokenSym 1,1
```

```
MaxIter 600
DIISMaxEq 20
directresetfreq 10
end
*xyzfile 0 3 g4.xyz
```

Transition state optimization, using the NEB's climbing image

```
!BP86 def2-SVP def2/J D3BJ PAL8 OptTS slowconv NumFreq
%geom
Calc_Hess true
NumHess true
Recalc_Hess 5
end
%scf
BrokenSym 1,1
MaxIter 600
DIISMaxEq 20
directresetfreq 10
end
*xyzfile 0 3 4-3_CI.xyz
```

MD simulation of **A.3** with explicit THF molecule

```
! MD PBEh-3c PAL8
%md
timestep 1.0_fs
initvel 250_K
thermostat berendsen 250_K timecon 10.0_fs
dump position stride 1 filename "trajectory.xyz"
run 5000
end
*xyzfile 0 1 md_thf.xyz
```

A.2 Structural data of relevant complexes

Optimized **A.2K** complex, in XYZ format

```
101
Coordinates from ORCA-job ga
  C   -0.07883610225069     21.39359663916554     22.78939122487010
  C   -1.08766359540147     20.40222065717644     22.96256440665080
  C   -1.02892555097725     19.48171745410627     24.04693660133042
  C   0.04821364827644     19.56827056889062     24.94665811387301
  C   1.05065297491450     20.53576181090074     24.78255959701728
  C   0.98402201574527     21.43701106896818     23.70873814842992
  N   -2.14779152673843     20.31888127611749     22.01668609151903
  C   -3.24775560513601     21.08779035480527     22.16619558331503
  C   -3.37142519741498     21.93352687162730     23.41741868060502
  C   -2.09454493333161     18.40089638243915     24.17364040040205
  C   -2.33555241264024     17.92583626762335     25.61192949599611
  C   -0.13667304462450     22.32154118303392     21.58221495487156
  C   0.48177828651217     23.70397358384894     21.83426885247031
  Ni  -1.82223988744401     19.21863869271571     20.55461919821208
  N   -3.39745965114924     19.66346769687622     19.52615031075573
  C   -4.32422243222648     20.54367582989221     19.92428327295358
  C   -4.27556152499384     21.16783037151130     21.19772691907347
  C   -3.41499403169869     19.10994859956636     18.17330586553161
  C   -2.38291273716905     18.01835041048718     18.10870476945475
  N   -1.49143427607768     17.96682531195434     19.14776179662079
  N   -0.67507029527851     16.89249661016864     18.96082996882055
  C   -1.03317321444893     16.27412211476232     17.79389981160287
  C   -2.12852000999422     16.95309397733587     17.21769532762029
  C   -0.23351987950354     15.05893398346974     17.41160522479380
  N   0.56688992485777     14.66025093490440     18.56614601258059
  C   1.38656961965653     13.60692539610993     18.50155658060711
  C   2.20669900814627     13.21521352294838     19.59613200780831
  C   2.27037500315353     13.78981364072584     20.88401750137416
  C   3.22970820096604     13.18841581372635     21.89352243002106
  K   -2.92657259574972     15.97149057918960     20.53005093758022
  Ni  0.49890224084636     15.86676124995948     20.06914046229490
  N   1.54280976050526     14.87001144056459     21.24849671713196
  C   1.37509394517718     15.19284981290200     22.61858396852964
  C   1.94184444439547     16.39319317908535     23.13739785863235
  C   1.78256972237333     16.68172540244953     24.50388605766018
  C   1.06411760982505     15.82187373789364     25.34813046908237
  C   0.46782903855005     14.66505865681644     24.82051608605965
  C   0.60147647945035     14.33089386925603     23.46060560769867
  C   2.64031824612750     17.35877523299543     22.19151627469496
  C   1.60981859563068     18.33008453230613     21.58542917246300
  C   -0.11082696402812     13.11556344959429     22.86267706009717
  C   -0.55481844154277     12.07344929042638     23.89614760635851
  C   1.47186346493619     12.79736921636136     17.22361491127134
  C   -1.29981547704178     13.56352288048817     21.98700430673312
  C   3.79129692927430     18.14011191978836     22.83822292472648
  C   -1.73090678473688     17.21628732566418     23.26087269300283
  C   0.50613203680184     21.63160092857875     20.36297166837445
  C   -5.46293616838009     20.90968825710082     18.99293947366772
  H   -2.64710022333700     16.72120964199075     16.28090934560333
  H   -0.91548617018384     14.24396628306885     17.06957854365789
  H   0.41108098370418     15.29621736476357     16.53013205974991
  H   0.47716217204980     12.40026324015470     16.92773833320753
  H   2.16348138864517     11.94195220463875     17.33239916110392
  H   1.82569677315561     13.42173355910417     16.37496741934577
  H   2.87625519214169     12.36290209546502     19.41554901629484
  H   3.88198293249917     13.97647218987802     22.32347659810805
  H   3.86572154643262     12.41641791339091     21.42236006018554
  H   2.70400706236190     12.72418982043744     22.75389906726402
  H   -0.11606818949908     14.01413208857591     25.48743771337862
  H   0.96100528991541     16.05510237383867     26.41924609231174
```

```
  H   2.22822623862756     17.59931902858255     24.91148418872084
  H   3.05024454398582     16.74726669051768     21.36060621221980
  H   4.33295188125421     18.72955143843496     22.06991969142655
  H   4.51995881938037     17.46457490461409     23.33138616998622
  H   3.42346369599992     18.86238920922097     23.59676117283059
  H   1.18175827051001     18.98657305736876     22.36724353639416
  H   0.75267927381923     17.79933979363605     21.10345636448560
  H   2.07003847138849     18.96683525509920     20.80322975258672
  H   0.59610667050065     12.61302783986992     22.17000603556886
  H   -1.78078433256521     12.69415455548640     21.49054376387830
  H   -0.91545646451888     14.25598130615566     21.19737801059969
  H   -2.05863104140559     14.07742316758430     22.61859782547885
  H   0.29043087806764     11.75025492512457     24.53656004776306
  H   -0.95969351459624     11.17507659924723     23.38738322790448
  H   -1.35544089615412     12.45914443012582     24.56272082089261
  H   -3.18495879681556     19.90127327766626     17.41802560926642
  H   -4.41293597835627     18.70316362891517     17.88169425780018
  H   -5.08069036573631     21.38485856153606     18.06410505177593
  H   -6.16766382606213     21.61446624990983     19.47222054708488
  H   -6.03543990377952     20.01228651948323     18.67313466846863
  H   -5.11433048015030     21.83348641580920     21.44381247144734
  H   -3.26896390171922     21.31593181795484     24.33356733905028
  H   -4.34227449171051     22.46134272084879     23.44976189970431
  H   -2.55845545881681     22.68844902242148     23.46971134416225
  H   0.10576254951277     18.86681586087943     25.79102890982269
  H   1.88671337414184     20.59033282372554     25.49726358363739
  H   1.77772913916807     22.18909989041580     23.58506015076265
  H   -1.20922236436474     22.46802416941368     21.33659346621567
  H   1.58587941317957     21.44435080249368     20.53612974677969
  H   0.39802959607324     22.25027344274441     19.44771075090774
  H   0.01437056295408     20.64962820924132     20.17113526412260
  H   0.04897356210303     24.18653055551515     22.73478755974363
  H   0.30043698762030     24.37047203233591     20.96590451296609
  H   1.58197763343406     23.64827248180155     21.97599946345136
  H   -3.03883374234334     18.83650036679485     23.78363851517224
  H   -1.61555957409585     17.58581759826308     22.21037936288165
  H   -2.52079461650858     16.43111234043050     23.30879772135571
  H   -0.77702178184355     16.74979084990613     23.56581023363114
  H   -3.20341385193276     17.23479638903879     25.65058321624166
  H   -2.54283465156310     18.77587356107122     26.29327504662908
  H   -1.46105114071106     17.36996944772365     26.00827567072235
```

Optimized **A.3** complex, in XYZ format

```
104
Coordinates from ORCA-job gd
  C   -0.37518617397377     20.99977384541864     22.51072702673551
  C   -1.46058162957891     20.21622689147698     23.00104136286686
  C   -1.36216086869867     19.52450246145612     24.23819748948732
  C   -0.16007475257462     19.61959873571800     24.97009607482352
  C   0.92643672443562     20.36987246313386     24.49191717275028
  C   0.81479205788449     21.05453820535158     23.26714959910645
  N   -2.65926208498170     20.14418293988104     22.23555870630674
  C   -2.67516240350369     19.26131500059433     21.21494498867276
  C   -1.47485639784289     18.36117720814399     20.98925507840430
  C   -2.52639379484096     18.69375145334129     24.76026226679522
  C   -2.16948773367051     17.19619036805749     24.80412410810868
  C   -0.53958712216126     21.79745943193231     21.21867101377527
  C   0.77681904450745     22.07133361106266     20.48108704901163
  Ni  -4.08893362589539     21.27498119190495     22.75599152931995
  N   -5.24150287055590     20.71069418291116     21.38488618915869
  C   -4.98846263401971     19.81578649600049     20.42501000352715
  C   -3.76308029408365     19.11747061549290     20.33987529530620
  C   -6.56636410643354     21.33887015452811     21.39710821237626
  C   -6.66660895014614     22.20365787939064     22.60288724422504
  N   -5.49725218349764     22.45609897233220     23.24545659718106
  N   -5.76173217737286     23.26170654794812     24.31205510979848
  C   -7.10424219168619     23.49818454431520     24.34087050821434
```

C	-7.72738325337203	22.84693741902559	23.26257765195267
C	-7.60867128516476	24.33342707949781	25.46825791729527
N	-6.45904908416873	24.85001331592381	26.20920067533865
C	-6.67680169573045	25.65649177555195	27.24743361208797
C	-5.61524321945559	26.27398252811930	27.95368710460934
C	-4.24722011581470	26.18415098562525	27.64936782838684
C	-3.29687966355832	27.03261187941978	28.47664498404708
Ni	-4.76548829914893	24.34643077898611	25.48915949202061
N	-3.75050871038262	25.40446607442091	26.65719724098737
C	-2.34307390201683	25.44030263906900	26.46437737878613
C	-1.80298511421321	26.19188978691587	25.37859992824351
C	-0.40254498379071	26.26353156462746	25.23725854688659
C	0.45532599215121	25.61461705161218	26.14266304331852
C	-0.08968046634538	24.84570387572836	27.18553410291371
C	-1.48531259619931	24.73319647024294	27.35859886327028
C	-2.74494401213073	26.88122601847734	24.40374211782106
C	-3.07601700089539	28.31521876703682	24.85748248187770
C	-2.08233303867756	23.79840737482826	28.40735501337484
C	-2.42412236886127	22.44499320250243	27.75319111238397
C	-8.09332353624827	25.96651397636075	27.68408987837460
C	-1.20443547049249	23.61515457573544	29.65144289584882
C	-2.24970144532877	26.83729287573700	22.95300030152100
C	-6.04786779471126	19.49977920705831	19.38932554988302
C	-3.02381004161153	19.20907101539899	26.12223728535404
C	-1.31509638496804	23.10411457988989	21.48629708563832
K	-1.08560580139068	23.13445032682525	24.72995132759976
H	-8.79088218933679	22.83909934894849	23.00149112100446
H	-8.24358717374397	25.16501553647088	25.08161070994286
H	-8.27601658819911	23.72102929857322	26.12177113099560
H	-8.66053737632475	26.47987220124395	26.87785144962504
H	-8.10352274581198	26.61526538783878	28.57868059462025
H	-8.65384407583699	25.03742092524195	27.92092512848611
H	-5.89266715420314	26.93373720701734	28.78652378976270
H	-2.63358382526599	26.41516380730548	29.11778915225749
H	-3.86495885877111	27.71706894989020	29.13299294199632
H	-2.62387632896917	27.63614719587909	27.83460158499426
H	0.02515555524910	26.84903254296562	24.40893622757039
H	1.54753676479500	25.70489085157606	26.03403513858089
H	0.58534625425040	24.32166239653322	27.87882242315159
H	-3.04836832459277	24.23658681960616	28.72847687290593
H	-1.74415394781453	23.02066826134280	30.41627538145442
H	-0.92548470899955	24.58756325478603	30.10618983565683
H	-0.26611066046598	23.06728011035123	29.42154206456408
H	-1.50873994714270	21.90931757521350	27.41761525961606
H	-3.09865689954161	22.58865585413166	26.88267379683738
H	-2.94712201487777	21.77413905628087	28.46410115551516
H	-3.68778820950536	26.29189053578982	24.45270120988306
H	-3.01860272972254	27.25826397013775	22.27402735418186
H	-2.05867141846449	25.79459346368083	22.62451645957721
H	-1.32042768900708	27.42509620701654	22.79858303722840
H	-3.56109496144382	28.31763685539057	25.85302958369611
H	-3.77865514330170	28.79551774678675	24.14496667862095
H	-2.16218639701883	28.94380517274807	24.91704674741173
H	-7.37623232985601	20.57359058532734	21.40353683589041
H	-6.72925614893725	21.94931525423245	20.47595955893527
H	-6.96315072991745	19.07974082431334	19.85788767415576
H	-5.67367183909892	18.76511888943885	18.65337879027738
H	-6.36520141979585	20.41030669163965	18.83809377425996
H	-3.66233726413831	18.37674080401178	19.53603696330719
H	-0.55801937522891	18.93997228394712	20.75258804728476
H	-1.66729580986666	17.65968109967626	20.15728132534485
H	-1.23928112264626	17.77506407179079	21.90079414349879
H	1.67337173111687	21.63172333522546	22.89175356414548
H	1.86498843937164	20.41675135160103	25.06652211718075
H	-0.07372118131533	19.08877922267164	25.93107662059240
H	-3.35612806364896	18.83349921883872	24.03813289439388
H	-2.23858401415094	19.13625255649195	26.90614684487824
H	-3.89681277840963	18.61748248921077	26.46735740090426
H	-3.32556412223425	20.26757045645950	26.00674050832208

```
  H   -1.84338021208062     16.82336580782610     23.81150052055386
  H   -3.04777608251464     16.59461065932021     25.11735547719578
  H   -1.34874860729266     16.99290216345134     25.52461573479022
  H   -1.18339658009130     21.19335881481737     20.54736814647536
  H   -2.23952757398952     22.89900541766037     22.06910914072398
  H   -1.61338978520260     23.59638818008840     20.53922480846083
  H   -0.68077380647645     23.83589022794122     22.03657362540599
  H   0.57542377586965     22.54201530137839     19.49758051775824
  H   1.34810967861427     21.13752427154145     20.30312332176584
  H   1.43287701855720     22.76806212375605     21.04486818391895
  O   -3.13409597716746     21.76715289211809     24.25818264065606
  H   -3.56564625661139     24.08995851181879     24.69287411412569
  H   -3.68609330757272     22.46631361563904     24.68243882887567
```

Optimized **A.4** complex, in XYZ format

```
104
Coordinates from ORCA-job gd
  C   -0.30767808778248     21.11372809681496     22.64847936958234
  C   -1.45274910976448     20.34813206134561     23.03679625289170
  C   -1.49339679548864     19.70570979872203     24.31757447225201
  C   -0.43621622954224     19.92682134214899     25.22051001817596
  C   0.66675017733275     20.72855874583006     24.87069750256063
  C   0.72828695372531     21.29976906994650     23.58737960164094
  N   -2.57238740145962     20.23312568078572     22.17723265302817
  C   -2.58260302920830     19.32284964691195     21.17388026848643
  C   -1.37363051609754     18.42824693107312     20.99384837986643
  C   -2.69901680235304     18.85181546453437     24.69015557426699
  C   -2.31293477066123     17.54337831810973     25.39719078735497
  C   -0.22515712174066     21.75803255346297     21.26548088755892
  C   1.13247812317627     21.49952139824044     20.58975695463101
  Ni  -4.03692489835570     21.25767095193499     22.69245407703201
  N   -5.26414763719819     20.62525412116703     21.38900181900547
  C   -4.97393986812080     19.73659536493374     20.43728786165064
  C   -3.69063414049795     19.13380811877200     20.32747725482508
  C   -6.62137145833880     21.14482213374670     21.53087623337434
  C   -6.67530294852250     22.01271154496270     22.75303209015671
  N   -5.49026887295947     22.29555825448057     23.36819720813030
  N   -5.74204635883012     23.11460384511227     24.43250595156267
  C   -7.08789077780482     23.33367466374262     24.48785349793915
  C   -7.72532765843355     22.65058334516052     23.43622233462284
  C   -7.59668676283487     24.21453269255831     25.58806967493082
  N   -6.45421866483776     24.79827617497392     26.28275280215846
  C   -6.63897045412743     25.60754565863781     27.32601459383984
  C   -5.55597028212552     26.21192256928643     28.01923485658666
  C   -4.18689998831119     26.11105936595823     27.71104246108543
  C   -3.20095633330724     26.88209929422920     28.56737306154182
  Ni  -4.76075822746439     24.26344212731648     25.59686722018355
  N   -3.71506831657583     25.35666455218079     26.69018722964214
  C   -2.34217371217879     25.41084366759023     26.35397844638049
  C   -1.91484498293735     26.25899376770459     25.28195965502753
  C   -0.55028442100493     26.26055223683437     24.93122114507746
  C   0.38322357969585     25.46618333834957     25.61982414244985
  C   -0.04675854730376     24.63790365545360     26.67237683850664
  C   -1.40162156484031     24.59114715272529     27.05403253965264
  C   -2.93775175720999     27.10373925289167     24.53333346849871
  C   -3.26902993161904     28.40769757606459     25.28650998232150
  C   -1.90474919751190     23.60749470488515     28.10500074639868
  C   -2.50195575432625     22.37206786742401     27.40497327184168
  C   -8.04581760960491     25.91357993696962     27.79805559401192
  C   -0.84996291714824     23.20510596011724     29.14177157542160
  C   -2.54652147149386     27.39999843962886     23.08004670956639
  C   -6.04587442986420     19.31017821321519     19.45513868992516
  C   -3.71201925628412     19.66514855393205     25.51871341568487
  C   -0.53972799253079     23.26708704530060     21.31268545515706
  K   -1.64752449596007     23.21091146593586     24.36001559705059
  H   -8.79512070986194     22.62585190286502     23.20132958483477
  H   -8.26308950568921     25.00397797646963     25.16559698594843
```

```
  H   -8.23580979800266     23.62054627468493     26.28560854538208
  H   -8.64574107452019     26.38755601805324     26.99155967624162
  H   -8.03969267202109     26.59320326119427     28.66982528802392
  H   -8.58278483132569     24.98430696166801     28.08595157501967
  H   -5.81771109009281     26.85105235584954     28.87330354455260
  H   -2.55491761314835     26.19718389115729     29.15712913487720
  H   -3.72982014165453     27.54655641050661     29.27526618038483
  H   -2.51488247118690     27.49712428315887     27.95040397129356
  H   -0.21051526856266     26.89480282356802     24.09916075261534
  H   1.44629507285626     25.49013265118341     25.33503821976423
  H   0.68752888175961     24.01088544470269     27.19974811825702
  H   -2.74452063647226     24.09760017989205     28.63694157462517
  H   -1.30832878565444     22.57934284858586     29.93438350881885
  H   -0.39476217119601     24.09268889439693     29.62603204052336
  H   -0.03111822941892     22.60532861953889     28.69056231078611
  H   -1.71583259995924     21.78547403494636     26.88222443797079
  H   -3.28697177580722     22.68286240372916     26.67169010659972
  H   -2.99297060129925     21.69260412209551     28.12963123142185
  H   -3.87132189746698     26.49226245225538     24.53399884393576
  H   -3.38308580983375     27.91613082988971     22.56631320450455
  H   -2.33630167602220     26.46933864045172     22.51930607950871
  H   -1.66468045821972     28.07251697241025     23.01600059172643
  H   -3.70591979703587     28.20895646855103     26.28219030888159
  H   -4.01075538857028     29.00040574731963     24.71203891654365
  H   -2.35995408352124     29.03178276968554     25.41783646616317
  H   -7.37041807056306     20.32173701385570     21.61541249622435
  H   -6.92495282230865     21.73767159879354     20.63328854888371
  H   -6.90362461748137     18.83347060166255     19.97691782766962
  H   -5.65349470774121     18.58978518893624     18.71363537955934
  H   -6.45822058216451     20.18302847011064     18.90571899535367
  H   -3.56917907430686     18.38860612237674     19.52931409989286
  H   -0.44634596412689     19.00693817726759     20.80664451174561
  H   -1.52149353638131     17.72804697119041     20.15151918725964
  H   -1.18534121687971     17.83336274590929     21.91296779294917
  H   1.60676443673689     21.90319846902258     23.30916700961971
  H   1.48384381386732     20.89400285911524     25.58922376987304
  H   -0.46564454442341     19.45312992175950     26.21395020958384
  H   -3.20182706989105     18.59313524744776     23.73589011110425
  H   -3.31104954824283     19.90697673461970     26.52255897889227
  H   -4.65890378270818     19.10370591592095     25.64902653349160
  H   -3.96756167010951     20.61727009770430     24.99898642129248
  H   -1.57837654898261     16.96085418253055     24.80455844025496
  H   -3.21210247482095     16.91227741201362     25.54999203102183
  H   -1.87138273574346     17.72457130002644     26.39994728917485
  H   -1.01485283090477     21.28949672704384     20.64520679895780
  H   -1.57977932893683     23.46806699118748     21.63690961915398
  H   -0.43438665369719     23.72342098155112     20.30713931455357
  H   0.15969398532232     23.81089896505694     21.98687977943141
  H   1.12094942279468     21.86830262832940     19.54435923831432
  H   1.37962351419097     20.41859683811551     20.57095051303109
  H   1.96131433984040     22.02167897942071     21.11240384482860
  O   -3.46977516318054     24.34727958723284     22.74216045202557
  H   -4.08922809286689     24.63833474793221     23.46587504125720
  H   -3.91367062373015     23.49901256295021     22.46114134185370
```

Optimized **A.TS1** complex, in XYZ format

```
104
Coordinates from ORCA-job gt
  C   2.83250175659584     -1.69807037120924     -1.87810084529316
  C   1.55199002467078     -2.27939781214511     -1.63171977945812
  C   1.30486021258679     -2.98050364970029     -0.40933234479314
  C   2.36037302893419     -3.13790575261251      0.51101716684993
  C   3.63439872793987     -2.59838759226294      0.26011862219545
  C   3.85298444030152     -1.86891747586499     -0.92120644129697
  N   0.50784837225550     -2.19821217759150     -2.59306182967227
  C   0.48066434441184     -3.13629507416459     -3.56917996435965
  C   1.67481579534864     -4.05010106427581     -3.75902759092101
```

C	-0.08885785392223	-3.49736904200098	-0.07154508040745
C	-0.09602436942592	-5.00132969358598	0.23943999765141
C	3.08042901753023	-0.84662938450343	-3.11629314260437
C	4.34412443834987	-1.25334976619445	-3.89271004160752
Ni	-0.99452278059382	-1.17528304188692	-2.04886483919650
N	-2.25951515425657	-2.09540903539223	-3.11083451167405
C	-1.96164152842166	-2.89721936034723	-4.13556933576694
C	-0.64402395186949	-3.35952753797603	-4.38316237590174
C	-3.66667519332176	-1.82308341376184	-2.78916484653377
C	-3.70669617765276	-1.03521790287757	-1.51940949732765
N	-2.52477047822855	-0.47578363265590	-1.14447176772091
N	-2.69805835522230	0.18653659677386	0.02484315668489
C	-4.00558348121309	0.04992051186503	0.39178425876759
C	-4.69124088019320	-0.72560832638508	-0.56536346489663
C	-4.41918206956886	0.71764811427700	1.66510671341481
N	-3.30829799915978	1.53713424207743	2.12948455232582
C	-3.49759218045610	2.39584802889624	3.12839487636564
C	-2.46432585012370	3.26600878018909	3.57416707415135
C	-1.14669715867095	3.34103304390953	3.09268330783382
C	-0.24170773510777	4.40525462215364	3.69024585369643
Ni	-1.65591637920888	1.31257400571496	1.12151656573395
N	-0.65776461063106	2.54088970572101	2.10838541773380
C	0.73130648525887	2.53779843708821	1.87963266017353
C	1.26216378137238	3.11512697302551	0.67799494069051
C	2.65422230355023	3.10311803985976	0.47915844117563
C	3.52839576843840	2.56933530374717	1.44814919765995
C	3.00155465825231	2.01667855663602	2.63199154134664
C	1.61292384893753	1.97764300211671	2.86777754231695
C	0.28619221614127	3.65141816256362	-0.35532407519024
C	-0.33901429214994	4.99980420799481	0.04741969345279
C	1.02079538220218	1.27277579577857	4.09136378119931
C	0.40790163128346	-0.08900213808321	3.70087225483582
C	-4.84645927729983	2.48948787560325	3.81378123766010
C	2.00232316548161	1.12590564020272	5.25859975742061
C	0.85509914262054	3.71870303274928	-1.77565659313949
C	-3.07015392968999	-3.40359231697035	-5.03481436922185
C	-0.71153506430762	-2.66706836583724	1.06895671658652
C	3.13107075326907	0.64079137697384	-2.71905301809101
K	1.78144360922058	-0.12734324576385	0.80647278638216
H	-5.74682619145223	-1.01791055874125	-0.56215291070409
H	-5.34471873949191	1.31577897982644	1.49257879472556
H	-4.69671886697624	-0.04917903736794	2.42933368162891
H	-5.64388845437809	2.78738739468875	3.09897418189855
H	-4.83098208841025	3.22664591522631	4.63804066428447
H	-5.15303782099478	1.50751700727998	4.23370917103842
H	-2.73471659542244	3.98115924619792	4.36351352442993
H	0.60175562187867	3.97492567783780	4.26898249421420
H	-0.81576869299251	5.06922354371966	4.36262809128877
H	0.22130450456045	5.02489643283905	2.89556147756853
H	3.07301581710699	3.52924393734403	-0.44459816444504
H	4.61716320622867	2.59776542748132	1.28767879529732
H	3.69239259543082	1.60547486686521	3.38398895852273
H	0.16639889744353	1.88616833143736	4.44380272508026
H	1.48648982040392	0.70447485316611	6.14503276450456
H	2.44005800015684	2.10187743486886	5.55170416878286
H	2.83941427909196	0.43797500275640	5.01403116985411
H	1.19444324469598	-0.83468635439566	3.44315299681145
H	-0.30006836109149	0.03412744005049	2.84817364987344
H	-0.16752341287978	-0.52215751426123	4.54414561357083
H	-0.55261502031900	2.90279045140165	-0.33233220327119
H	0.04961369729939	3.95128261593916	-2.50168852794256
H	1.32723715216473	2.76265654938897	-2.08180480695438
H	1.62864200555310	4.50942703844167	-1.88291717849898
H	-0.90191911233220	4.91123778537646	0.99412812436902
H	-1.05216583572378	5.33741326902219	-0.73334879686124
H	0.43816902820701	5.78393102980261	0.16646451867361
H	-4.24527974272556	-2.76869704588360	-2.67593821517082
H	-4.15885130924061	-1.26021691335854	-3.61906387683597
H	-3.78884716305127	-4.03868734854480	-4.47302190601626

H	-2.66487011020505	-4.00335983465348	-5.87026078486490
H	-3.65596911962306	-2.56252142654771	-5.46141191109498
H	-0.51717967332084	-4.05992301136117	-5.21945180210688
H	2.62115847942207	-3.49142813091711	-3.89618259286013
H	1.52572991664219	-4.70986454126088	-4.63306520746731
H	1.82121659003645	-4.68937408234164	-2.86265170585017
H	4.84535807215888	-1.42901278950562	-1.10650377340047
H	4.45249486992526	-2.74444091574335	0.98228088336729
H	2.18221719099752	-3.69718791212605	1.44382299617319
H	-0.72034682364178	-3.32721949453979	-0.96780265186272
H	-0.13484993765696	-2.77040282561243	2.01317512663051
H	-1.75020016236500	-2.99665593626406	1.27113020157466
H	-0.78636710947155	-1.58805929885886	0.80751233365799
H	0.34225941152660	-5.58629602293629	-0.59446198265253
H	-1.13395685642055	-5.35873911194056	0.39763999855386
H	0.47875009341858	-5.23915957525299	1.15949748444464
H	2.20189705849533	-0.98292800120230	-3.77840079262441
H	2.20198877483555	0.92385522375145	-2.18815935086357
H	3.23163465107496	1.29525524182695	-3.60824080265140
H	3.98805582239622	0.85015840490273	-2.04322391502196
H	4.42712361587926	-0.66678792250149	-4.82944256728936
H	4.33393274491944	-2.32825494980566	-4.16452571970897
H	5.26712688729614	-1.06667896699007	-3.30454283270603
O	0.09004563883216	0.35625926962646	-1.09802049001487
H	-0.54130024694584	0.79783120259538	-0.26405867882309
H	0.04775360479635	1.07226306738527	-1.76890280148631

Appendix B

Supplemental material for Chapter 4

B.1 CP-PAW input files

*.strc file for the optimization of pairwise constrained $[Fe^{II}(NH_3)_6]^{2+}$ model system using PBE0r

```
!STRUCTURE
 !GENERIC LUNIT[AA]=1. !END
 !OCCUPATIONS EMPTY=10 NSPIN=2 SPIN[HBAR]=2. CHARGE[E]=2. !END
 !CONSTRAINTS
    !BOND ATOM1='N_01' ATOM2='N_02' MOVE=T NSTEP=1 VALUE=4.724 !END
    !BOND ATOM1='N_03' ATOM2='N_04' MOVE=T NSTEP=1 VALUE=4.724 !END
    !BOND ATOM1='N_05' ATOM2='N_06' MOVE=T NSTEP=1 VALUE=4.724 !END
 !END
 !SPECIES NAME='FE' NPRO=1 1 1  LRHOX=4
    !NTBO    NOFL=1 0 1 CV=T  raug/rcov=1.15 LHFWEIGHT=0.080
             focksetup=F cv=T NDDO=F 31=F BONDX=F !END
    !AUGMENT  ID='FE_NDLSS_V0' Z=  26.00000 ZV= 8.
             TYPE='NDLSS' RBOX/RCOV=  1.200 RCSM/RCOV=  0.250
             RCL/RCOV=  0.800  0.800  0.800  0.800  0.800
      !GRID DMIN=   0.100E-05 DMAX=     0.100 RMAX=    20.000 !END
      !POT  POW=  3.000 RC/RCOV=  0.702 !END
      !CORE POW=  3.000 RC/RCOV=  0.702 !END
    !END
```

```
 !END
 !SPECIES   NAME='N_'   NPRO=1 1 1 LRHOX=4 RAD/RCOV=1.4
    !NTBO    NOFL=1 1 0 CV=T  RAUG/RCOV=1.2 LHFWEIGHT=0.080
             FOCKSETUP=F CV=T NDDO=F 31=F BONDX=F !END
    !AUGMENT ID='MY_NDLSS_N' EL='N' ZV= 5.
             TYPE='NDLSS' RBOX/RCOV=1.2 RCSM/RCOV=.25
             RCL/RCOV=0.75 0.75 0.75  0.75
      !GRID  DMIN=1.E-6 DMAX=.15 RMAX=9. !END
      !POT   POW=3. RC/RCOV=0.75 VAL0_X=-4.3 !END
      !CORE  POW=2. RC/RCOV=0.75  !END
    !END
 !END
 !SPECIES   NAME='C_'   NPRO=1 1 1 LRHOX=4 RAD/RCOV=1.4
    !NTBO    NOFL=1 1 0 CV=T  RAUG/RCOV=1.2 LHFWEIGHT=0.080
             FOCKSETUP=F CV=T NDDO=F 31=F BONDX=F !END
    !AUGMENT ID='MY_NDLSS_C' EL='C' ZV= 4.
             TYPE='NDLSS' RBOX/RCOV=1.2 RCSM/RCOV=.25
             RCL/RCOV=0.85 0.85 0.85 0.85
      !GRID  DMIN=1.E-6 DMAX=.15 RMAX=9. !END
      !POT   POW=3. RC/RCOV=0.75  VAL0_X=-2.7 !END
      !CORE  POW=2. RC/RCOV=0.75  !END
    !END
 !END
 !SPECIES   NAME='H_'  M=2. NPRO=1 1 LRHOX=2 RAD/RCOV=1.2
    !NTBO    NOFL=1 0 CV=T  RAUG/RCOV=1.2 LHFWEIGHT=0.080
             FOCKSETUP=F CV=T NDDO=F 31=F BONDX=F !END
    !AUGMENT ID='MY_NDLSS_H' EL='H' ZV= 1.
             TYPE='NDLSS' RBOX/RCOV=1.2 RCSM/RCOV=.25
             RCL/RCOV=1.2 1.2  1.2  1.2
      !GRID  DMIN=1.E-6 DMAX=.15 RMAX=9. !END
      !POT   POW=3. RC/RCOV=1. VAL0_X=-1.6 !END
      !CORE  POW=2. RC/RCOV=1. !END
    !END
 !END
!LATTICE T=   0.00000 6.90000 6.90000
              6.90000 0.00000 6.90000
```

```
              6.90000  6.90000 0.0000 !END
 !ATOM NAME= 'FE1' R=    0.78135    3.03110   12.31354 !END
 !ATOM NAME= 'N_01' R=    -0.38282    3.30934   10.52564 !END
 !ATOM NAME= 'N_02' R=    -0.54065    1.35312   12.07401 !END
 !ATOM NAME= 'N_03' R=     2.47003    2.14026   11.31866 !END
 !ATOM NAME= 'N_04' R=     2.24845    4.55400   11.93017 !END
 !ATOM NAME= 'N_05' R=     1.39773    2.68495   14.34201 !END
 !ATOM NAME= 'N_06' R=    -0.53750    4.10138   13.63647 !END
 !ATOM NAME= 'H_01' R=    -0.24074    4.17232    9.96608 !END
 !ATOM NAME= 'H_02' R=    -1.37693    4.56787   13.24192 !END
 !ATOM NAME= 'H_03' R=    -0.33027    2.62500    9.74887 !END
 !ATOM NAME= 'H_04' R=    -1.56828    1.49211   12.05918 !END
 !ATOM NAME= 'H_05' R=    -0.51014    0.58817   12.77534 !END
 !ATOM NAME= 'H_06' R=     3.38076    2.12723   11.81349 !END
 !ATOM NAME= 'H_07' R=     2.46407    4.80044   10.94669 !END
 !ATOM NAME= 'H_08' R=     2.06357    5.51685   12.27294 !END
 !ATOM NAME= 'H_09' R=     2.26719    2.14322   14.51056 !END
 !ATOM NAME= 'H_10' R=     2.43216    1.13026   11.08004 !END
 !ATOM NAME= 'H_11' R=     1.59441    3.47852   14.97880 !END
 !ATOM NAME= 'H_12' R=    -0.99859    3.62098   14.43059 !END
 !ATOM NAME= 'H_13' R=    -0.15737    4.92145   14.14454 !END
 !ATOM NAME= 'H_14' R=     0.77476    2.13293   14.95971 !END
 !ATOM NAME= 'H_15' R=     3.21643    4.45779   12.28865 !END
 !ATOM NAME= 'H_16' R=     2.79258    2.49364   10.39885 !END
 !ATOM NAME= 'H_17' R=    -1.41404    3.37299   10.61104 !END
 !ATOM NAME= 'H_18' R=    -0.44779    0.76295   11.22736 !END
 !ISOLATE !END
!END
!EOB
```

B.2 Structural data of $[Fe^{II}(NH_3)_6]^{2+}$ model

Table B.1: N-N pair distance of 2.5 Å. a) high-spin, b) low-spin, in XYZ format

(a)

FE	0.78135	3.03110	12.31354
N	-0.38282	3.30934	10.52564
N	-0.54065	1.35312	12.07401
N	2.47003	2.14026	11.31866
N	2.24845	4.55400	11.93017
N	1.39773	2.68495	14.34201
N	-0.53750	4.10138	13.63647
H	-0.24074	4.17232	9.96608
H	-1.37693	4.56787	13.24192
H	-0.33027	2.62500	9.74887
H	-1.56828	1.49211	12.05918
H	-0.51014	0.58817	12.77534
H	3.38076	2.12723	11.81349
H	2.46407	4.80044	10.94669
H	2.06357	5.51685	12.27294
H	2.26719	2.14322	14.51056
H	2.43216	1.13026	11.08004
H	1.59441	3.47852	14.97880
H	-0.99859	3.62098	14.43059
H	-0.15737	4.92145	14.14454
H	0.77476	2.13293	14.95971
H	3.21643	4.45779	12.28865
H	2.79258	2.49364	10.39885
H	-1.41404	3.37299	10.61104
H	-0.44779	0.76295	11.22736

(b)

FE	0.84908	3.00986	12.33825
N	-0.21820	3.18064	10.70853
N	-0.23274	1.38088	12.44341
N	2.30667	2.18910	11.32266
N	1.96856	4.57742	11.97896
N	1.69689	2.78426	14.08995
N	-0.43064	3.94914	13.48509
H	-0.13751	4.03582	10.12640
H	-1.31644	4.31314	13.08462
H	-0.11354	2.47812	9.95265
H	-1.26398	1.46192	12.52459
H	-0.07841	0.70284	13.21368
H	3.26584	2.24186	11.71256
H	2.20086	4.80525	10.99486
H	1.64486	5.52030	12.26859
H	2.61013	2.29724	14.16794
H	2.29129	1.17003	11.12574
H	1.92920	3.62675	14.64836
H	-0.83198	3.45280	14.30257
H	-0.12653	4.81892	13.96062
H	1.19073	2.24647	14.81745
H	2.92325	4.61991	12.38267
H	2.50588	2.52244	10.36074
H	-1.25129	3.16694	10.79513
H	-0.18743	0.70986	11.65492

Table B.2: N-N pair distance of 2.8 Å. a) high-spin, b) low-spin, in XYZ format

(a)

FE	8.08091	6.59883	5.92752
N	6.87245	7.05523	7.68722
N	7.59348	4.58055	6.59388
N	6.35472	6.74433	4.58644
N	8.23774	8.68549	5.31130
N	9.98238	6.60132	7.01563
N	9.43954	5.96423	4.34379
H	9.08518	5.84944	3.37676
H	8.99305	9.28127	5.69645
H	10.27848	6.53680	4.13751
H	10.58247	5.75626	7.01165
H	9.96775	6.77533	8.03774
H	6.53006	6.96717	3.58923
H	7.43477	9.30882	5.51121
H	7.85946	3.78232	5.98899
H	6.81880	8.04092	8.00268
H	5.76103	5.90662	4.44502
H	6.59738	4.33374	6.73825
H	7.12517	6.62136	8.59369
H	5.85900	6.83663	7.68396
H	7.97544	4.23029	7.49157
H	5.60408	7.43558	4.76846
H	8.36168	8.90956	4.30665
H	10.70046	7.30429	6.76227
H	9.90110	5.04198	4.44494

(b)

FE	8.09750	6.58190	5.91287
N	7.18000	7.26004	7.54556
N	7.73184	4.71502	6.51715
N	6.38601	6.56397	4.89131
N	8.39805	8.46279	5.32196
N	9.82926	6.56698	6.90882
N	9.05923	5.91425	4.29725
H	8.55387	5.85680	3.39443
H	9.07353	9.05502	5.83905
H	9.89780	6.43188	3.97626
H	10.44895	5.74279	6.80722
H	9.81274	6.62291	7.94390
H	6.25570	7.24736	4.12326
H	7.58954	9.11085	5.32711
H	7.75340	3.94409	5.82510
H	7.51008	8.14960	7.96287
H	6.13359	5.70051	4.37644
H	6.81011	4.51285	6.94590
H	7.18780	6.67415	8.40041
H	6.16598	7.47316	7.51355
H	8.33846	4.29046	7.24237
H	5.48916	6.71398	5.38856
H	8.73906	8.64390	4.35993
H	10.52842	7.30947	6.72566
H	9.46460	4.96048	4.31064

Table B.3: N-N pair distance of 3.1 Å. a) high-spin, b) low-spin, in XYZ format

(a)

FE	1.67865	6.57736	-0.37345
N	2.04971	4.38831	-0.37834
N	3.66827	6.88660	0.48672
N	0.87690	6.45765	1.66167
N	-0.32198	6.23306	-1.18819
N	1.31621	8.76746	-0.42901
N	2.48935	6.70392	-2.42275
H	1.23321	5.72775	2.30498
H	2.89857	7.60535	-2.72765
H	0.82223	9.15545	-1.25340
H	0.73853	9.20382	0.31233
H	-0.13757	6.28097	1.77311
H	-1.13118	6.29156	-0.54539
H	-0.67677	6.85228	-1.93966
H	3.86472	7.76608	0.99795
H	1.89138	3.86781	-1.26060
H	4.02935	6.21279	1.18605
H	2.99910	4.03238	-0.16378
H	3.27588	6.07716	-2.67103
H	-0.53258	5.31757	-1.62535
H	0.96355	7.27689	2.28995
H	2.11950	9.42150	-0.41096
H	1.88019	6.52290	-3.24073
H	4.47664	6.89398	-0.16031
H	1.50450	3.77854	0.25793

(b)

FE	1.74681	6.59135	-0.38339
N	1.86318	4.55940	-0.56911
N	3.62144	6.93933	0.35497
N	1.17047	6.31638	1.55526
N	-0.08997	6.45963	-1.27322
N	1.39164	8.58413	-0.09661
N	2.52523	6.68398	-2.26776
H	1.72296	5.64145	2.11353
H	2.80957	7.60047	-2.65881
H	1.43027	9.23270	-0.90336
H	0.45994	8.84295	0.27438
H	0.22094	5.95524	1.75976
H	-0.94613	6.47433	-0.69044
H	-0.33709	7.20905	-1.94357
H	3.72192	7.33074	1.30869
H	1.77961	4.13276	-1.50915
H	4.29750	6.15827	0.43189
H	2.71302	4.06186	-0.24708
H	3.40127	6.15776	-2.43535
H	-0.31134	5.63271	-1.85611
H	1.17662	7.11908	2.20933
H	1.98806	9.11718	0.56129
H	1.96602	6.34038	-3.06893
H	4.21304	7.61251	-0.16394
H	1.14944	4.00009	-0.06900

B.3 Absolute energies (Eh) from SPE calculations

Using PBE, BP86, TPSS and M06-L

	PBE	BP86	TPSS	M06-L
2.5 Å, HS	-1611.31394182704	-1612.21181225286	-1612.04541650429	-1611.8312296385
2.5 Å, LS	-1611.33504264393	-1612.23203305343	-1612.06943423148	-1611.82617037154
2.6 Å, HS	-1611.32669581554	-1612.22458186504	-1612.05819837707	-1611.84543307343
2.6 Å, LS	-1611.34489446973	-1612.24198183326	-1612.0794918585	-1611.83691670181
2.7 Å, HS	-1611.33581983985	-1612.23372142758	-1612.06728580552	-1611.85489181217
2.7 Å, LS	-1611.35084864319	-1612.248039278	-1612.08563838146	-1611.84367729907
2.8 Å, HS	-1611.34174799896	-1612.23970247011	-1612.07307793425	-1611.86089127433
2.8 Å, LS	-1611.35387535836	-1612.25111882385	-1612.08887837626	-1611.84808257695
2.9 Å, HS	-1611.34546305524	-1612.2434864492	-1612.07701036119	-1611.86492073313
2.9 Å, LS	-1611.35464639159	-1612.25190109507	-1612.08984512315	-1611.85059770242
3.0 Å, HS	-1611.34789125528	-1612.24553346853	-1612.07906433559	-1611.86717974695
3.0 Å, LS	-1611.35434760779	-1612.25164217608	-1612.0897802799	-1611.85213183204
3.1 Å, HS	-1611.34703690399	-1612.24497736748	-1612.07845143695	-1611.86621919722
3.1 Å, LS	-1611.35214635849	-1612.2494748855	-1612.08773294594	-1611.85178194351

Using B3LYP with 10, 15, 20 and 25% exact exchange

	B3LYP(10%)	B3LYP(15)	B3LYP(20)	B3LYP(25%)
2.5 Å, HS	-1610.94952594267	-1611.33284328771	-1611.71736748635	-1612.10304650325
2.5 Å, LS	-1610.95982682662	-1611.33402051468	-1611.70983687101	-1612.08721943538
2.6 Å, HS	-1610.96271412583	-1611.34636099819	-1611.73120044291	-1612.11718169432
2.6 Å, LS	-1610.97047172445	-1611.34506518765	-1611.72127420517	-1612.09904226486
2.7 Å, HS	-1610.97217288164	-1611.35610715504	-1611.74122273941	-1612.12747017399
2.7 Å, LS	-1610.97709332561	-1611.35202710027	-1611.72857203556	-1612.1066711232
2.8 Å, HS	-1610.97826791859	-1611.3624037942	-1611.74773319818	-1612.13415231224
2.8 Å, LS	-1610.98071558478	-1611.35597638502	-1611.73284655096	-1612.11126838357
2.9 Å, HS	-1610.98218728739	-1611.36649115501	-1611.75196277805	-1612.13855274433
2.9 Å, LS	-1610.98194828978	-1611.35747163195	-1611.73460230896	-1612.11328218151
3.0 Å, HS	-1610.98431129668	-1611.36873438923	-1611.75432275792	-1612.14102661488
3.0 Å, LS	-1610.98243579007	-1611.35838715145	-1611.7359427516	-1612.11504346795
3.1 Å, HS	-1610.98381943511	-1611.36825944887	-1611.75385919713	-1612.14057173513
3.1 Å, LS	-1610.98093853655	-1611.35728324445	-1611.73523147549	-1612.11472270883

Using PBE0 with 10, 15, 20 and 25% exact exchange

	PBE0(10%)	PBE0(15%)	PBE0(20%)	PBE0(25%)
2.5 Å, HS	-1610.19032949751	-1610.57443830335	-1610.95974208347	-1611.34619005557
2.5 Å, LS	-1610.2034804874	-1610.57788548789	-1610.95390384975	-1611.33148349425
2.6 Å, HS	-1610.20265934361	-1610.58710726414	-1610.97273611442	-1611.35949646403
2.6 Å, LS	-1610.2128425653	-1610.58765273006	-1610.96407110037	-1611.34204471464
2.7 Å, HS	-1610.21125206993	-1610.59599630844	-1610.98191177494	-1611.36894841734
2.7 Å, LS	-1610.21828956788	-1610.59344298127	-1610.97020205597	-1611.34851340839
2.8 Å, HS	-1610.21681329215	-1610.60171221025	-1610.98781482125	-1611.37504807853
2.8 Å, LS	-1610.22093900877	-1610.59642377858	-1610.97351412287	-1611.35215618729
2.9 Å, HS	-1610.2202669135	-1610.60539465663	-1610.99171872331	-1611.37907052025
2.9 Å, LS	-1610.2215300658	-1610.59728131866	-1610.9746375486	-1611.35354408794
3.0 Å, HS	-1610.22235497658	-1610.60760914915	-1610.9937569479	-1611.38151452511
3.0 Å, LS	-1610.22070085199	-1610.59688653808	-1610.9746765613	-1611.35401470996
3.1 Å, HS	-1610.22167243693	-1610.60692282577	-1610.99334317653	-1611.38087573236
3.1 Å, LS	-1610.217934554	-1610.5945209746	-1610.97271333933	-1611.35245399318

Using CAM-B3LYP with (α_0, μ_0), (α_1, μ_0), (α_2, μ_0), (α_0, μ_1), (α_0, μ_2)

	CAM-B3LYP	(α_0, μ_1)	(α_0, μ_2)	(α_1, μ_0)	(α_2, μ_0)
2.5 Å, HS	-1611.89097577089	-1611.38747833672	-1611.34299951079	-1611.32222823265	-1611.39591141635
2.5 Å, LS	-1611.88502938301	-1611.38712082845	-1611.3352590941	-1611.32594234899	-1611.38469827048
2.6 Å, HS	-1611.90462900745	-1611.40066280693	-1611.35661406234	-1611.3354673646	-1611.40946764075
2.6 Å, LS	-1611.89623137055	-1611.39789258956	-1611.3464137077	-1611.33666790873	-1611.39587739764
2.7 Å, HS	-1611.9143714551	-1611.40998418537	-1611.36627554501	-1611.34482354735	-1611.41908369007
2.7 Å, LS	-1611.9033706846	-1611.40465986678	-1611.35349645168	-1611.34340933566	-1611.40296421048
2.8 Å, HS	-1611.92072680228	-1611.4160269421	-1611.3725759077	-1611.35090858822	-1611.4253387383
2.8 Å, LS	-1611.90750911106	-1611.40849385138	-1611.35757995123	-1611.34716155503	-1611.40710894382
2.9 Å, HS	-1611.92487100184	-1611.41991707505	-1611.37666955806	-1611.35481991459	-1611.42940894953
2.9 Å, LS	-1611.90921614652	-1611.40998443155	-1611.35926313759	-1611.34857109198	-1611.40886083442
3.0 Å, HS	-1611.92716104295	-1611.42202476781	-1611.37888774683	-1611.35693627744	-1611.43160961759
3.0 Å, LS	-1611.91037039356	-1611.41074158913	-1611.36034750735	-1611.34923305786	-1611.41001186591
3.1 Å, HS	-1611.92671882773	-1611.42158427981	-1611.37845776168	-1611.35648840979	-1611.43118697517
3.1 Å, LS	-1611.90942223563	-1611.40943538083	-1611.35931037198	-1611.34781841344	-1611.40905120747

Using PBE0r with 8, 9, 11 and 12.5% exact exchange

	PBE0r(8.00%)	PBE0r(9.00%)	PBE0r(11.00%)	PBE0r(12.50%)
2.5 Å, HS	-92.3344956	-92.3300055	-92.3233405	-92.320538
2.5 Å, LS	-92.3311828	-92.3232491	-92.3100367	-92.3026846
2.6 Å, HS	-92.3462091	-92.3414424	-92.3341483	-92.3308191
2.6 Å, LS	-92.3405257	-92.3323971	-92.3187345	-92.3109804
2.7 Å, HS	-92.3543663	-92.3493436	-92.3414466	-92.3376116
2.7 Å, LS	-92.3460165	-92.3377	-92.3235982	-92.3154653
2.8 Å, HS	-92.3588657	-92.3536212	-92.345276	-92.3410611
2.8 Å, LS	-92.3480944	-92.3396194	-92.3251619	-92.3167136
2.9 Å, HS	-92.3611994	-92.355807	-92.347126	-92.3426369
2.9 Å, LS	-92.3481381	-92.3395613	-92.3248698	-92.316218
3.0 Å, HS	-92.3628447	-92.3573201	-92.3483529	-92.3436116
3.0 Å, LS	-92.3474557	-92.3387272	-92.3236782	-92.3147042
3.1 Å, HS	-92.3612848	-92.3566503	-92.3474327	-92.3424879
3.1 Å, LS	-92.3447425	-92.3358379	-92.3203811	-92.3110351

B.4 UCCSD(T*)-F12B reference energies

d_{N-N} / Å	$\Delta E_{\mathrm{HL}}^{\mathrm{UCCSD\text{-}F12B}}$	$\Delta E_{\mathrm{HL}}^{\mathrm{UCCSD(T^*)\text{-}F12B}}$	$\Delta E_{\mathrm{HL}}\,(\mathrm{DK})$	$\Delta E_{\mathrm{HL}}^{\mathrm{UCCSD(T^*)\text{-}F12B}} + \Delta E_{\mathrm{HL}}\,(\mathrm{DK})$
2.5	-16.9678	-7.0318	2.7643	-4.2675
2.6	-18.5519	-8.7567	2.7098	-6.0468
2.7	-20.1476	-10.4659	2.6602	-7.8057
2.8	-21.5542	-12.0082	2.5865	-9.4216
2.9	-23.0885	-13.6150	2.5470	-11.0680
3.0	-23.5710	-14.4150	2.3962	-12.0188
3.1	-23.8446	-15.1072	2.1977	-12.9095

Table B.4: Breakdown of energy composition, values given in kcal/mol.

Appendix C

Supplemental material for Chapter 5

C.1 Structural data of extended model set

Table C.1: Complex **B.04**. a) high -spin, b) low -spin, in XYZ format

(a)

C	-4.03919	2.74058	1.17980
N	-4.23759	2.57732	-0.09666
FE	-2.54894	2.84874	-1.32974
N	-2.56108	0.85866	-2.08646
C	-2.95835	0.72512	-3.31604
C	-3.38380	1.86534	-4.03365
N	-3.33950	2.98000	-3.33371
C	-3.69832	4.17565	-3.75732
C	-3.50025	5.20039	-2.80692
N	-2.98278	4.90508	-1.65227
C	-2.72561	2.95514	1.63903
N	-1.82808	2.97784	0.67000
C	-0.52436	3.10695	0.84167
C	0.19588	3.10834	-0.36526
N	-0.45465	2.97844	-1.48657
H	-4.09564	4.36814	-4.75361
H	-3.73607	1.81315	-5.06378
H	-3.77808	6.22297	-3.07509
H	-2.98463	-0.24672	-3.81624
H	-2.30668	-0.06658	-1.70725
H	-2.89882	5.76207	-1.08323
H	-0.04780	3.20692	1.81606
H	-2.47756	3.05528	2.69500
H	-4.85550	2.70454	1.90452
H	1.28156	3.22298	-0.33696
H	-5.24192	2.42521	-0.27502
H	0.20607	3.02223	-2.27725

(b)

C	-4.69435	2.66647	0.61049
N	-4.56617	2.70882	-0.68004
FE	-2.71656	2.83720	-1.27685
N	-2.60351	0.92502	-1.52558
C	-2.71629	0.54629	-2.76173
C	-2.91100	1.57076	-3.69866
N	-2.95632	2.76871	-3.11406
C	-3.13914	3.92034	-3.76419
C	-3.13777	5.01494	-2.88894
N	-2.94660	4.74185	-1.63476
C	-3.50457	2.73080	1.34909
N	-2.43717	2.84526	0.55534
C	-1.17961	2.93400	0.98967
C	-0.27275	3.04394	-0.07334
N	-0.79039	3.02643	-1.26333
H	-3.27161	3.97954	-4.83991
H	-3.02566	1.42773	-4.76824
H	-3.28961	6.03260	-3.25181
H	-2.66864	-0.50136	-3.06155
H	-2.47267	0.13544	-0.87795
H	-2.96927	5.58053	-1.03880
H	-0.91255	2.91773	2.04129
H	-3.43734	2.70520	2.43205
H	-5.66520	2.59037	1.10177
H	0.79993	3.13968	0.09969
H	-5.47075	2.67404	-1.16958
H	-0.08220	3.11474	-2.00543

Table C.2: Complex **B.05**. a) high -spin, b) low -spin, in XYZ format

(a)

C	-4.67581	2.52599	1.03123
C	-3.37562	2.60454	1.61238
N	-2.41927	2.74014	0.73928
C	-1.11382	2.81604	1.17211
C	-0.17275	2.95047	0.24434
N	-0.60016	3.01872	-1.12483
FE	-2.92040	2.78940	-1.22056
N	-3.09715	4.77771	-1.71044
C	-3.03488	5.08543	-2.97507
C	-2.82713	4.05294	-3.91595
N	-2.77059	2.86019	-3.36177
C	-2.58659	1.70840	-3.97184
C	-2.57987	0.60913	-3.08481
N	-2.70603	0.83216	-1.80755
N	-4.71623	2.59608	-0.25690
H	-2.73881	4.23401	-4.98561
H	-2.46916	1.60141	-5.04878
H	-3.14175	6.11435	-3.32316
H	-2.46624	-0.39962	-3.48479
H	-2.72074	-0.06407	-1.29671
H	-3.29063	5.62601	-1.15615
H	-0.87743	2.76043	2.23345
H	-3.20714	2.55073	2.68742
H	-5.56434	2.41878	1.65311
H	0.88396	3.01348	0.49605
H	-5.69489	2.53394	-0.58449
H	-0.20312	3.90211	-1.50077
H	-0.01687	2.33316	-1.64235

(b)

C	-4.69278	2.70755	0.53929
C	-3.52669	2.80642	1.34484
N	-2.45926	2.87889	0.59687
C	-1.18741	2.98442	1.12828
C	-0.21788	3.05014	0.22882
N	-0.64047	3.00512	-1.15511
FE	-2.64227	2.82950	-1.21162
N	-2.73138	4.72490	-1.59393
C	-3.04453	4.99280	-2.82820
C	-3.20416	3.89265	-3.68058
N	-2.96875	2.74450	-3.05028
C	-2.99918	1.53620	-3.60541
C	-2.66412	0.53425	-2.68533
N	-2.41313	0.92844	-1.47118
N	-4.42386	2.70663	-0.72759
H	-3.45462	3.95176	-4.73471
H	-3.22840	1.36959	-4.65261
H	-3.16475	6.01471	-3.18824
H	-2.60970	-0.51415	-2.97862
H	-2.18702	0.14876	-0.83788
H	-2.63075	5.57096	-1.01607
H	-1.02372	3.00700	2.20260
H	-3.50790	2.82265	2.43128
H	-5.70094	2.64213	0.94207
H	0.83770	3.13297	0.47310
H	-5.27788	2.63952	-1.30727
H	-0.23718	3.84427	-1.61559
H	-0.08979	2.25012	-1.60774

Table C.3: Complex **B.06**. a) high -spin, b) low -spin, in XYZ format

(a)

C	-4.78097	2.88944	0.84422
N	-4.66920	2.68972	-0.41143
FE	-2.68696	2.81583	-1.18209
N	-2.54630	0.61018	-1.54613
C	-2.73069	0.32051	-2.94809
C	-2.94515	1.33676	-3.77717
N	-2.98796	2.59279	-3.20864
C	-3.24737	3.63436	-3.91530
C	-3.25422	4.88185	-3.16659
N	-3.00162	4.79240	-1.91847
C	-3.54323	3.12625	1.57186
N	-2.48367	3.10108	0.84478
C	-1.23559	3.29274	1.40007
C	-0.20855	3.29089	0.55743
N	-0.48342	3.13364	-0.85066
H	-3.42956	3.60764	-4.99281
H	-3.09442	1.20197	-4.84698
H	-3.47671	5.82086	-3.67776
H	-2.68219	-0.71214	-3.29247
H	-3.23811	0.01777	-1.04520
H	-3.03463	5.73573	-1.48896
H	-1.11347	3.41157	2.47552
H	-3.53251	3.29915	2.65085
H	-5.73397	2.88092	1.37699
H	0.81842	3.43445	0.89104
H	-5.60852	2.53673	-0.82343
H	-0.08124	3.97714	-1.30668
H	0.20540	2.43551	-1.19212
H	-1.68590	0.09482	-1.27331

(b)

C	-4.67732	2.68593	0.56782
N	-4.47544	2.67293	-0.70189
FE	-2.66842	2.82837	-1.27011
N	-2.52237	0.84088	-1.51037
C	-2.74458	0.52334	-2.91063
C	-2.97073	1.55036	-3.71324
N	-2.95913	2.78639	-3.08260
C	-3.14505	3.89369	-3.72972
C	-3.07801	5.02240	-2.84225
N	-2.84234	4.69523	-1.62166
C	-3.46476	2.79112	1.33195
N	-2.43361	2.87309	0.55175
C	-1.14031	2.97161	1.04415
C	-0.20274	3.02710	0.11238
N	-0.66457	2.99463	-1.26471
H	-3.33253	3.95411	-4.80100
H	-3.15402	1.46347	-4.78186
H	-3.21671	6.05136	-3.17677
H	-2.70822	-0.51499	-3.23464
H	-3.19940	0.25803	-0.97847
H	-2.82375	5.52428	-1.00076
H	-0.94165	2.99318	2.11330
H	-3.41032	2.80122	2.41942
H	-5.66602	2.62558	1.02409
H	0.86351	3.10113	0.31811
H	-5.36567	2.62681	-1.22991
H	-0.27505	3.84883	-1.71195
H	-0.08138	2.28220	-1.74761
H	-1.64573	0.34880	-1.24378

Table C.4: Complex **B.07**. a) high -spin, b) low -spin, in XYZ format

(a)

FE	-1.80596	3.11574	0.02073
N	-0.46377	2.71792	-1.59572
N	-3.13904	2.64204	1.62102
N	-0.86539	4.64474	1.08989
N	-2.88582	4.53437	-1.04214
N	-3.08099	1.50606	-0.68469
N	-0.34055	1.70078	0.76519
C	-3.95566	1.68603	1.45422
C	-3.93436	1.04291	0.12837
C	0.55378	1.31230	-0.04287
C	0.46013	1.87020	-1.40484
C	-3.45350	5.26919	-1.64575
C	-0.37161	5.41303	1.71699
H	-4.00808	5.97609	-2.25433
H	0.11053	6.15267	2.34812
H	1.35887	0.61930	0.21475
H	1.15789	1.53243	-2.17847
H	-4.62346	0.22552	-0.09938
H	-4.64594	1.32047	2.22259
H	-0.18494	1.26263	1.69309
H	-0.44148	3.04032	-2.58213
H	-3.14520	0.99442	-1.58537
H	-3.23556	3.01754	2.58398

(b)

FE	-1.67054	3.02118	0.03397
N	-0.43934	3.33884	-1.37852
N	-2.82788	2.43944	1.42539
N	-1.03585	4.41502	1.05090
N	-2.93474	4.11975	-0.72532
N	-2.49910	1.49873	-0.78938
N	-0.19807	1.93333	0.58583
C	-3.56145	1.41861	1.21942
C	-3.36434	0.85681	-0.11127
C	0.83373	1.91024	-0.15934
C	0.68969	2.74989	-1.34163
C	-3.68920	4.76968	-1.20092
C	-0.67163	5.23457	1.69417
H	-4.42677	5.40456	-1.67008
H	-0.31441	6.04000	2.31934
H	1.73087	1.32894	0.05634
H	1.46591	2.85667	-2.10054
H	-3.90251	-0.01859	-0.47937
H	-4.25930	1.00318	1.94915
H	-0.08830	1.33638	1.42628
H	-0.53972	3.93606	-2.22057
H	-2.36284	1.09464	-1.73506
H	-2.97382	2.83974	2.37188

Table C.5: Complex **B.08**. a) high -spin, b) low -spin, in XYZ format

(a)

N	-1.69729	-0.66066	-0.02221
FE	-1.72497	1.43751	-0.00001
N	0.37373	1.46091	0.02051
N	-1.70146	1.46015	-2.09240
N	-1.74855	1.41487	2.09238
N	-1.75276	3.53566	0.02219
N	-3.82372	1.41414	-0.02051
C	-1.77582	1.39009	3.19853
C	1.47964	1.47997	0.04464
C	-1.65424	-1.76589	-0.04505
C	-1.67421	1.48488	-3.19853
C	-1.79573	4.64090	0.04503
C	-4.92963	1.39500	-0.04463
H	-1.80130	1.36673	4.27919
H	-1.61612	-2.84663	-0.06671
H	2.56092	1.50082	0.06768
H	-1.64868	1.50818	-4.27919
H	-1.83393	5.72163	0.06672
H	-6.01092	1.37418	-0.06765

(b)

N	-1.33573	-0.40253	-0.04749
FE	-1.80747	1.39691	-0.04407
N	-0.03577	1.85319	0.29134
N	-1.48347	1.48784	-1.87362
N	-2.13229	1.30519	1.78552
N	-2.27767	3.19627	-0.03962
N	-3.57935	0.94166	-0.38110
C	-2.33816	1.24543	2.86594
C	1.01587	2.11483	0.48883
C	-1.04459	-1.46499	-0.04705
C	-1.27729	1.54658	-2.95406
C	-2.56654	4.25929	-0.03794
C	-4.63094	0.68163	-0.58107
H	-2.53984	1.18514	3.92518
H	-0.75858	-2.50649	-0.04398
H	2.04596	2.37349	0.68382
H	-1.07558	1.60581	-4.01334
H	-2.85038	5.30139	-0.03914
H	-5.66092	0.42423	-0.77835

Table C.6: Complex **B.09**. a) high -spin, b) low -spin, in XYZ format

(a)

FE	-1.59760	1.60383	0.13280
C	-2.36323	3.80238	1.94311
C	-2.28799	2.60613	2.81292
N	-1.92250	1.53113	2.25354
N	-3.58005	1.00575	-0.44459
C	-3.74963	-0.21960	-0.71357
C	-2.54971	-1.08061	-0.61772
N	-1.49819	-0.51365	-0.19917
N	0.47172	1.95228	0.24712
C	1.06201	2.31186	-0.82070
C	0.21049	2.39748	-2.01134
N	-1.01738	2.12519	-1.82391
N	-2.15785	3.60023	0.71112
H	2.12761	2.54853	-0.88906
H	0.63822	2.68331	-2.97518
H	-2.62146	-2.13706	-0.89311
H	-4.70806	-0.66069	-1.00109
H	-2.54430	2.69315	3.87342
H	-2.59317	4.77636	2.38337
H	-4.48250	1.51277	-0.51404
H	-0.71816	-1.19763	-0.17312
H	-1.53587	2.20804	-2.71844
H	1.15050	1.92315	1.03077
H	-2.21787	4.49826	0.19413
H	-1.92482	0.75440	2.94123

(b)

FE	-1.72488	1.58158	-0.00130
C	-2.25184	3.74509	1.60218
C	-2.16296	2.61087	2.50572
N	-1.90915	1.52343	1.88732
N	-3.55173	1.19173	-0.33579
C	-3.88670	-0.02499	-0.52582
C	-2.75135	-0.92706	-0.43651
N	-1.66454	-0.30709	-0.18383
N	0.16369	1.76635	0.05855
C	0.78313	2.01877	-1.02863
C	-0.11927	2.10602	-2.16388
N	-1.33570	1.91482	-1.82854
N	-2.06029	3.40875	0.38608
H	1.86315	2.15828	-1.10773
H	0.21221	2.30919	-3.18257
H	-2.83009	-2.00724	-0.57495
H	-4.90515	-0.35689	-0.72950
H	-2.30239	2.69082	3.58568
H	-2.45633	4.76385	1.93262
H	-4.36708	1.82919	-0.39436
H	-0.85767	-0.95495	-0.12294
H	-1.97336	1.97193	-2.64382
H	0.81180	1.70689	0.86532
H	-2.11849	4.22330	-0.25240
H	-1.84845	0.71738	2.53622

Table C.7: Complex **B.10**. a) high -spin, b) low -spin, in XYZ format

(a)

C	-1.97443	4.18340	1.80618
N	-2.14039	3.81816	0.37270
FE	-1.74684	1.65131	0.04316
N	0.45081	1.94350	0.00110
C	0.98833	1.79089	-1.38067
C	0.04034	2.48710	-2.31855
N	-1.31994	1.91885	-2.09836
C	-2.53248	3.07295	2.65448
N	-1.91158	1.78802	2.22668
N	-1.65101	-0.54778	-0.11540
C	-2.92158	-1.10363	-0.65489
C	-4.06732	-0.41182	0.02982
N	-3.87679	1.06163	-0.10845
H	2.00586	2.18121	-1.47934
H	0.36186	2.40270	-3.36001
H	-2.99210	-2.19013	-0.54395
H	-4.07050	-0.64928	1.09904
H	-2.38166	3.27680	3.71884
H	-2.45806	5.13492	2.04675
H	-4.62010	1.48165	0.47999
H	-1.50127	-1.04076	0.78483
H	-1.96688	2.52053	-2.63764
H	1.01849	1.30909	0.58976
H	-1.62330	4.55519	-0.14077
H	-0.98247	1.76930	2.68673
H	-5.02481	-0.75107	-0.37674
H	-2.95167	-0.89888	-1.73122
H	-3.61424	2.98555	2.50261
H	-0.90138	4.30403	1.99029
H	1.03074	0.72074	-1.60828
H	0.00801	3.55717	-2.08659
H	0.82193	2.85599	0.32936
H	-1.34704	1.06877	-2.69189
H	-3.10481	4.10850	0.12629
H	-2.38422	1.05837	2.79118
H	-0.90199	-1.00373	-0.66711
H	-4.25884	1.29689	-1.04370

(b)

C	-2.58721	3.49398	2.05304
N	-2.46253	3.41442	0.56632
FE	-1.63845	1.68055	-0.00593
N	0.21844	2.31430	0.42959
C	0.98986	2.58907	-0.81959
C	0.04230	3.25565	-1.77101
N	-1.18348	2.40328	-1.82006
C	-2.96464	2.12491	2.53632
N	-2.02852	1.15730	1.88735
N	-0.99705	-0.15443	-0.47749
C	-1.98862	-0.87433	-1.33228
C	-3.35173	-0.53455	-0.80766
N	-3.40131	0.94949	-0.64065
H	1.88971	3.18757	-0.64828
H	0.49626	3.41619	-2.75354
H	-1.82881	-1.95643	-1.35304
H	-3.50694	-0.98863	0.17649
H	-2.94652	2.07076	3.62948
H	-3.31192	4.24550	2.38260
H	-4.27256	1.12863	-0.10717
H	-0.84460	-0.77577	0.33939
H	-1.89594	2.97574	-2.30973
H	0.82974	1.70084	0.99974
H	-2.05033	4.32146	0.27829
H	-1.19548	1.13922	2.50599
H	-4.13541	-0.91424	-1.47140
H	-1.87433	-0.50960	-2.35859
H	-3.98155	1.87444	2.21559
H	-1.61132	3.78471	2.45639
H	1.32658	1.62966	-1.22589
H	-0.24423	4.24409	-1.39671
H	0.29902	3.18685	0.98657
H	-0.99215	1.70705	-2.56571
H	-3.42440	3.55979	0.20493
H	-2.41617	0.22076	2.10881
H	-0.08389	-0.28995	-0.94966
H	-3.70036	1.31083	-1.56702

Table C.8: Complex **B.11**. a) high -spin, b) low -spin, in XYZ format

(a)

N	-1.82371	4.20214	1.33145
N	-1.63909	3.75970	-0.33441
N	-1.72143	2.55969	-0.39547
FE	-1.86079	1.15105	1.19426
N	-1.36164	-0.64451	0.07163
N	-0.28748	-1.19296	0.05525
N	0.82725	-0.20270	0.90576
N	0.21703	0.73925	1.34786
N	-1.84604	3.18748	1.97920
N	-2.44338	0.22725	3.07419
N	-3.55297	-0.13931	3.36028
N	-4.63368	0.31277	2.07254
N	-3.98301	0.75701	1.16254
H	0.93833	1.32912	1.84815
H	-2.01294	-1.27571	-0.47257
H	-1.82867	-0.06143	3.88652
H	-4.68211	1.00979	0.40933
H	-1.95361	3.48893	2.98781
H	-1.60758	2.31997	-1.41989

(b)

N	-1.78430	3.95983	1.42156
N	-1.81985	3.68387	-0.00513
N	-1.86433	2.45460	-0.18509
FE	-1.89096	1.22289	1.21701
N	-1.64797	-0.29754	0.16456
N	-0.53184	-0.79690	-0.05746
N	0.48836	-0.01589	0.62797
N	-0.05138	0.93708	1.21465
N	-1.81795	2.88649	2.04659
N	-2.21620	0.25952	2.77935
N	-3.35804	-0.00409	3.19012
N	-4.34002	0.53127	2.25480
N	-3.74846	1.10055	1.32225
H	0.72020	1.46845	1.68478
H	-2.34365	-0.89529	-0.34256
H	-1.55000	-0.14599	3.47991
H	-4.49263	1.46283	0.67900
H	-1.79223	3.13690	3.06423
H	-1.88649	2.30922	-1.22287

Table C.9: Complex **B.12**. a) high -spin, b) low -spin, in XYZ format

(a)

FE	-1.73810	2.88822	-0.01008
N	-3.41605	2.87828	1.22366
N	-2.80810	1.18973	-0.73701
N	-0.26549	1.97838	1.24970
N	-0.06214	2.90143	-1.24567
N	-0.66376	4.58228	0.72363
N	-3.21080	3.78930	-1.27785
N	-4.59182	2.63027	0.95097
N	0.92554	2.27378	1.35534
N	0.55176	4.70659	0.87645
N	1.11475	3.14445	-0.97319
N	-4.02311	1.06248	-0.89196
N	-4.40177	3.49278	-1.38124
C	-4.75992	2.31963	-0.51721
C	1.28535	3.44939	0.49564
H	2.34341	3.64131	0.65414
H	-5.81737	2.12488	-0.67626
H	-3.08115	4.61436	-1.91494
H	-3.41723	3.07391	2.25660
H	-2.40174	0.26157	-1.01639
H	-0.39615	1.15152	1.88426
H	-0.06244	2.70897	-2.27922
H	-1.06775	5.51044	1.00650

(b)

FE	-1.86866	2.80310	0.07190
N	-3.37133	2.72243	1.20333
N	-2.69375	1.37217	-0.83016
N	-0.77699	1.71822	1.15675
N	-0.36599	2.88376	-1.05954
N	-1.04357	4.23403	0.97394
N	-2.96034	3.88800	-1.01295
N	-4.54912	2.57054	0.86528
N	0.41335	1.89798	1.43153
N	0.15254	4.34458	1.26023
N	0.81180	3.03563	-0.72149
N	-3.88986	1.26162	-1.11645
N	-4.15069	3.70824	-1.28772
C	-4.64712	2.45839	-0.62567
C	0.90979	3.14781	0.76946
H	1.95733	3.27658	1.02937
H	-5.69465	2.32962	-0.88558
H	-2.67695	4.77107	-1.50205
H	-3.37154	2.79338	2.24970
H	-2.22369	0.50786	-1.19288
H	-1.06039	0.83516	1.64587
H	-0.36577	2.81279	-2.10591
H	-1.51363	5.09835	1.33665

Table C.10: $[Fe^{II}(NH_3)_6]^{2+}$. a) high -spin, b) low -spin, in XYZ format

(a)

FE	8.07222	6.59657	5.92788
N	6.82730	7.18765	7.67111
N	7.68101	4.49563	6.50803
N	6.26123	6.59558	4.60496
N	8.37914	8.71583	5.35188
N	9.91203	6.62282	7.20885
N	9.36684	5.99924	4.22552
H	8.94801	5.95307	3.27978
H	9.15358	9.23850	5.79790
H	10.20833	6.57291	4.03690
H	10.48351	5.76076	7.26187
H	9.78650	6.82993	8.21599
H	6.41200	6.86607	3.61634
H	7.58631	9.35627	5.53421
H	7.92708	3.76986	5.81207
H	6.90847	8.17312	7.97828
H	5.76003	5.69896	4.47350
H	6.70149	4.23010	6.71587
H	6.99132	6.69833	8.56922
H	5.79879	7.09537	7.59099
H	8.15976	4.12610	7.34866
H	5.47154	7.22097	4.84534
H	8.55885	8.92484	4.35334
H	10.64502	7.31513	6.97297
H	9.79548	5.05886	4.28902

(b)

FE	8.09587	6.58167	5.91205
N	7.16780	7.27092	7.56833
N	7.72674	4.68666	6.51776
N	6.35688	6.55768	4.87718
N	8.40750	8.49156	5.32287
N	9.85069	6.56153	6.91981
N	9.07085	5.91017	4.27310
H	8.54901	5.86540	3.37863
H	9.07826	9.06662	5.86552
H	9.90814	6.44299	3.97340
H	10.45081	5.72443	6.80413
H	9.81410	6.62009	7.95454
H	6.23653	7.25915	4.12359
H	7.58378	9.12061	5.32600
H	7.74496	3.93337	5.80600
H	7.52428	8.15588	7.97416
H	6.13525	5.68859	4.35727
H	6.80223	4.50696	6.95114
H	7.17680	6.66540	8.40975
H	6.15611	7.49196	7.51347
H	8.35043	4.27569	7.23671
H	5.46944	6.69022	5.39638
H	8.76194	8.65490	4.36225
H	10.54046	7.30897	6.71968
H	9.46776	4.95284	4.30317

C.2 Cross-validation results

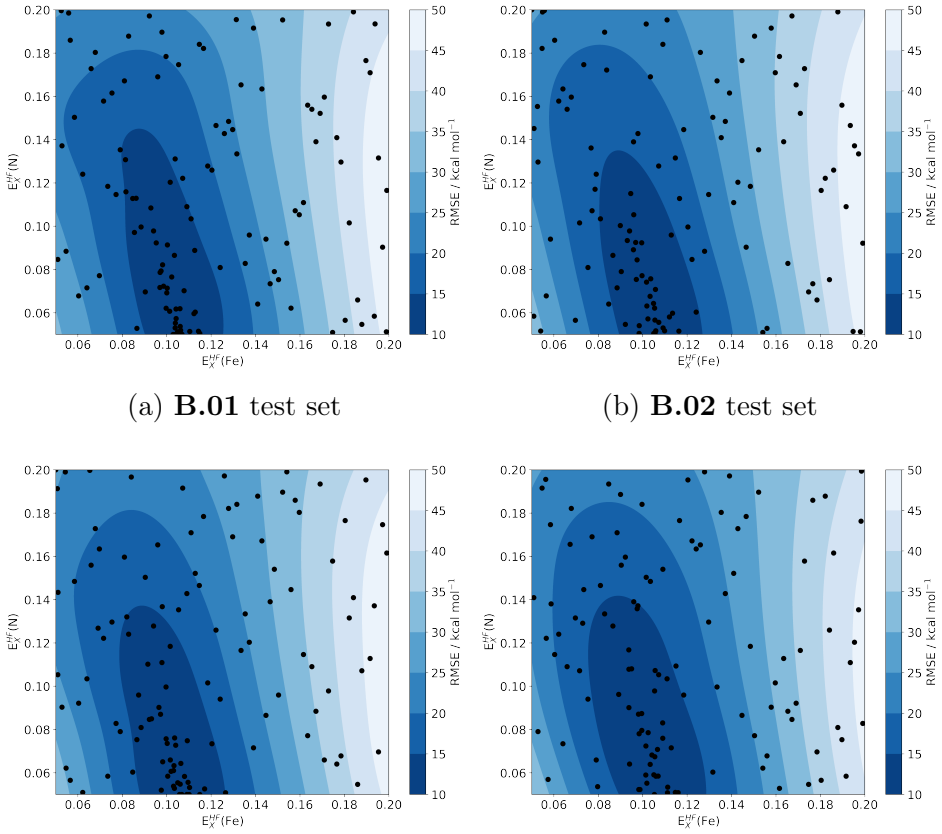

(a) **B.01** test set

(b) **B.02** test set

(c) **B.03** test set

(d) **B.04** test set

Figure C.1: 2D representation of the result of the BO procedure using a training set composed of all systems from the extended (10) model set, except for the noted test set complex. Each point reflects an iteration, with a unique set of HF exchange parameters and resulting RMSE. The color gradient is derived from the mean of the Gaussian process regression, reflecting the predicted RMSE values inbetween sampled points.

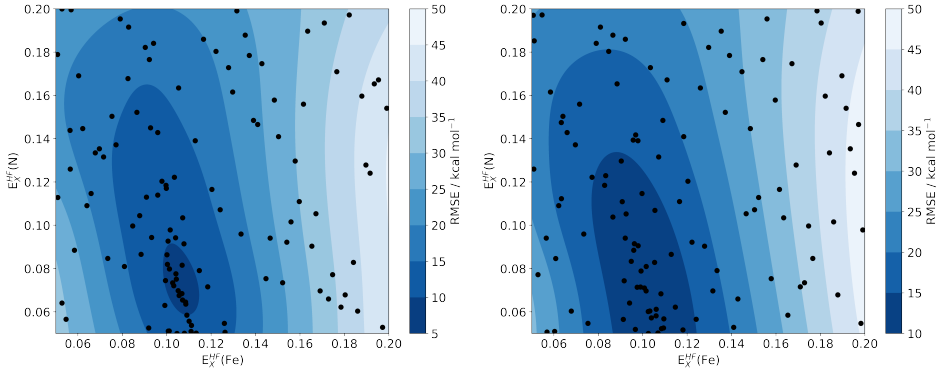

(a) **B.05** test set (b) **B.06** test set

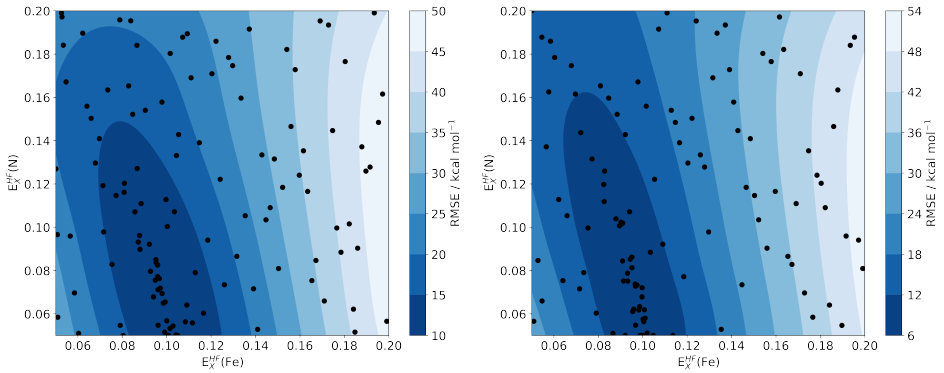

(c) **B.07** test set (d) **B.08** test set

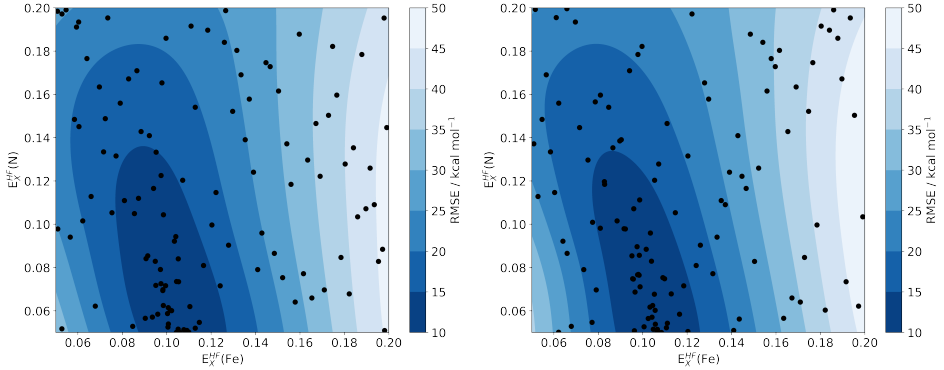

(e) **B.09** test set (f) **B.10** test set

Figure C.2: 2D representation of the result of the BO procedure using a training set composed of all systems from the extended (10) model set, except for the noted test set complex. Each point reflects an iteration, with a unique set of HF exchange parameters and resulting RMSE. The color gradient is derived from the mean of the Gaussian process regression, reflecting the predicted RMSE values inbetween sampled points.

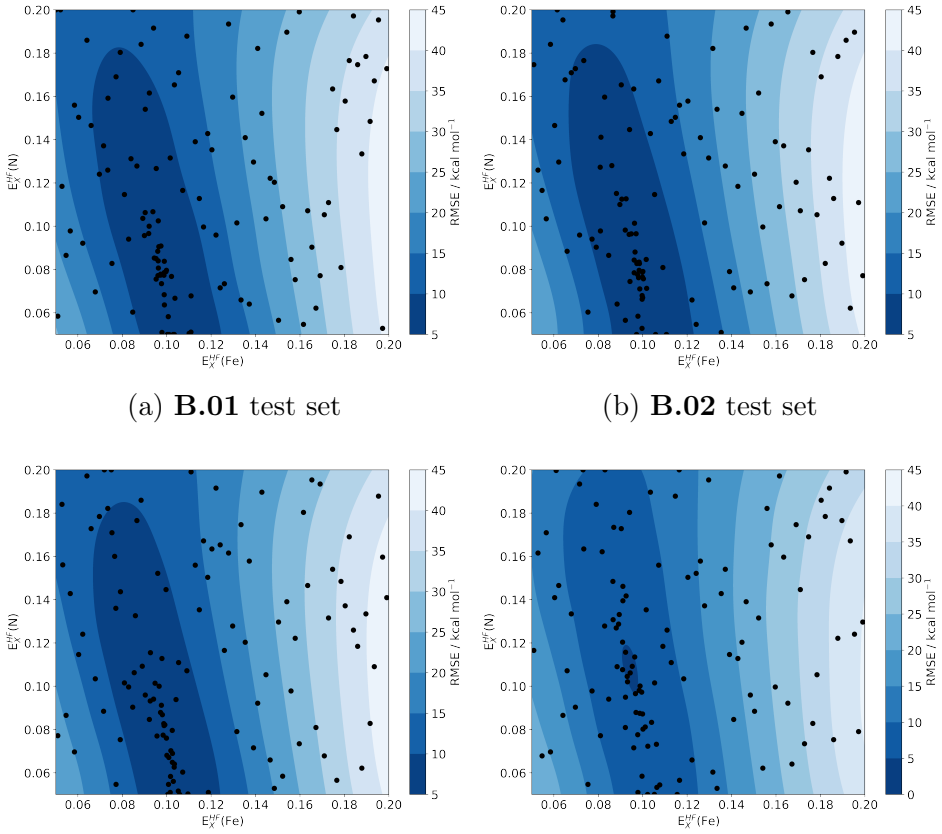

(a) **B.01** test set

(b) **B.02** test set

(c) **B.03** test set

(d) **B.04** test set

Figure C.3: 2D representation of the result of the BO procedure using a training set composed of all systems from the reduced (8) model set, except for the noted test set complex. Each point reflects an iteration, with a unique set of HF exchange parameters and resulting RMSE. The color gradient is derived from the mean of the Gaussian process regression, reflecting the predicted RMSE values inbetween sampled points.

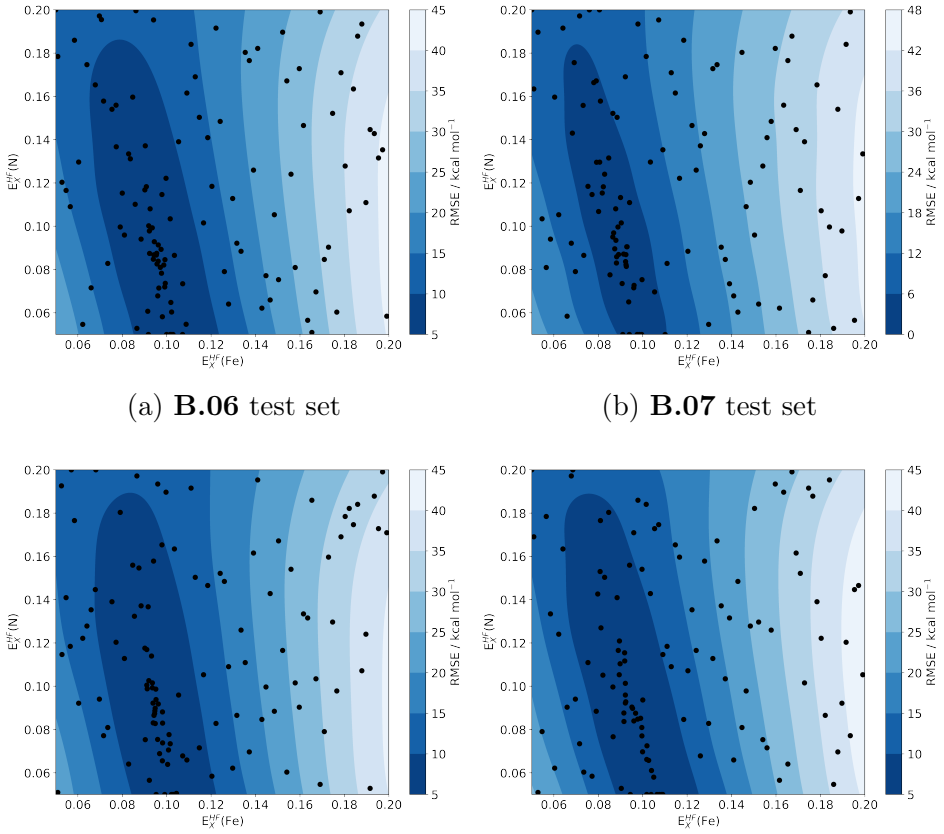

(a) **B.06** test set

(b) **B.07** test set

(c) **B.09** test set

(d) **B.10** test set

Figure C.4: 2D representation of the result of the BO procedure using a training set composed of all systems from the reduced (8) model set, except for the noted test set complex. Each point reflects an iteration, with a unique set of HF exchange parameters and resulting RMSE. The color gradient is derived from the mean of the Gaussian process regression, reflecting the predicted RMSE values inbetween sampled points.

Appendix D

Supplemental material for Chapter 6

D.1 ORCA input files

Frequency calculation of **B.05** model system in HS state

```
!PBE0 DKH-def2-TZVPP SARC/J D3BJ PAL8 tightscf slowconv Numfreq DKH2 grid6

%method
ScalHFX = 0.10
end

%scf
MaxIter 200
DIISMaxEq 10
directresetfreq 10
end

*xyzfile 1 5 *.xyz
```

D.2 CP-PAW input files

*.strc file for the optimization of $(Fe_{HS})_3(Fe_{LS})_1$ using PBE0r with 6% HF exchange. Structural data omitted for brevity

```
!STRUCTURE
 !GENERIC LUNIT[AA]=1. !END
 !OCCUPATIONS EMPTY=10 NSPIN=2 SPIN[HBAR]=6. CHARGE[E]=4. !END
 !SPECIES NAME='Fe' NPRO=1 1 1  LRHOX=4
    !NTBO    NOFL=1 0 1 CV=T  raug/rcov=1.15 LHFWEIGHT=0.06
             focksetup=F cv=T NDDO=F 31=F BONDX=F !END
    !AUGMENT  ID='FE_NDLSS_V0' Z=  26.00000 ZV= 8.
             TYPE='NDLSS' RBOX/RCOV=  1.200 RCSM/RCOV=  0.250
             RCL/RCOV=  0.800  0.800  0.800  0.800  0.800
      !GRID DMIN=   0.100E-05 DMAX=     0.100 RMAX=    20.000 !END
      !POT  POW=  3.000 RC/RCOV=  0.702 !END
      !CORE POW=  3.000 RC/RCOV=  0.702 !END
    !END
 !END
 !SPECIES   NAME='N_'   NPRO=1 1 1 LRHOX=4 RAD/RCOV=1.4
    !NTBO    NOFL=1 1 0 CV=T  RAUG/RCOV=1.2 LHFWEIGHT=0.06
             FOCKSETUP=F CV=T NDDO=F 31=F BONDX=F !END
    !AUGMENT ID='MY_NDLSS_N' EL='N' ZV= 5.
             TYPE='NDLSS' RBOX/RCOV=1.2 RCSM/RCOV=.25
             RCL/RCOV=0.75 0.75 0.75  0.75
      !GRID  DMIN=1.E-6 DMAX=.15 RMAX=9. !END
      !POT   POW=3. RC/RCOV=0.75 VAL0_X=-4.3 !END
      !CORE  POW=2. RC/RCOV=0.75  !END
    !END
 !END
 !SPECIES   NAME='C_'   NPRO=1 1 1 LRHOX=4 RAD/RCOV=1.4
    !NTBO    NOFL=1 1 0 CV=T  RAUG/RCOV=1.2 LHFWEIGHT=0.06
             FOCKSETUP=F CV=T NDDO=F 31=F BONDX=F !END
    !AUGMENT ID='MY_NDLSS_C' EL='C' ZV= 4.
             TYPE='NDLSS' RBOX/RCOV=1.2 RCSM/RCOV=.25
             RCL/RCOV=0.85 0.85 0.85 0.85
```

```
      !GRID  DMIN=1.E-6 DMAX=.15 RMAX=9. !END
      !POT   POW=3. RC/RCOV=0.75  VAL0_X=-2.7 !END
      !CORE  POW=2. RC/RCOV=0.75  !END
    !END
 !END
 !SPECIES   NAME='H_'  M=2. NPRO=1 1 LRHOX=2 RAD/RCOV=1.2
    !NTBO    NOFL=1 0 CV=T  RAUG/RCOV=1.2 LHFWEIGHT=0.06
             FOCKSETUP=F CV=T NDDO=F 31=F BONDX=F !END
    !AUGMENT ID='MY_NDLSS_H' EL='H' ZV= 1.
             TYPE='NDLSS' RBOX/RCOV=1.2 RCSM/RCOV=.25
             RCL/RCOV=1.2 1.2  1.2  1.2
      !GRID  DMIN=1.E-6 DMAX=.15 RMAX=9. !END
      !POT   POW=3. RC/RCOV=1. VAL0_X=-1.6 !END
      !CORE  POW=2. RC/RCOV=1. !END
    !END
 !END
!LATTICE T=  0.00000 17.00000 17.00000
              17.00000 0.00000 17.00000
             17.00000  17.00000 0.0000 !END
  !ATOM NAME= 'Fe1'      R=      3.50707    14.65479    15.03014 !END
  !ATOM NAME= 'Fe2'      R=      4.94646    10.36137    16.23403 !END
                  [...]
 !ISOLATE !END
!ORBPOT_x
 !POT ATOM='Fe1' Value=+0.1 TYPE='D' RC=1.5 S=1 !END
 !POT ATOM='Fe2' Value=+0.1 TYPE='D' RC=1.5 S=1 !END
 !POT ATOM='Fe3' Value=+0.1 TYPE='D' RC=1.5 S=1 !END
 !POT ATOM='Fe4' Value=+0.1 TYPE='D' RC=1.5 S=1 !END
    !END
!END
!EOB
```

D.3 Structural data of converged [2x2] Fe^{II} grid systems

Optimized $(Fe_{LS})_4$ complex, in XYZ format

```
      180
c8s0
Fe     3.59659   14.71786   15.31269
Fe     4.98745   10.35807   16.14063
Fe     9.13302   11.34609   14.30240
Fe     8.03795   15.85687   14.57871
N      4.59061   13.52803   16.64888
N      5.08489   12.29429   16.82962
N      4.05269   16.03967   16.57621
N      2.82956   16.36225   14.42328
N      6.26247   10.11326   17.49518
N      5.41796    8.43900   15.85998
N      5.95386   10.76838   14.38628
N      7.13237   11.15065   13.87316
N      3.50412   10.28503   14.98564
N      3.51068    9.96691   17.46260
N      9.15375   11.99738   12.54002
N     11.04376   11.88611   14.15672
N      8.84877   12.90533   15.60569
N      8.42323   14.17449   15.68959
N      9.43979   10.42272   15.91506
N      9.45878    9.47587   13.60415
N      7.57118   16.52204   16.26995
N      7.39432   17.66462   14.06696
N      6.36698   15.08435   13.68816
N      5.11604   14.66596   13.93061
N      8.75990   15.53358   12.87250
N      9.94323   16.46434   14.86403
N      2.76668   13.64045   14.01587
N      1.90201   14.28342   16.25962
C      5.65802   13.51886   18.65009
C      4.93671   14.27413   17.75131
C      5.75873   12.29364   18.02790
C      4.56162   15.65427   17.76546
C      4.60548   16.51732   18.85578
C      4.13711   17.80988   18.70772
C      3.63528   18.21491   17.48209
C      3.59457   17.30188   16.43636
C      2.97770   17.51327   15.13956
C      2.54382   18.74801   14.67402
C      1.91421   18.83579   13.44876
C      1.73728   17.67114   12.72269
C      2.20525   16.47724   13.23944
C      6.42021   11.08786   18.41620
C      7.06200   10.84975   19.62887
C      7.52200    9.57623   19.90651
C      7.34117    8.56838   18.97167
C      6.70612    8.86747   17.77516
C      6.31746    7.92019   16.74489
C      6.78092    6.61423   16.65970
C      6.31836    5.78968   15.65300
C      5.39797    6.30433   14.75563
C      4.98135    7.61512   14.89452
C      5.67141   10.98542   12.14688
C      5.06452   10.66599   13.34209
C      6.95741   11.31295   12.51912
C      3.71413   10.30917   13.65233
C      2.72265    9.93724   12.75000
C      1.48476    9.55469   13.23306
```

C	1.25953	9.55029	14.59979
C	2.29392	9.91099	15.45328
C	2.27426	9.83342	16.90288
C	1.12915	9.61420	17.65773
C	1.22490	9.50052	19.03002
C	2.47842	9.60590	19.60683
C	3.57531	9.83702	18.79765
C	8.07545	11.77544	11.75744
C	8.14326	11.89136	10.37113
C	9.35137	12.21493	9.78188
C	10.46368	12.42587	10.58231
C	10.33390	12.30751	11.95876
C	11.40832	12.36985	12.93423
C	12.68341	12.85225	12.67099
C	13.63604	12.84460	13.67069
C	13.27839	12.34839	14.91289
C	11.99067	11.88511	15.10825
C	8.89928	13.48868	17.79723
C	9.13781	12.48541	16.88298
C	8.42365	14.52187	17.01965
C	9.55924	11.12997	17.05884
C	10.11010	10.57317	18.20862
C	10.52073	9.25317	18.18475
C	10.37525	8.51706	17.02072
C	9.84197	9.13395	15.89660
C	9.74718	8.55593	14.56862
C	9.95828	7.21246	14.28570
C	9.90017	6.77018	12.97955
C	9.63340	7.69889	11.98888
C	9.42144	9.01877	12.34167
C	7.95324	15.82733	17.36288
C	7.97030	16.40903	18.62788
C	7.61311	17.73792	18.76068
C	7.24025	18.45901	17.63650
C	7.23101	17.82323	16.40357
C	6.99873	18.44692	15.11239
C	6.45235	19.71076	14.93457
C	6.30520	20.21805	13.65838
C	6.71444	19.43630	12.59135
C	7.24589	18.18414	12.83814
C	5.53499	14.29193	11.73332
C	6.62497	14.85979	12.35602
C	4.61917	14.15634	12.75403
C	7.92832	15.18909	11.86660
C	8.32709	15.25231	10.53521
C	9.61586	15.65633	10.23873
C	10.47891	15.98769	11.27027
C	10.01792	15.92638	12.57863
C	10.73850	16.36256	13.76089
C	12.09103	16.67783	13.77920
C	12.67039	17.13875	14.94404
C	11.86677	17.27487	16.06247
C	10.53069	16.92990	15.97833
C	3.30754	13.58851	12.77941
C	2.58071	13.12979	11.68340
C	1.26514	12.74498	11.86330
C	0.70250	12.81493	13.12848
C	1.47862	13.26854	14.18536
C	1.02389	13.52640	15.54054
C	-0.17951	13.07613	16.06663
C	-0.52255	13.40316	17.36367
C	0.35785	14.17862	18.09892
C	1.54116	14.59114	17.51536
H	6.08055	13.82986	19.59739
H	4.98126	16.16107	19.81181
H	4.14302	18.49762	19.55131
H	3.23115	19.21598	17.35460
H	2.69518	19.63713	15.28182
H	1.55850	19.79286	13.07138

```
H      1.23416   17.67369   11.75825
H      2.06613   15.56341   12.67178
H      7.15023   11.65030   20.36008
H      7.99924    9.35831   20.86029
H      7.65716    7.55093   19.18683
H      7.50102    6.24976   17.38922
H      6.66146    4.75955   15.57480
H      4.99009    5.69729   13.95034
H      4.25673    8.02886   14.19931
H      5.22960   11.01237   11.15857
H      2.93815    9.92766   11.68434
H      0.69979    9.24033   12.54783
H      0.30436    9.22113   15.00114
H      0.16496    9.52689   17.16215
H      0.34022    9.31964   19.63793
H      2.61973    9.50556   20.68072
H      4.55909    9.91910   19.24770
H      7.26345   11.67907    9.76753
H      9.43626   12.28060    8.69863
H     11.43204   12.64192   10.13826
H     12.92257   13.22942   11.67896
H     14.64403   13.20992   13.48223
H     13.99078   12.30678   15.73396
H     11.70078   11.48868   16.07672
H      9.01606   13.45430   18.87325
H     10.23280   11.18443   19.09941
H     10.97190    8.80103   19.06600
H     10.72028    7.48737   16.97150
H     10.17595    6.51862   15.09442
H     10.07129    5.72289   12.73685
H      9.59255    7.41467   10.93967
H      9.21413    9.74803   11.56585
H      8.30921   15.83064   19.48459
H      7.64789   18.22306   19.73455
H      6.99660   19.51556   17.71210
H      6.14866   20.29247   15.80226
H      5.88833   21.21076   13.49810
H      6.63490   19.78975   11.56560
H      7.57421   17.56338   12.00967
H      5.43951   13.98660   10.69875
H      7.61876   15.00851    9.74717
H      9.94437   15.73259    9.20393
H     11.48550   16.33871   11.05754
H     12.68316   16.56655   12.87375
H     13.72685   17.39925   14.97669
H     12.26203   17.65209   17.00309
H      9.89853   17.03689   16.85352
H      3.03635   13.12605   10.69557
H      0.66725   12.41297   11.01643
H     -0.34153   12.55595   13.28486
H     -0.84390   12.47259   15.45196
H     -1.46566   13.06790   17.79164
H      0.13441   14.47704   19.12084
H      2.23740   15.20301   18.08108
```

Optimized $(Fe_{HS})_1(Fe_{LS})_3$ complex, in XYZ format

```
      180
c8s2
Fe     3.54987   14.79800   15.34781
Fe     4.84057   10.40365   15.96449
Fe     9.02795   11.45052   14.44362
Fe     8.02486   15.93637   14.79400
N      4.49853   13.53158   16.63350
N      5.01199   12.29796   16.72225
N      3.99790   16.04618   16.68058
N      2.84998   16.48990   14.51379
N      6.22063   10.09796   17.19300
```

N	5.20971	8.47432	15.59768
N	5.74390	10.83847	14.25622
N	6.96466	11.12615	13.79589
N	3.33778	10.39633	14.84567
N	3.42261	10.00821	17.30805
N	9.17942	11.64991	12.36864
N	11.21511	12.02095	13.94328
N	8.93717	13.12918	15.83175
N	8.41580	14.35523	15.94924
N	9.80556	10.61682	16.20064
N	9.49789	9.20322	14.03957
N	7.50626	16.64577	16.44999
N	7.36490	17.68862	14.19596
N	6.40302	15.08437	13.85855
N	5.11622	14.74381	14.02553
N	8.84651	15.47165	13.16387
N	9.90261	16.61763	15.11199
N	2.73152	13.78750	13.99313
N	1.81376	14.38178	16.22464
C	5.67798	13.43373	18.56767
C	4.89234	14.22366	17.75494
C	5.75885	12.24345	17.87614
C	4.50708	15.59938	17.84842
C	4.54578	16.40444	18.98225
C	4.06488	17.69896	18.90255
C	3.56162	18.16629	17.69954
C	3.53290	17.31204	16.60555
C	2.94828	17.59513	15.30683
C	2.51438	18.85027	14.89923
C	1.95345	19.00777	13.64765
C	1.84805	17.89264	12.83432
C	2.30200	16.67302	13.30131
C	6.47584	11.03240	18.13458
C	7.29699	10.75922	19.22374
C	7.87218	9.50597	19.33347
C	7.60993	8.54700	18.36793
C	6.76363	8.86855	17.31557
C	6.25105	7.95410	16.30940
C	6.72369	6.66485	16.10489
C	6.11457	5.85377	15.16813
C	5.03420	6.36042	14.46641
C	4.62293	7.65785	14.70850
C	5.60027	10.84651	12.00762
C	4.90054	10.68488	13.18875
C	6.88897	11.13159	12.42581
C	3.52854	10.40403	13.50546
C	2.50155	10.07967	12.62728
C	1.25587	9.75844	13.13983
C	1.06006	9.75278	14.51121
C	2.12896	10.06108	15.34372
C	2.16044	9.93886	16.79286
C	1.04288	9.72097	17.58713
C	1.19513	9.54086	18.94799
C	2.47422	9.58283	19.47593
C	3.54294	9.81935	18.63125
C	8.07858	11.37249	11.64227
C	8.12154	11.26636	10.25254
C	9.33509	11.41163	9.61004
C	10.47084	11.67786	10.35553
C	10.35911	11.80461	11.73613
C	11.49210	12.10962	12.62327
C	12.74581	12.48787	12.15012
C	13.75185	12.78191	13.05094
C	13.47273	12.70436	14.40534
C	12.20093	12.32230	14.79516
C	9.04576	13.71599	18.01720
C	9.33408	12.73579	17.08381
C	8.44423	14.71269	17.26789
C	9.96976	11.44817	17.24801

```
C     10.73306   11.09693   18.35899
C     11.34882    9.86045   18.37960
C     11.17559    8.99901   17.31019
C     10.39106    9.40326   16.23463
C     10.12607    8.56674   15.05450
C     10.46953    7.21849   14.99054
C     10.16205    6.49136   13.85658
C      9.50812    7.13117   12.81731
C      9.20382    8.47398   12.95718
C      7.90894   16.00798   17.57571
C      7.89084   16.64210   18.81329
C      7.47343   17.96018   18.88651
C      7.08896   18.62193   17.73045
C      7.12397   17.93967   16.52123
C      6.92097   18.50629   15.19554
C      6.37161   19.75542   14.94200
C      6.27079   20.20572   13.63930
C      6.72396   19.38336   12.62090
C      7.25575   18.14765   12.94034
C      5.67484   14.21947   11.89155
C      6.74678   14.76060   12.56590
C      4.67642   14.20237   12.84005
C      8.09642   14.98621   12.15350
C      8.62039   14.79246   10.87906
C      9.95178   15.08627   10.65085
C     10.72937   15.56982   11.69087
C     10.14534   15.76199   12.93606
C     10.77604   16.36800   14.09472
C     12.12019   16.71322   14.15953
C     12.60858   17.36226   15.27541
C     11.72314   17.65643   16.29754
C     10.40169   17.26884   16.17606
C      3.33355   13.71453   12.78742
C      2.64189   13.30316   11.65042
C      1.30134   12.98346   11.76026
C      0.67909   13.06687   12.99675
C      1.42141   13.47195   14.09662
C      0.92291   13.70891   15.44037
C     -0.32316   13.30655   15.90213
C     -0.69492   13.59332   17.20117
C      0.20314   14.27472   18.00526
C      1.42853   14.64505   17.48318
H      6.15316   13.70100   19.50303
H      4.92598   16.00124   19.91780
H      4.06495   18.34057   19.78174
H      3.15464   19.17149   17.62400
H      2.61452   19.70060   15.57005
H      1.60011   19.98167   13.31355
H      1.40936   17.95361   11.84077
H      2.21911   15.79485   12.66898
H      7.46057   11.52165   19.98173
H      8.50797    9.26539   20.18316
H      8.02024    7.54451   18.45839
H      7.56781    6.30149   16.68664
H      6.46703    4.83819   14.99751
H      4.50028    5.75891   13.73409
H      3.77720    8.06554   14.16271
H      5.22063   10.77810   10.99530
H      2.69066   10.05792   11.55664
H      0.44148    9.48643   12.47102
H      0.10091    9.45990   14.93119
H      0.05566    9.68428   17.13192
H      0.33184    9.35679   19.58505
H      2.65510    9.42879   20.53746
H      4.55178    9.85415   19.03251
H      7.21825   11.03534    9.69269
H      9.40238   11.30296    8.52873
H     11.43589   11.76712    9.86436
H     12.93786   12.55446   11.08203
```

```
H     14.74230   13.06651   12.69895
H     14.23013   12.92335   15.15503
H     11.95082   12.24680   15.85267
H      9.23092   13.69991   19.08473
H     10.86281   11.80230   19.17678
H     11.97474    9.56944   19.22170
H     11.66817    8.03049   17.30641
H     10.97444    6.73584   15.82381
H     10.43196    5.43880   13.78471
H      9.24556    6.60559   11.90170
H      8.69558    9.00385   12.15316
H      8.24545   16.11595   19.69726
H      7.47552   18.48430   19.84056
H      6.80543   19.67095   17.76211
H      6.03066   20.37305   15.77029
H      5.85418   21.18750   13.42143
H      6.67823   19.69341   11.57920
H      7.62255   17.48795   12.15778
H      5.63831   13.85899   10.87139
H      7.97991   14.42580   10.08080
H     10.38182   14.95780    9.65939
H     11.77096   15.83241   11.52598
H     12.77802   16.47786   13.32618
H     13.65675   17.64871   15.34037
H     12.04264   18.18774   17.19137
H      9.70757   17.50072   16.97680
H      3.14815   13.28151   10.68787
H      0.73157   12.68871   10.88081
H     -0.38151   12.85157   13.09831
H     -0.99806   12.77216   15.23694
H     -1.67138   13.29548   17.57905
H     -0.03884   14.53291   19.03392
H      2.14034   15.18238   18.10316
```

Optimized $(Fe_{HS})_3(Fe_{LS})_1$ complex, in XYZ format

```
      180
c8s6
Fe     3.60190   14.60556   15.17045
Fe     4.94132   10.36174   16.11563
Fe     9.07830   11.33959   14.58332
Fe     7.93887   15.69699   14.68141
N      4.52934   13.38789   16.69990
N      5.09229   12.18973   16.86164
N      3.89169   15.98618   16.69654
N      2.80925   16.67038   14.42583
N      6.32485   10.06833   17.34374
N      5.32887    8.46014   15.72425
N      5.80942   10.84045   14.41046
N      7.02717   11.11566   13.94499
N      3.41637   10.42216   15.02384
N      3.53424    9.94303   17.46473
N      9.20801   11.77158   12.54728
N     11.26519   12.00815   14.12411
N      8.88245   12.88410   15.99593
N      8.37907   14.12037   16.05455
N      9.86231   10.46875   16.32604
N      9.52324    9.14436   14.13181
N      7.66934   16.60494   16.54845
N      7.09906   17.77507   14.30973
N      6.35656   14.86770   13.50918
N      5.07782   14.51384   13.66385
N      8.78252   15.59489   12.76434
N     10.14802   16.47063   14.81354
N      2.54207   13.83879   13.54279
N      1.53410   14.09375   15.90540
C      5.74633   13.45341   18.60928
C      4.91219   14.16461   17.76404
```

```
C      5.85689   12.21719   17.99583
C      4.45020   15.53182   17.83758
C      4.54194   16.32299   18.97952
C      4.04434   17.61079   18.93724
C      3.48463   18.08647   17.76366
C      3.42571   17.25012   16.65321
C      2.87297   17.65602   15.35046
C      2.46547   18.95912   15.07692
C      1.97746   19.27269   13.82309
C      1.91742   18.27327   12.86764
C      2.34012   17.00289   13.21789
C      6.58005   11.01157   18.28205
C      7.39020   10.73914   19.37775
C      7.95109    9.47883   19.49991
C      7.68548    8.51286   18.54206
C      6.85101    8.83301   17.47898
C      6.34166    7.92225   16.46445
C      6.79445    6.62501   16.26816
C      6.20238    5.83265   15.30382
C      5.16460    6.36694   14.55852
C      4.76629    7.66898   14.79819
C      5.61726   11.03961   12.17414
C      4.93852   10.80038   13.35430
C      6.92343   11.24458   12.58288
C      3.56556   10.55080   13.68498
C      2.49196   10.39089   12.81774
C      1.24276   10.10752   13.34421
C      1.08892    9.97994   14.71549
C      2.20141   10.13222   15.53411
C      2.26133    9.92100   16.97200
C      1.15573    9.68180   17.77726
C      1.33051    9.43724   19.12526
C      2.61962    9.43917   19.63026
C      3.67610    9.69531   18.77619
C      8.09887   11.56474   11.80945
C      8.11626   11.63369   10.41764
C      9.30944   11.90920    9.78045
C     10.44852   12.13404   10.53546
C     10.36488   12.06558   11.92172
C     11.50603   12.29038   12.82380
C     12.73499   12.77401   12.38249
C     13.75598   12.96956   13.29296
C     13.51744   12.68551   14.62691
C     12.26677   12.21376   14.98604
C      9.24314   13.64765   18.08367
C      9.41820   12.58164   17.21382
C      8.57527   14.59362   17.31854
C     10.05437   11.28958   17.37737
C     10.83348   10.91625   18.46783
C     11.43585    9.67035   18.45750
C     11.23793    8.82392   17.37974
C     10.43709    9.25298   16.32484
C     10.14304    8.45799   15.12118
C     10.45055    7.10558   15.00673
C     10.11331    6.42803   13.84996
C      9.46711    7.11943   12.83874
C      9.20010    8.46440   13.02618
C      8.12595   15.93533   17.62590
C      8.19955   16.53113   18.88141
C      7.82317   17.85640   19.01060
C      7.37400   18.55116   17.90042
C      7.30108   17.89176   16.67683
C      6.86516   18.51725   15.41754
C      6.25171   19.76489   15.35915
C      5.86078   20.27173   14.13401
C      6.08942   19.51504   12.99682
C      6.70683   18.28442   13.13697
C      5.52864   14.42733   11.45899
C      6.64790   14.82399   12.17810
```

C	4.55948	14.23637	12.43251
C	7.97309	15.21967	11.75063
C	8.38501	15.25803	10.42283
C	9.66099	15.70357	10.13449
C	10.49821	16.07973	11.16958
C	10.03253	16.00642	12.47964
C	10.83528	16.39192	13.65129
C	12.20061	16.65339	13.57389
C	12.88783	17.02983	14.71195
C	12.18914	17.13239	15.90231
C	10.83628	16.84034	15.89920
C	3.16334	13.85617	12.34633
C	2.47793	13.59385	11.16392
C	1.11637	13.34999	11.22596
C	0.47363	13.35935	12.45240
C	1.22080	13.59929	13.60217
C	0.67079	13.63757	14.96772
C	-0.61724	13.22010	15.28801
C	-1.03863	13.26766	16.60437
C	-0.15632	13.72367	17.57056
C	1.10797	14.12339	17.17267
H	6.22566	13.79235	19.51932
H	4.97676	15.91795	19.89011
H	4.08089	18.24456	19.82183
H	3.07838	19.09336	17.72463
H	2.52789	19.73054	15.84025
H	1.64547	20.28464	13.59609
H	1.53727	18.46514	11.86652
H	2.29784	16.19624	12.48796
H	7.55628	11.50535	20.13166
H	8.57753	9.23823	20.35648
H	8.08650	7.50773	18.64526
H	7.60849	6.23932	16.87782
H	6.53828	4.81005	15.14173
H	4.65365	5.78228	13.79673
H	3.95266	8.10625	14.22523
H	5.21196	11.08184	11.17074
H	2.64532	10.47334	11.74450
H	0.39002	9.96259	12.68363
H	0.12171	9.72698	15.14215
H	0.15953	9.68101	17.34060
H	0.47669	9.23636	19.76987
H	2.81772	9.23826	20.68083
H	4.69222	9.69764	19.16014
H	7.20793	11.44555	9.85019
H	9.35910	11.94215	8.69323
H	11.39566	12.33815	10.04401
H	12.89637	12.99628	11.33050
H	14.72799	13.33337	12.96325
H	14.28899	12.81465	15.38293
H	12.05005	11.97867	16.02711
H	9.55634	13.72337	19.11846
H	10.98316	11.60398	19.29741
H	12.07193	9.36075	19.28520
H	11.72413	7.85208	17.35221
H	10.94992	6.58173	15.81862
H	10.35535	5.37221	13.73836
H	9.18517	6.63185	11.90797
H	8.70386	9.04147	12.24648
H	8.57432	15.96971	19.73462
H	7.89683	18.35676	19.97493
H	7.10924	19.60177	17.98417
H	6.07388	20.33515	16.26795
H	5.38694	21.24972	14.06690
H	5.80574	19.87330	12.00959
H	6.91073	17.66483	12.26397
H	5.43379	14.30129	10.38692
H	7.70365	14.95759	9.63046
H	10.00138	15.77097	9.10243

```
H     11.49437   16.45644   10.95434
H     12.72822   16.56037   12.62804
H     13.95361   17.24828   14.66796
H     12.67812   17.44105   16.82381
H     10.26316   16.91285   16.82180
H      2.99935   13.61540   10.20929
H      0.54922   13.17062   10.31389
H     -0.60050   13.20224   12.50747
H     -1.28807   12.85523   14.51370
H     -2.04711   12.95601   16.87228
H     -0.44361   13.78520   18.61808
H      1.82845   14.49622   17.90094
```

Optimized $(Fe_{HS})_4$ complex, in XYZ format

```
       180
c8s8
Fe     3.70677   14.73857   15.26925
Fe     5.07929   10.59554   16.13712
Fe     9.10595   11.42891   14.33234
Fe     8.01783   15.74462   14.59898
N      4.74475   13.71702   16.80120
N      5.26448   12.50628   17.00446
N      3.91594   16.20606   16.75769
N      2.89256   16.74262   14.42683
N      6.28693   10.24083   17.80984
N      5.75308    8.43692   16.03718
N      5.91329   10.96131   14.22177
N      7.09109   11.29496   13.69165
N      3.45848   10.24919   14.86230
N      3.23458   10.10730   17.44759
N      9.22554   11.85490   12.28067
N     11.23418   12.10047   13.89301
N      8.89060   12.90481   15.82874
N      8.44910   14.15902   15.92210
N      9.72890   10.43006   16.07199
N      9.53159    9.21674   13.77883
N      7.74016   16.61165   16.48325
N      7.20532   17.82514   14.26374
N      6.39943   14.92078   13.50409
N      5.13736   14.54851   13.72150
N      8.79793   15.60434   12.66363
N     10.20823   16.48836   14.66231
N      2.64084   13.77584   13.73858
N      1.70431   14.08223   16.13164
C      5.61000   13.70309   18.88128
C      4.94181   14.45913   17.92786
C      5.80171   12.47814   18.25799
C      4.45100   15.82104   17.93631
C      4.48900   16.66605   19.04009
C      3.95821   17.93749   18.92143
C      3.42534   18.34248   17.71028
C      3.42385   17.45267   16.63879
C      2.90383   17.77662   15.29937
C      2.47782   19.05280   14.94216
C      2.02784   19.28643   13.65670
C      2.02465   18.23689   12.75439
C      2.46182   16.99703   13.18673
C      6.41004   11.24191   18.70450
C      7.02729   11.04938   19.93689
C      7.50285    9.78834   20.25089
C      7.37178    8.75825   19.33407
C      6.76285    9.01992   18.11063
C      6.55234    8.02208   17.04823
C      7.13530    6.75870   17.06080
C      6.89421    5.88993   16.01282
C      6.07986    6.30838   14.97338
C      5.53885    7.58072   15.03223
```

C	5.67427	10.91099	11.98195
C	5.04037	10.72256	13.20160
C	6.96541	11.27546	12.33272
C	3.69100	10.31882	13.53441
C	2.71566	9.99376	12.59802
C	1.47537	9.58068	13.04731
C	1.23082	9.51422	14.40794
C	2.24459	9.86149	15.29615
C	2.10042	9.83622	16.76167
C	0.89267	9.57041	17.40098
C	0.83729	9.57871	18.78173
C	1.99168	9.86294	19.49086
C	3.15305	10.11716	18.78208
C	8.13221	11.59135	11.53654
C	8.17727	11.58030	10.14546
C	9.38628	11.82488	9.51817
C	10.51070	12.09220	10.28076
C	10.39559	12.10749	11.66789
C	11.50970	12.36658	12.59446
C	12.74326	12.86348	12.18422
C	13.72922	13.09417	13.12538
C	13.45245	12.83119	14.45695
C	12.20130	12.33945	14.78570
C	9.12334	13.53565	17.97853
C	9.30487	12.50597	17.06516
C	8.57334	14.55942	17.21964
C	9.82047	11.15949	17.20491
C	10.38064	10.64486	18.36898
C	10.85769	9.34661	18.35910
C	10.74882	8.58985	17.20578
C	10.17199	9.15969	16.07341
C	9.98856	8.45016	14.79572
C	10.24041	7.08969	14.64328
C	10.02044	6.48857	13.41857
C	9.54411	7.26394	12.37567
C	9.31928	8.60965	12.60644
C	8.15886	15.90675	17.55369
C	8.21412	16.47171	18.82416
C	7.85154	17.79868	18.97688
C	7.43148	18.52605	17.87550
C	7.37907	17.89775	16.63500
C	6.96388	18.55009	15.38175
C	6.35607	19.80098	15.33680
C	5.98224	20.32999	14.11562
C	6.22140	19.59207	12.96795
C	6.83066	18.35593	13.09468
C	5.51713	14.36069	11.50826
C	6.64978	14.81623	12.16780
C	4.58573	14.19909	12.52298
C	7.96249	15.19156	11.68685
C	8.34605	15.16983	10.35041
C	9.62151	15.58724	10.01866
C	10.48374	16.00351	11.01806
C	10.04328	15.99791	12.33817
C	10.86653	16.42500	13.48223
C	12.21946	16.73345	13.36987
C	12.92262	17.13020	14.49161
C	12.25573	17.20024	15.70265
C	10.91209	16.86958	15.73354
C	3.20681	13.76009	12.51468
C	2.48901	13.39482	11.37962
C	1.15414	13.05732	11.51823
C	0.57306	13.06746	12.77530
C	1.34991	13.42547	13.87343
C	0.86096	13.47946	15.26096
C	-0.35562	12.93653	15.66258
C	-0.72729	13.01374	16.99180
C	0.13129	13.62678	17.88925
C	1.32510	14.14001	17.41304

```
H      5.91693   14.00229   19.87647
H      4.91412   16.32060   19.97957
H      3.95156   18.61351   19.77501
H      2.99557   19.33544   17.61062
H      2.49660   19.86533   15.66414
H      1.68084   20.27627   13.36431
H      1.67678   18.36702   11.73186
H      2.46315   16.14913   12.50347
H      7.10857   11.87184   20.64434
H      7.96579    9.60147   21.21855
H      7.71959    7.75890   19.58184
H      7.77742    6.45605   17.88468
H      7.33276    4.89330   16.01031
H      5.85402    5.65763   14.13138
H      4.88745    7.94367   14.23725
H      5.25650   10.80352   10.98791
H      2.93710   10.05100   11.53504
H      0.69908    9.29861   12.33788
H      0.26520    9.17265   14.77060
H     -0.00377    9.35613   16.82468
H     -0.09621    9.36064   19.29813
H      2.00219    9.87526   20.57858
H      4.08017   10.33755   19.30960
H      7.28254   11.35380    9.56948
H      9.45820   11.79330    8.43208
H     11.47031   12.26026    9.79897
H     12.93207   13.07216   11.13371
H     14.70503   13.47024   12.82187
H     14.19712   12.99054   15.23391
H     11.95104   12.11180   15.82171
H      9.34715   13.53522   19.03873
H     10.45478   11.26319   19.26054
H     11.32368    8.92454   19.24810
H     11.13255    7.57352   17.18390
H     10.60577    6.49740   15.47848
H     10.22169    5.42750   13.28007
H      9.35933    6.84087   11.39060
H      8.95169    9.24716   11.80393
H      8.56244   15.88452   19.67115
H      7.91133   18.27479   19.95433
H      7.17257   19.57629   17.98040
H      6.17025   20.35661   16.25305
H      5.51402   21.31139   14.05935
H      5.95289   19.96988   11.98377
H      7.04357   17.74935   12.21445
H      5.39167   14.16995   10.44897
H      7.64618   14.84165    9.58574
H      9.94278   15.60084    8.97844
H     11.48056   16.35437   10.76524
H     12.72477   16.66520   12.40977
H     13.97837   17.38678   14.41958
H     12.76118   17.51570   16.61276
H     10.35812   16.91759   16.67010
H      2.96699   13.40264   10.40230
H      0.55975   12.79650   10.64394
H     -0.47954   12.82373   12.89308
H     -1.00814   12.45111   14.94048
H     -1.68070   12.60493   17.32280
H     -0.12030   13.71922   18.94357
H      2.02309   14.63496   18.08800
```